Dissertation

Targeting atherosclerosis: chemical, genetic and proteomic approaches

Submitted by

M.Sc.

Prakash DODDAPATTAR

for the Academic Degree of
Doctor of Philosophy
(Ph.D.)

at the

Medical University of Graz

under the Supervision of
Univ.-Prof. Dr. Dagmar Kratky
Institute of Molecular Biology and Biochemistry

Submitted
2013

Preface

The work presented in this thesis was financed by the PhD program 'Molecular Medicine', Medical University of Graz, Austria, through the academic years 2009-2013. The complete study was carried out in its entirety at the institute of Molecular biology and Biochemistry, Medical University of Graz, Austria.

This work benefited financially from the following grants, the Grants F30 SFB LIPOTOX, W1226 DK-MCD, P19186, and P22832, which are all funded by the Austrian Science Fund (FWF).

Acknowledgement

My most sincere thanks go to my mentor Prof. Dagmar Kratky for believing in me and offering a position to fulfill my dream in her group. I express deep sense of gratitude for continuous encouragement as well as constant and extremely patient support to carry out my experiments. I have been very fortunate to have a mentor who offered me the freedom to explore many new ideas on my own and guiding to correct me when my steps faltered. I learnt a lot from her amazing management skills both personally and professionally. I am in debt to her for understanding and encouraging my scientific skills.

I am highly grateful to my colleague Branislav Radovic for believing and letting me work on xanthohumol. I am extremely lucky and grateful to him in this regard.

I would like to thank Prof. Ruth Birner-Grünberger for collaborating a part of our project and for one of my thesis committee members along with Prof. Gerhard M. Kostner.

It is my pleasure to acknowledge my collaborators, Prof. Wolfgang Sattler, Prof. Helmut Ahammer and Prof. Gerald Hoefler.

I am indeed very grateful to Anton Ibovnik, Silvia Povoden and Sabrina for their technical help and Isabella Hindler, Fiona and Sabine Donner for assisting me in animal facility.

My special thanks to all my past and present colleagues including, Nora Rathke, Elma Aflaki, Jay Patankar, Katharina Jandl, Prakash Chandak, Lalit Doshi, Dagmar Kolb, Sascha Obrowsky, Madeleine Göritzer, Nemanja Vujic, Vinay Sachdev and Stefanie Schlager, Melanie, Julia, Martin and Christoph Nusshold for a wonderful co-operation and making my stay comfortable

I am very grateful to Markus Absenger for helping in microscopy studies all the time and office secretaries Regina Knöbl and Birgit Vogel for explaining many official issues.

I would also like to thank all members of Institute of Molecular biology and Biochemistry for lively interactions and making me feel very comfortable over the years.

I am thankful to Institute of Molecular biology and Biochemistry for providing excellent working environment with advanced equipment facility, animal facility for taking care of my animals and Molecular Medicine PhD program, Medical University of Graz for funding.

I am extremely lucky and blessed to have a beautiful family: My biggest gift and strength; mother Kasturi, father Krishnamurti for always fulfilling my demands. My all-time two encouraging people; sister Jyoti and a wonderful motivating best friend cum brother, Kirankumar, moral support from brother-in-law Vinayak Bengeri and sister-in-law Savita, finally, smile on face from my beautiful niece Paavana and cheerful nephew Bhargav. Last but not the least I would like to thank all my friends and Indian families in Graz for having me as one of their family members.

Above all, I thank the almighty for helping me in each and every situation and bringing positive energy to work with positive approach.

Dedicated to

My parents and all my teachers

Declaration

I hereby declare that this doctoral thesis is my own original work and that I have fully acknowledged by name all of those individuals and organizations that have contributed to research for this thesis. Due acknowledgement has been made in the text to all other material used. I followed the guidelines of "Good Scientific Practice" for the completion of this thesis and related research work.

Please note that parts of my thesis have already been published and/or are under scrutiny for future publications.

Xanthohumol ameliorates atherosclerotic plaque formation, hypercholesterolemia, and hepatic steatosis in ApoE-deficient mice

Prakash Doddapattar[†], Branislav Radović[†], Jay V. Patankar, Sascha Obrowsky, Katharina Jandl, Christoph Nusshold, Dagmar Kolb, Nemanja Vujić, Lalit Doshi, Prakash G. Chandak, Madeleine Goeritzer, Helmut Ahammer, Gerald Hoefler, Wolfgang Sattler and Dagmar Kratky
Molecular Nutrition & Food Research 2013 May 3.

doi: 10.1002/mnfr.201200794

[†] Equal contribution

Graz, July 2013 Prakash Doddapattar

Abstract

During my doctoral studies, I worked mainly on three projects. The first project was to study the role of xanthohumol as atheroprotective compound, the second project was to check the role of perilipin1 (PLIN1) on atherosclerotic plaque formation and the third project was to identify lipid droplet-associated proteins in macrophage-derived foam cells.

Accumulation of cholesterol and other lipids in the arteries constitute most prominent manifestation of atherosclerosis. In addition to lipid build up, circulating inflammatory markers fuel the disease condition. To counter-balance variations in physiology, metabolic and immune responses play a very basic role in homeostasis of multicellular organisms.

Xanthohumol (XN) is a prenylated anti-oxidative and anti-inflammatory compound with positive effects on lipid and glucose metabolism. Herein, we demonstrate a role of XN as a potent lipid lowering compound, down-regulating inflammation and thereby reducing atherosclerosis. In addition to improving hypercholesterolemia, oral supplementation of XN leads to phosphorylation/activation of AMPK and its downstream target acetyl-CoA carboxylase leading to reduced hepatic lipid accumulation in Apolipoprotein E-deficient (*ApoE*(-/-)) mice. Likewise, XN feeding down-regulated protein expression of mature SREBP-2 and reduced transcriptional expression of SREBP-1c and its well-known target stearoyl-CoA desaturase 1. Concomitant induction of hepatic mRNA expression of carnitine palmitoyltransferase-1a in *ApoE-/-* mice administered with XN suggests increased fatty acid beta-oxidation. Fecal cholesterol concentrations were also markedly increased in XN-fed *ApoE-/-* mice compared with mice fed western-type diet alone. Our work reveals potential action of XN as atheroprotective compound, improving hypercholesterolemia, inflammation and hepatic steatosis. Therefore XN may constitute a therapeutic compound for the treatment of atherosclerosis.

PLIN1 is the most abundant protein associated with lipid droplet (LD)s of many cell types. LD-rich macrophage-derived foam cells are a defining feature of atherosclerotic plaque development. Increased expression of PLIN1 during differentiation of human

monocytes to macrophages prompted us to study the role of PLIN1 in foam cell formation and atherosclerosis.

We show that *Plin1* inactivation in *ApoE-/-* (*ApoE-/-Plin1-/-*) mice reduced accumulation of LDs in macrophage-derived foam cells and protected mice against atherosclerosis. Mechanistically, decreased atherosclerosis in *ApoE-/-Plin1-/-* mice might be the result of increased cholesterol efflux and low levels of circulating triglyceride concentrations in the plasma and the ability of macrophages to maintain reduced foam cell formation. We further show that whole body deletion of *Plin1* (*Plin1-/-*) in mice results in the increased macrophage cell spreading. In conclusion, *Plin1* deletion in *ApoE-/-* mice protects against atherosclerosis and therefore inhibition of PLIN1 might be atheroprotective.

The structural proteins and hydrolases on lipid droplets (LDs) of macrophage-derived foam cells have a regulatory role in lipid storage and release. PERILIPINs constitute the most abundant structural proteins on LDs. In order to gain insight into the distribution of proteins that govern the flux of lipids into/from LDs, we studied protein composition in macrophage LDs. Since we have found reduced atherosclerosis and decreased number of foam cells in an atherosclerotic mouse model lacking *perilipin1* (*Plin1*), we were interested in differences in LD-associated proteins of wild type (Wt) and *Plin1*-deficient (-/-) foam cells. Foam cell formation was induced by incubating peritoneal macrophages in the presence of acetylated low density lipoprotein (acLDL). LDs were purified by density gradient centrifugation; the LD proteomes were compared by LC-MS/MS after isotopic labelling of peptides. We found a number of LD-associated proteins both that are known to be expressed on LDs and some of unknown functions. Among many differentially expressed proteins, we found reduced expression of ATGL, CGI-58 and Rab18 on the LDs of *Plin1-/-* compared to Wt macrophages.

Zusammenfassung

Im Rahmen meiner Dissertation arbeitete ich an drei Projekten. Das erste Projekt umfasste die Untersuchung der Funktion und Wirkungsweise von Xanthohumol als atheroprotektiver Wirkstoff. Im zweiten Projekt untersuchte ich die Auswirkung der Abwesenheit von Perilipin1 (PLIN1), einem wichtigen Lipidtropfen-assoziierten Protein, hinsichtlich atherosklerotischer Plaquebildung. Im dritten Projekt ging es darum, Lipidtropfen-assoziierte Proteine in lipidgeladenen Makrophagen, sogenannten Schaumzellen, zu identifizieren.

Eine Akkumulierung von Cholesterin und anderen Lipiden in der Arterie stellt ein charakteristisches Merkmal von Atherosklerose dar. Die daraus resultierenden entzündlichen Prozesse in der Arterienwand fördern die Bildung von atherosklerotischen Plaques. Xanthohumol (XN), das aus Hopfen gewonnen wird, ist eine prenylierte, anti-oxidative und anti-inflammatorische Verbindung mit positiven Auswirkungen auf den Lipid- und Glukosestoffwechsel. In dieser Studie zeigen wir, dass XN Cholesterin Konzentrationen im Plasma reduziert und die Bildung atherosklerotischer Plaques in Apolipoprotein E-defizienten (ApoE-/-) Mäusen, welche mit Atherosklerose-auslösender Diät (WTD) gefüttert wurden, vermindert. Neben einer Verbesserung der Hypercholesterinämie hat XN auch positive Auswirkungen auf den hepatischen Lipidstoffwechsel. Der zugrundeliegende Mechanismus könnte auf der Aktivierung von AMP-aktivierter Protein Kinase (AMPK) in der Leber und der dadurch verringerten Lipogenese beruhen, wodurch es in weiterer Folge zu reduzierten Lipidkonzentrationen in der Leber sowie im Plasma kommt. Weiters kommt es infolge von XN Fütterung zu einer Hinunterregulation von SREBP-2 und SREBP-1c, was in einer verminderten Expression von Stearoyl-CoA Desaturase 1 resultiert. XN Verabreichung induziert weiters die Expression von Carnitinpalmitoyltransferase-1a in der Leber, was auf einen erhöhten Abbau von Fettsäure durch ß-Oxidation hinweist. Zusätzlich haben wir in XN-gefütterten Mäusen eine erhöhte Cholesterinausscheidung über den Stuhl beobachtet.

Diese Arbeit zeigt, dass die atheroprotektive Wirkungsweise von XN auf einen positiven Effekt auf Leber - und peripheren Cholesterinmetabolismus sowie auf eine Abschwächung von Entzündungsreaktionen zurückzuführen ist. Basierend auf diesen

Ergebnissen kann XN als potenieller pharmakologischer Wirkstoff zur Vorbeugung und Behandlung metabolischer Erkrankungen eingesetzt werden.

Lipidtropfen-assoziierte Proteine haben wichtige Funktionen bei der Bildung, dem Transport, der Mobilisation und der Stabilisation von Lipidtropfen. PERILIPINE sind wichtige Lipidtropfen-assoziierte Proteine, die vor allem der Stabilisation dieser Organellen dienen. PLIN1, das an der Oberfläche von Fetttröpfchen unterschiedlichster Zelltypen vorzufinden ist, gehört zu den am besten charakterisierten Lipidtropfen-assoziierten Proteinen. Differenzierung von humanen Monozyten zu Makrophagen ist assoziiert mit einer erhöhten Expression von PLIN1. Diesen Beobachtungen zufolge habe wir die Funktion von PLIN1 hinsichtlich Schaumzellbildung und Entstehung von Atherosklerose genauer untersucht. Wir zeigen, dass es in Abwesenheit von PLIN1 in Apolipoprotein E-defizienten Mäusen (ApoE-/-Plin1-/-) zu einem reduzierten Vorkommen von Lipidtropfen in Schaumzellen und in weiterer Folge zu reduzierter Ausbildung von Atherosklerose kommt. Dieser Beobachtung liegt zugrunde, dass ApoE-/-Plin1-/- Mäuse eine erhöhte Fähigkeit zum Makrophagen-vermittelten Cholesterinefflux aufweisen, was sich positiv auf die Schaumzellbildung auswirkt. Weiters konnten wir verminderte Plasma Triglyzerid Konzentrationen beobachten, was einen atheroprotektiven Phänotyp unterstützt. PLIN1-Defizienz führt außerdem zu einer erhöhten Fähigkeit der Makrophagen zur Zellausbreitung. Diese Beobachtungen deuten darauf hin, dass die Abwesenheit von PLIN1 vor Atherosklerose schützt und somit eine Inhibierung von PLIN1 eine neue Strategie zur Vorbeugung von Atherosklerose darstellt.

Ein Ziel dieses Projektes war es, die Proteinzusammensetzung von Lipidtropfen in Makrophagen zu charakterisieren, um somit einen Einblick in die Rolle von Perilipinen als regulierende Faktoren im Lipidmetabolismus von Makrophagen zu bekommen. Aufgrund der beobachteten verminderten Ausbildung von Atherosklerose in PLIN1-defizienten Mäusen waren wir speziell daran interessiert, das Lipidtropfen Proteom zwischen Wildtyp (WT) und Plin1-/- Schaumzellen zu vergleichen. Durch Beladung mit acetyliertem Low-density Lipoprotein (acLDL) wurden Makrophagen zur Schaumzellbildung angeregt, die Lipidtropfen durch Dichtegradientenzentrifugation isoliert und dessen Proteom mittels LC-MS/MS durch Isotopenmarkierung der Peptide analysiert. Diese Untersuchungen zeigten eine Expression von bereits charakterisierten

Lipidtropfen-assoziierten Proteinen sowie auch von Proteinen am Lipidtropfen mit bisher nicht beschriebener Funktion. Diese Beobachtungen konnten durch Western-Blot Experimente bestätigt werden.

Table of Contents

The important thing is not to stop questioning.

Albert Einstein

1. Introduction

Atherosclerosis is one of the leading causes of mortality in the modern world. Synergistic effects of increased cholesterol and inflammatory markers in the blood contribute to the atheroma plaque formation in the arteries, which finally ends in the blockade of arteries. Hardening of arteries is a slow process that matures with aging. Plaque formation is an irreversible process once it has occurred. Moreover, increased plasma cholesterol at young age can also promote plaque formation with faster pace. However, lowering plasma cholesterol and changes in life style can repress or slow down the process of plaque formation. It is estimated that each year about seventeen million people die from cardiovascular diseases worldwide, with atherosclerosis being the main cause of disease. In addition to dysregulation of lipid metabolism, involvement of innate and adaptive immune responses have been identified in atherosclerosis, with components of low density lipoproteins (LDL) targeting inflammation and immune cell activation throughout the course of disease (Hansson and Hermansson, 2011). Dysfunction in the immune response to metabolic regulation or vice versa can lead to chronic metabolic syndrome, mainly type 2 diabetes, obesity and cardiovascular disorders. Therefore it is one of the utmost important challenges in the field of cardiovascular diseases to find out an effective treatment to improve the disease condition.

1.1. Overview of atherosclerosis

Circulating lipids in LDL particles are the key components during the initiation and progression of atherosclerosis. With age, damage to the endothelium recruits immune cells such as macrophages and initiates the deposition of excess lipids in the vascular intima. Prolonged entry and modification of LDL by oxidation recruits immune cells via activated endothelial cells that express adhesion molecules such as intracellular adhesion molecule (ICAM-1), vascular cell adhesion molecule (VCAM-1), E-selectin and P-selectin. These molecules are essential for attracting and trapping of monocyte (Fig 1) (Libby, 2002). As a primary line of defense, macrophages take up oxidized or other modified LDL in order to clear LDL from the intima.

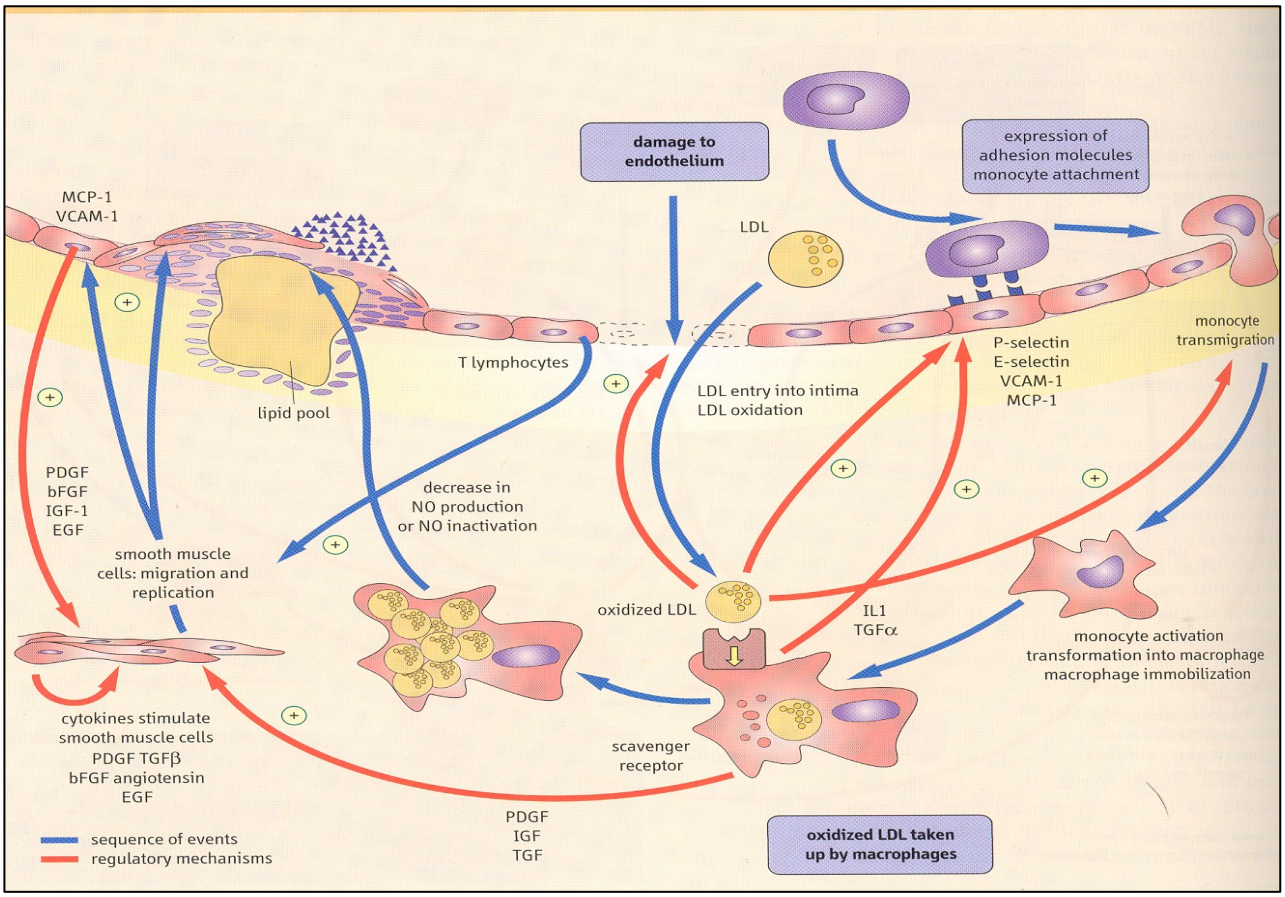

Figure 1. Lipid entry into the damaged intima is the main event in the initiation of atherosclerosis. Monocytes are attracted via chemokines like MCP-1 and adhesion molecules such as and P-and E-selectins. Monocytes undergo differentiation to macrophages and engulf oxidized LDL via scavenger receptors to become foam cells. Foam cells regulate SMC proliferation by secreting PDGF, IGF and TGF along with endothelial cell secreted cytokines. SMCs then form a fibrous cap as a protective mechanism. Figure adopted from (Libby, 2002).

Plaque formation results in the development of different diseases depending on which organs it affects, including heart, brain, pelvis, lungs, and kidneys. The exact basis of atherosclerosis is not known. However, certain habits may worsen the risk of the disease, called risk factors. One can control risk factors like physical activity, an unhealthy diet, and smoking. Other factors are not possible to be controlled, such as a family history of the condition which are otherwise called genetic factors. High circulating levels of LDL are one of the major causes of atherosclerosis. Although high cholesterol concentrations are associated with cardiovascular complications in approximately 50% of all patients, inflammation contributes as a pathologically important factor for atherosclerosis.

1.2. Lipoproteins and atherosclerosis

Adherence of circulating monocytes to the arterial wall and then migrating into sub-endothelial space where they are activated into macrophages is one of the initial steps in the progression of atherosclerosis. Increased modification of lipoproteins into oxidized lipoproteins is the key process in the activation of macrophages into foam cells and other inflammatory white blood cells and platelets.

1.2.1. Lipoproteins

Lipoproteins are lipid-protein complexes that are involved in the transport and metabolism of lipids from diet and endogenous synthesis. High plasma lipoprotein levels are associated with the higher risk of coronary artery disease, a well noted and leading cause of death and morbidity. Lipoproteins are mainly composed of insoluble triglycerides (TG) and cholesterol esters (CE) at their core and are covered by a monolayer of phospholipids (PL) and free cholesterol (FC) (Fig 3). Apolipoproteins are the structural components that are encapsulated in the monolayer and can interact with the core and surface lipids.

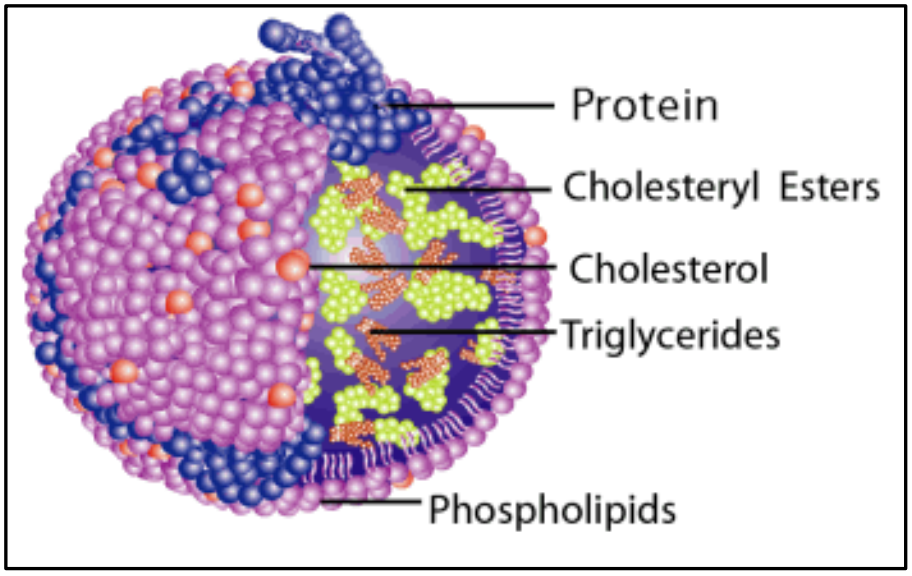

Figure 3. Structure of a lipoprotein particle

Lipoproteins are broadly classified into five major types (Fig 4): chylomicrons having a diameter of 100-1000 nm, VLDL (30-80 nm), IDL (25-50 nm), LDL (18-28 nm) and HDL (5-15 nm).

Relative size of lipoprotein particles

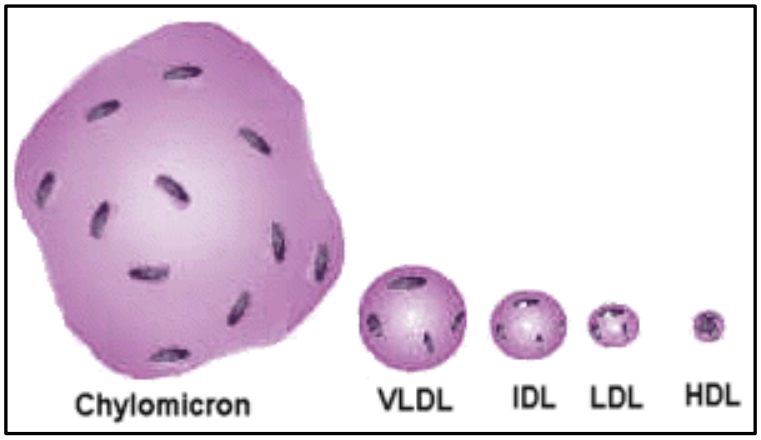

Figure 4. Relative size of lipoproteins
(http://www.scientificpsychic.com/health/lipoproteins-LDL-HDL.html)

Lipoprotein levels are one of the biomarkers during the progression of atherosclerosis. LDL are taken up by macrophages in the arterial wall as soon as they undergo oxidative modification. LDL vary in shape, size and their contents (van Antwerpen et al., 1999) (Ren et al., 2010). LDL comprise of small but dense and large subclasses, the former being more prone to oxidation (Austin, 1994). Each LDL particle is composed of one apolipoprotein B-100 (ApoB-100). ApoB-100 is a ligand for hepatic removal of plasma cholesterol by LDLRs (Rudenko et al., 2002).

HDL are secreted from liver and intestine and are the smallest among all lipoprotein particles. The main function of HDL is to take up cholesterol from peripheral tissues and transfer it to the liver, a mechanism called reverse cholesterol transport (RCT). The initial step in HDL metabolism is the synthesis of lipid-poor ApoA-I, mainly from liver. During RCT, lipid-poor ApoA-I particles take up additional PL and cholesterol from the liver via ATP-binding cassette, sub-family A (ABC1), member 1 (ABCA1) receptor mediated efflux. Lipid poor apoA-I becomes nascent HDL particle by additionally taking up PL and free cholesterol (FC) delivered by lipoprotein lipase (LPL)-mediated hydrolysis of chylomicrons and VLDL particles. CE are formed by the action of lecithin-cholesterol acyltransferase (LCAT) which is bound to lipoproteins resulting in the formation of large, mature spherical HDL particles. Cholesterol efflux from macrophages during RCT contributes to the improvement of atherosclerosis.

Macrophage cholesterol efflux takes place mainly via ABCA1 and ATP-binding cassette sub-family G member 1 (ABCG1) receptors to lipid-poor ApoA-I and mature HDL, respectively. The direct pathway of cholesterol delivery back to liver takes place by selective uptake of CE via liver scavenger receptor class B member 1 (SRB-I) receptors. An indirect pathway involves cholesterol ester transfer protein (CETP) mediated exchange of CE and TG between HDL and ApoB-containing chylomicrons, VLDL, LDL, and their remnants (Lewis and Rader, 2005).

1.3. Adenosine monophosphate-activated protein kinase (AMPK)

The liver is the central organ for maintaining energy balance and glucose metabolism. Liver produces lipoproteins, detoxifies foreign chemical compounds and synthesizes enzymes necessary for digestion. Liver lipid metabolism involves many interdependent and cross-regulated pathways and plays a very pivotal role in lipid homeostasis.

Increased lipid biosynthesis in the liver results in elevated levels of plasma lipoproteins that promote atherosclerosis. Adenosine monophosphate-activated protein kinase (AMPK) is a metabolic regulator activated by low energy levels that act on a switch from ATP-consuming anabolic pathways to ATP-generating catabolic pathways (Viollet et al., 2003). AMPK, a serine/ threonine protein kinase, maintains energy balance at cellular and whole body levels. Recent studies over the last decade recognized multifaceted roles of AMPK in the equilibrium of lipid, glucose and energy metabolism. The physiological importance of AMPK function is validated by the use of AMPK activators. Activation of hepatic AMPK leads to inhibition of lipogenesis, cholesterol synthesis, and glucose production with concomitant increase in fatty acid oxidation (Fig 5). AMPK serves as an inter-tissue signaling switch that responds to various hormones such as leptin and adiponectin, connecting peripheral tissues and hypothalamus and controlling whole body energy homeostasis (Long and Zierath, 2006).

In the liver, AMPK targets rate-limiting enzymes of fatty acid and sterol synthesis such as acetyl-CoA carboxylase 1 (ACC1) (Munday et al., 1988) and 3-hydroxy-3-methylglutaryl-CoA reductase (HMGCR) (Clarke and Hardie, 1990). Phosphorylation of ACC1 at Ser-79 inhibits ACC activity, leading to decreased fatty acid biosynthesis and increased carnitine palmitoyltransferase1 (CPT1), the rate limiting step in fatty acid

oxidation in mitochondria (Merrill et al., 1997). AMPK enhances fatty acid oxidation by inhibitory phosphorylation of ACC2, which produces the CPT1 inhibitor malonyl-CoA (Merrill et al., 1997). AMPK affects the hepatic lipid metabolism by down-regulating mRNA expression of the transcription factor sterol regulatory element binding protein 1 (SREBP1) (Zhou et al., 2001). In brown adipose tissue, phosphorylation of AMPK activates adipose triglyceride lipase (ATGL) for brown adipose phenotype (Ahmadian et al., 2011). Reduced body weight, fat mass, increased oxidation of fatty acids and reduced hepatic lipid accumulation in stearoyl CoA desaturase (SCD) 1-deficient mice is shown to be regulated via increased AMPK activation (Dobrzyn et al., 2004).

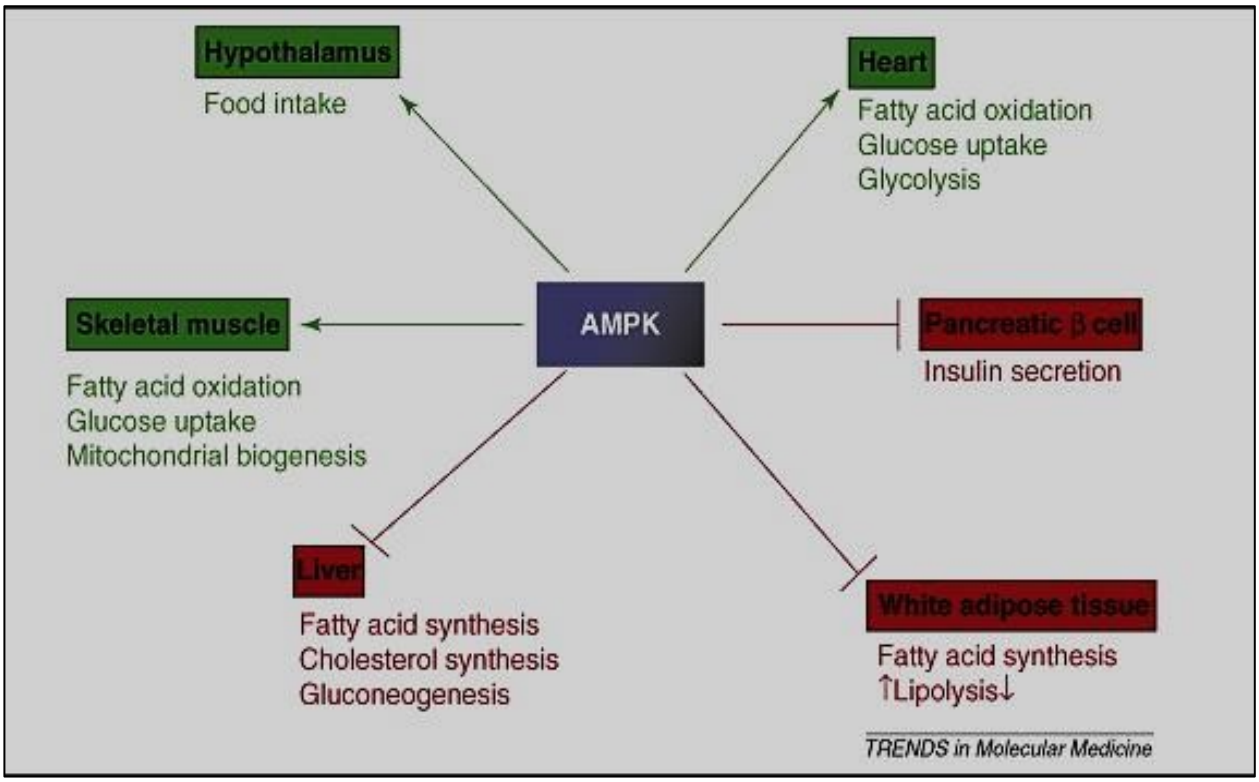

Figure 5. AMPK activation in different tissues leads to number of downstream metabolic effects: Activation of AMPK (green arrows) stimulates energy-generating pathways in several tissues and results in increased FA oxidation, while inhibiting (red lines) energy-consuming pathways. AMPK activation decreases FA and cholesterol synthesis normalizing hepatic lipid and glucose metabolism. Figure adopted from (Lage et al., 2008).

1.5. SREBS and regulation of lipid metabolism

Sterol regulatory element-binding proteins (SREBPs) are membrane-bound transcription factors that regulate genes involved in cholesterol and fatty acid syntheses (Horton et al.,

2002, Brown and Goldstein, 1999). SREBP-1c regulates fatty acid metabolism, whereas SREBP-2 is involved in cholesterol biosynthesis pathway (Fig 6). Within a cell, transport of SREBS between endoplasmic reticulum and Golgi compartments is regulated via the insulin-induced gene 1 protein (INSIG1) with SREBP cleavage-activating protein (SCAP). Under normal conditions, the SREBP-SCAP complex is bound to INSIG1. When cellular cholesterol levels fall, SREBP-SCAP complex moves to Golgi, where it is cleaved and an active form is released into the nucleus, which then acts as transcription factor.

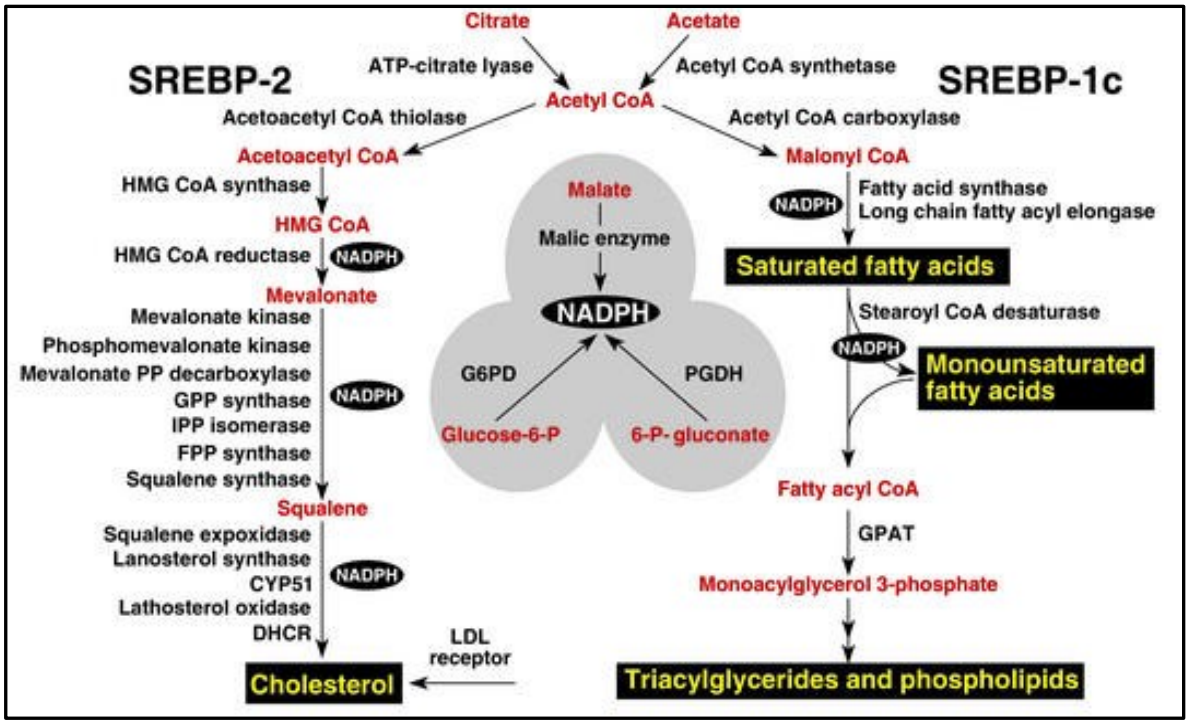

Figure 6. SREBP-mediated cellular lipid metabolism; SREBP-1c regulates genes involved in fatty acid and phospholipid metabolism and SREBP-2 controls cholesterol metabolism (Horton et al., 2002).

1.6. Inflammation and atherosclerosis

While increased levels of lipids in the plasma are the major factors for atheroma development, inflammation is the boosting factor for disease condition if left untreated. The idea of the involvement of inflammation in accelerating atheroma formation dates back to initial studies by Rudolf Virchow, Karl Rokitansky, and others since 1800s (Wong et al., 2012). Signs of inflammation occur conjointly with lipid accumulation in the arteries (Libby, 2002). Numerous studies show a very strong link between the

regulation of metabolism and inflammation with respect to atherosclerosis. Thus, the major driving force for atherosclerosis progression is the release of pro-inflammatory stimuli by macrophage-foam cell apoptosis in plaques and inflammation (Fig 7).

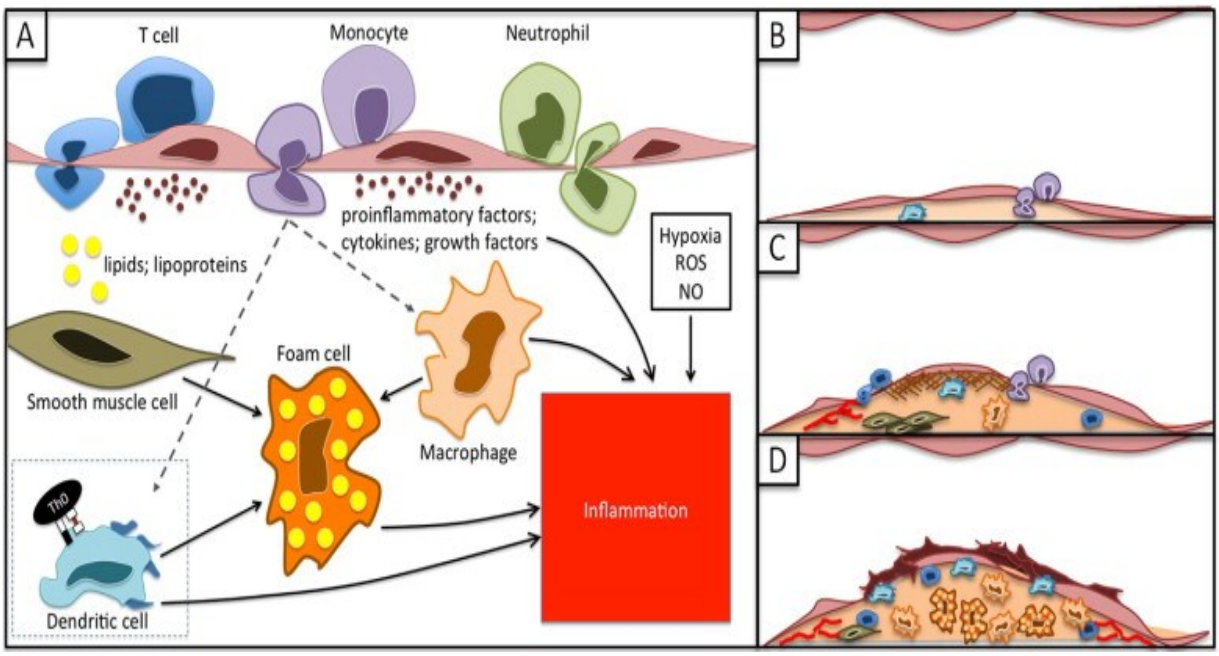

Figure 7. Involvement of inflammation in all stages of atherosclerosis. (**A**) Numerous cells like T-cells, monocytes, and neutrophils engulf oxidized lipids and mediate the inflammatory response to atherosclerosis. Initial accumulation and retention of lipid and lipoproteins contribute to the early and progressive inflammatory response, especially when the lipids are oxidatively modified. Proinflammatory cytokines, chemokines, and growth factors further elaborate this response. In addition to external factors such as hypoxia, reactive oxygen species (ROS) and nitric oxide (NO) (in excess), inflammation within the lesion fuels plaque formation. (**B**) During the initial progression, monocytes and dendritic cells infiltrate into the vessel wall. (**C**) Infiltrating monocytes differentiate into macrophages and T-cells and other leukocytes enter the vessel wall. (**D**) Toward the later stages of plaque development macrophage foam cells alter the microenvironment, changing extracellular matrix composition and decreasing smooth muscle cell content, predisposing to plaque rupture (Wong et al., 2012).

1.7. Atherosclerosis prone mouse models

Wild type (Wt) mice have increased levels of plasma high density lipoproteins (HDL) and low levels of LDL and very low density lipoproteins (VLDL). Wt mice are therefore not a good model to study atherosclerosis. Mice need to be genetically modified in order to recapitulate the phenotype of atherosclerosis. Most widely used mouse models for

atherosclerosis study are apolipoprotein E knockout (*ApoE-/-*) and LDL receptor knockout (*Ldlr-/-*) mice.

1.7.1. *ApoE-/-* mice

ApoE is one of the constituents of plasma lipoproteins which facilitates LDL uptake via LDLR-related receptors thereby clearing atherogenic particles from the circulation (Knowles and Maeda, 2000). In normal mice, ApoE is made predominantly by the liver and then incorporated into all lipoprotein particles except LDLs (Plump and Breslow, 1995). *ApoE-/-* mice exhibit shift from the normal distribution of plasma high density lipoprotein (HDL) particles to VLDL and intermediate density lipoprotein (IDL) particles (Zhang et al., 1992). *ApoE-/-* mice have highly increased cholesterol levels and develop spontaneous atherosclerotic lesion even on chow diet (Zadelaar et al., 2007, Breslow, 1996). Lesion development can be accelerated by feeding Western type diet (WTD) or High fat, high cholesterol diet. Plaque progression in *ApoE-/-* mice from initial events to complex lesions appears like human lesion progression (Nakashima et al., 1994). ApoE is also immunomodulatory in function as it can inhibit T-cell proliferation (Tenger and Zhou, 2003). ApoE is a strong acceptor of cellular cholesterol and therefore involved in foam cell formation. Many anti-atherosclerotic drug development studies are designed in *ApoE-/-* mice (Zadelaar et al., 2007).

1.7.2. *Ldlr−/−* mice

The LDLR is responsible for endocytosis of cholesterol-rich LDL. LDLR recognizes ApoE and protein present on VLDL and chylomicron remnants (Brown and Goldstein, 1979). Compared to *ApoE-/-* mice, *Ldlr-/-* mice develop atherosclerosis rather slowly on regular chow diet feeding as a result of modest increase in plasma cholesterol. They rapidly develop rapid lesions on high fat/high cholesterol diet feeding (Ishibashi et al., 1994). The lipoprotein profile in *Ldlr-/-* mice is more similar to humans in cholesterol being confined mainly to LDL fraction (Zadelaar et al., 2007).

1.8. Xanthohumol

Xanthohumol (Fig 8) (Greek: Xantho=yellow, XN) is a prenylated flavonoid found in hops, inflorescences of the female hop plant (*Humulus lupulus* L.). XN, the most

abundant chalcone present in hops, potentially inhibits oxidation of LDL proving its antioxidant property (Miranda et al., 2000).

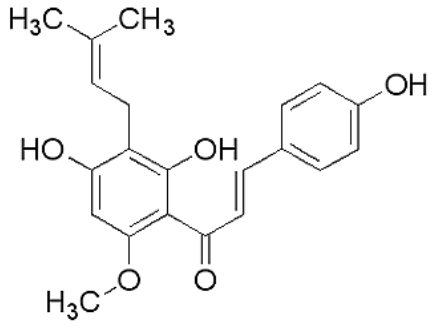

Figure 8. Structure of xanthohumol

Female hop plant rich in polyphenols is used to give a bitter taste and aroma to beer. XN inhibits acyl-CoA:diacylglycerol acyltransferase (DGAT) activity, one of the key enzymes in the final step of triglyceride (TG) synthesis (Tabata et al., 1997). XN has been used as an anti-rheumatic, anti-diuretic and anti-analgesic compound. It shows anti-pyretic properties, induces phase 2 enzymes of xenobiotic detoxification (Miranda et al., 2000) and inhibits NO and prostaglandin E (2) production in carcinogenesis (Zhao et al., 2003). Very recently, XN was found to be an anti-lymphocytic leukaemia drug having AKT/NF-kB inhibitory activity (Benelli et al., 2012). XN regulates lipid and glucose metabolism in HepG2 cells. Casaschi et al. showed inhibition of TG and ApoB secretion associated with increased cellular ApoB degradation and lower activity of TG transfer protein (Casaschi et al., 2004). XN-fed KK-Ay mice exhibited lower plasma glucose levels, plasma and hepatic TG concentrations and adipose tissue weight as well as increased plasma adiponectin levels. XN reduces arterial cholesterol content by inhibiting CETP activity (Hirata et al., 2012b). Among all the beneficial activities of XN, chemo-preventive and anti-inflammatory properties are extensively studied. Since the last two decades studies on XN emerged significantly proving more and more beneficial impacts on health issues. However, its molecular mechanisms are not well characterized.

Though various studies have shown a role of XN as an anti-inflammatory, anti-lymphocytic, neuro-protective, anti-carcinogenic, anti-angiogenic and pro-apoptototic

activities in different cellular and animal models, very little is known about its anti-atherogenic property.

2. Aims and objectives

WTD feeding causes lipid accumulation in many tissues and results in increased circulating plasma cholesterol. Increased concentration of cholesterol promotes inflammation and thereby progression of atherosclerotic plaques in the arteries. XN exerts anti-oxidative, lipid lowering and anti-inflammatory effects.

XN improves insulin sensitivity, lipid levels in obese mice and anti-inflammatory responses by inhibition of MCP-1, interleukin-1 beta, tumor necrosis factor-alpha and induced nitro oxide synthase in lipopolysaccharide stimulated macrophages. Since most of these effects are observed in macrophages that are crucial for the initiation and progression of atherosclerosis we hypothesised that XN treatment reduces plaque formation in *ApoE-/-* mice.

With this background, the aim of the thesis was to investigate whether feeding of XN attenuates atherosclerosis in *ApoE-/-* mice.

Specifically I investigated:

- Influence of XN on atherosclerosis, hypercholesterolemia and inflammation
- Impact on liver steatosis

3. Materials and Methods

Table 1.

Chemical	Company
Bromo phenol blue	Merck
Chloroform	Fluka
DMSO	Merck
Dulbecco´s modified Eagle´s medium (DMEM)	Gibco
EDTA	Roth
Ethanol	Merck
Fetal calf serum (FCS)	PAA
Formaldehyde	Sigma-Aldrich
Glucose	Sigma
Glycerin	Merck
Isopropanol	Merck
KH2PO4	Merck
KCl	Merck
KOH	Merck
β - Mercaptoethanol	Merck
NaCl	Merck
NaOH	Roth
Oil Red O	Merck
Penicillin/streptomycin	Cambrex
Protease inhibitor cocktail (PIC)	Sigma
QuantiFastTM SYBR Green PCR Kit	Qiagen
RNAse Inhibitor	Qiagen
SDS	Serva
Sodium chloride	Roth
Sodium thioglycollate	Sigma
TEMED	Sigma-Aldrich
TRI-reagent	Peqlab

Tris	Roth
Triton X-100	Merck
Trypsin	PAA

Kits

Table 2.

Bradford protein assay	Bio-Rad
ECL chemiluminescence detection system	Thermo Scientific
Nuclear and Cytoplasmic extraction	Thermo Scientific
Triglyceride F	Diasys
Total Cholesterol	Greiner
Sybr Green Kit	Qiagen
TriFast	Peq Lab
TRIzol®	Invitrogen
High-Capacity cDNA Reverse Transcription	Applied Biosystems

3.1. Thioglycollate Medium

Agar: 0.7 g, L-cysteine: 0.25 g, Glucose: 6 g, Peptone 140: 17 g, Peptone 110: 2.5 g, NaCl: 2.5 g, Na_2SO_4: 0.1 g, Sodium thioglycollate: 0.5 g, Water: 1000 ml
All the ingredients were mixed and autoclaved. After cooling down to room temperature, 15 ml and 50 ml aliquots were prepared and stored at -20° C.

3.2. Diethyl pyrocarbonte (DEPC) water

Four hundred µl diethyl pyrocarbonate (DEPC) were mixed with 400 ml ddH_2O in open bottles and thereafter kept under the hood overnight and autoclaved the next day.

3.3. 0.5 M EDTA pH 8.0

EDTA: 186.1 g, NaOH: 20 g and 900 ml ddH_2O. Adjust the pH and make the volume up to 1000 ml with ddH_2O. Autoclave and store at room temperature.

3.4. Western blot buffers and reagents

3.4.1. RIPA buffer

Fifty mM KH_2PO_4, 150 mM NaCl, 1% Triton X-100, 0.5 % deoxycholate and 1:2000 protease inhibitor complex (PIC) (should be added just before use) and stored at 4°C.

3.4.2. 10X running buffer

Glycin 150.1 g, SDS 10 g and 30.3 g Tris were filled up to 1000 ml with ddH_2O.

3.4.3. Separating gel buffer (Buffer 1)

Four ml of 10 % SDS, 18.2 g Tris, and 80 ml ddH_2O were mixed and pH 8.8 was adjusted with with HCl and volume was adjusted up to 100 ml with ddH_2O.

3.4.4. Stacking gel buffer (Buffer 2)

Six g Tris was dissolved in 90 ml ddH_2O. pH 6.8 was adjusted with HCl and the volume was adjusted up to 100 ml with ddH_2O.

3.4.5. SDS sample buffer

SDS 2.15 g, Tris 0.76 g and 45 ml ddH_2O were mixed and pH 6.8 was adjusted with HCl. Thereafter, 10 ml glycerol (80 %) and a small quantity of bromo phenol blue were added.

3.4.6. 10 X Transfer buffer

One mg/ml EDTA, 30 g glycerin and 12.1 g Tris were mixed in 1000 ml ddH_2O.

3.4.7. 10X washing buffer (TBS)

Ninety g NaCl, 5 g Tween 20, 100 ml of 1 M Tris-HCl (pH 7.4) were mixed in 1000 ml ddH_2O.

3.4.8. Separating gel

Table 3.

Reagents	**10 % SDS gel**
Acrylamide	2866.25 µl

Buffer 1	2712.5 µl
ddH2O	5171.25 µl
10% SDS	100 µl
TEMED	4.4 µl
10% APS	7.6 µl
Final volume	87804.4 µl

3.4.9. Stacking gel

Table 4.

Reagents	**10 % SDS gel**
Acrylamide	326 µl
Buffer 1	500 µl
ddH2O	1650 µl
10 % SDS	21.5 µl
TEMED	1.25 µl
10 % APS	19 µl
Final volume	2517.75 µl

3.5. Animals and diets

Female *ApoE-/-* mice (The Jackson Laboratory, Bar Harbor, USA), maintained on a regular 12 h dark/light cycle, were fed chow diet containing 4.3 % fat and 21 % protein (Ssniff, Soest, Germany). At the age of 8-9 weeks, they were divided into 2 groups designed to have similar mean fasted plasma cholesterol concentrations and challenged with WTD (21 % fat, 0.2 % cholesterol; Ssniff) or WTD + XN (300 mg/kg body weight/day) for 8 weeks to induce atherosclerotic plaque formation. XN (Xantho-flav, 80 % purity) was obtained from Hopsteiner®, Mainburg, Germany. The purity of XN, extracted with 90 % ethanol, was determined by the manufacturer using HPLC by UV detection at 370 nm using pure XN as a calibrator. XN was mixed with WTD powder, lyophilized and administered as pellets to mice ad libitum. Blood was collected after 4 and 8 weeks of feeding. Animals were sacrificed at the age of 8 weeks and organs were

collected. One additional cohort was fed WTD ± XN for 4 weeks to determine fractional cholesterol absorption. In addition, plasma isolated from these mice was used for estimation of lipid parameters and added to the values obtained in the first cohort after 4 weeks of feeding. This explains the inconsistence in the number of mice used in different experiments.

LDL receptor *(Ldlr)-/-* mice (The Jackson Laboratory, Bar Harbor, ME) were fed WTD or WTD + XN (300 mg/kg body weight/day) for 4 weeks. Thereafter, blood was collected and plasma was isolated for lipid analysis.

All experimental protocols were approved by the Austrian Federal Ministry of Science and Research, Division of Genetic Engineering and Animal Experiments (Vienna, Austria) (BMWF-66.010/0057-II/3b/2011, BMWF-66.010/0159-II/3b/2012).

3.6. Cell culture

Mouse peritoneal macrophages (MPM) were collected by intraperitonial injection of 3 ml thioglycollate to each mouse. After three days of injection, MPMs were isolated by splashing the peritoneal cavity with 9-10 ml of PBS-EDTA (1 ml of 500 µM EDTA in 500 ml PBS). Cells were plated in DMEM containing 10 % lipoprotein-deficient serum (LPDS) and 1 % penicillin/ 1 % streptomycin (1 % P/S) for 2 h. MPMs were washed with warm PBS. Adherent cells were cultured in DMEM medium containing 10 % LPDS, 1 % P/S with or without 100 µg/ml acLDL for 24 h.

3.7. RNA isolation from cells

Prior to isolating RNA from cells, cells were washed three times with warm PBS. Total RNA was isolated using TriFast according to manufacturer's protocol.

3.8. RNA isolation from tissues

Mice were sacrificed by cervical dislocation. Small pieces of tissues were collected directly into homogenization tubes containing 1 ml TRIzol reagent and immediately frozen into liquid nitrogen and stored at -70°C until use.

For RNA isolation, tissues were thawed and homogenized using Precellys homogenizer (Peqlab, Austria) at 5000 rpm for 20 s. Two hundred micro liter of chloroform/ml of TRIzol reagent was added and vortexed thoroughly and incubated at room temperature (RT) for 10 min. Samples were centrifuged for 15 min at 8500 rpm at 4° C. The RNA-

rich aqueous phase was transferred to a new tube and 0.5 ml isopropanol/ml of Trizol reagent was added. The mixture was incubated for 10 min at RT. Samples were then centrifuged for 10 min at 8500 rpm, and 4° C. The supernatant was removed and the pellet was washed with 1 ml 75 % ethanol. Samples were centrifuged at 8500 rpm for 5 min. Lastly, the supernatant was removed carefully and the pellet was dried under the hood for about 10 min. RNA was dissolved in 50 to 200 µl sterile DEPC water depending on the amount of pellet. The samples were immediately stored at -70° C.

3.9. RNA quantification

Two µl of RNA was used for quantification on a Nano Drop, spectrophotometer, at a wavelength of 260 nm. For checking the quality, the absorption ratio at 260/280 nm (1.8-2) was considered along with determining the integrity of RNA by running on an RNA gel (The FlashGel™ RNA Kit, Lonza).

3.10. cDNA preparation by reverse transcription

Two µg RNA was reverse transcribed into cDNA using the High-capacity cDNA Reverse Transcription kit (Applied Biosystems, Foster City, USA).

3.11. Reaction mixture for reverse transcription

Table 5.

Components	Volume/ reaction (in µl)
10 X RT buffer	2
25 X dNTP Mix (100mM)	0.8
10 X RT random primers	2
Reverse transcriptase	1
RNase inhibitor	0.7
Nuclease-free water	3.5
2 µg RNA/ 10 µl DEPC-H_2O	10
Total volume	20

3.12. Thermal cycler conditions for reverse transcription

Table 6.

	Step 1	Step 2	Step 3	Step 4
Temperature	25° C	37° C	85° C	4° C
Time	10 min	120 min	5 sec	∞

3.13. Real time quantitative polymerase chain reaction (qPCR)

qPCR is a very sensitive technique that allows quantification of gene expression. PCR products were detected by SYBR Green I fluorescence dye that binds to a minor groove of double-stranded DNA.

Three µl of diluted cDNA (1:50 in ddH_2O) were mixed with 1 µl of forward and reverse primers and 5 µl of QuantiFast™ SYBER® Green. The mixture was pipetted into 96 well Light Cycler 480 Multiwell Plates. The plate was centrifuged at 1000 rpm for 1 min and then loaded on a Roche LightCycler 480.

3.14. Program set up for qPCR

Table 7.

	Temperature	**Time**	**Cycles**
Denaturation	95° C	5 min	1
Amplification	95° C 60° C	10 sec 30 sec	35
Melting curve	95° C 60° C 95° C	10 sec 20 sec continuous	1 1
Cool down	40° C	20 sec	1

3.15. Estimation of lipid parameters from plasma

Mice were weighed and blood was collected from overnight fasted mice by retro-orbital bleeding into an Eppendorf tube containing 7 µl EDTA. Plasma was prepared by centrifuging at 7000 rpm for 7 min at 4° C. TC, TG and FC concentrations were

estimated according to manufacturer's instructions. CE levels were calculated by subtracting FC from TC and multiplied by 1.7253.

3.16. Estimation of lipid parameters from macrophages

Peritoneal macrophages were plated in 6 well plates using DMEM. After 2 h of plating, cells were washed with warm PBS and treated with 100 µg/ml acLDL or 100 µg/ml VLDL for 24 h. Cells were washed with warm PBS and 2 ml of hexane:isopropanol (3:2 v/v) was added to each well and incubated for 1 h at 4° C under continuous shaking. The lipid extract was collected in clean tubes and dried under a stream of liquid nitrogen. One hundred µl of freshly made 1 % Triton-X 100 in chloroform was added and dried under liquid nitrogen. Samples were dissolved in 100 µl ddH_2O by incubating for 15 min at 37° C in a water bath. TG, TC and FC concentrations were estimated using commercially available enzymatic kits (Diagnostic systems, Holzheim, Germany). Absorbance values were normalized to protein concentrations.

3.17. Protein isolation and immunoblotting

Cells were lysed and tissues were homogenized in an ice-cold RIPA buffer containing PIC (1:2000). The proteins were separated by centrifuging at 1200 *g* for 10 min at 4° C and the pellet was discarded. The protein amount was estimated by Bradford protein assay (Bio-Rad, Munich, Germany). Forty micrograms of protein lysates were mixed with equal volumes of SDS sample buffer (freshly added 5 % β-mercaptoethanol) and cooked at 95° C for 5 min. Samples were separated on SDS PAGE. Protein blotting was done using PVDF membranes. Membrane blocking was done with 5 % skim milk in TBS for 1 h at room temperature. The blot was incubated overnight with the primary antibody and 1 h with the respective HRP-conjugated secondary antibody. Proteins were probed using ECL plus substrate (Amersham Biosciences, Piscataway, USA) and recorded using ChemiDoc System (ChemiDoc™ MP System #170-8280). Primary and secondary antibodies used in this study are listed in Table 8.

Table 4.

Primary antibody	Dilution	Company	Catalogue number
AMPK (Rabbit)	1:1000	Cell Signaling Technology	5832S

pAMPK (Rabbit)	1:1000	Cell Signaling Technology	4188S
ABCA1 (Rabbit)	1:1000	Novus Biologicals	NB400-105
ABCG1 (Rabbit)	1:1000	Novus Biologicals	NB400-132
ACC (Rabbit)	1:1000	Cell Signaling Technology	3676S
pACC (Rabbit)	1:1000	Cell Signaling Technology	3661S
SREBP-1c (Rabbit)	1:1000	Abcam	Ab44153
pSREBP-1c (Rabbit)	1:1000	Cell Signaling Technology	9874S
HMGCoR	1:1000	Biorbyt	orb6191
PLIN2 (Rabbit)	1:1000	Santa Cruz	sc-377429
PLIN1 (Guinea pig)	1:1000	Progen	GP29
β-actin (Mouse)	1:5000	Sigma	A5316
Cathepsin B (Rabbit)	1:1000	Cell Signaling Technology	3383S
Rab7 (Rabbit)	1:1000	Cell Signaling Technology	2094S
Rab18 (Rabbit)	1:1000	Calbiochem	552126
CGI58 (Mouse)	1:500	Abnova	H00051099-M01
ATGL (Rabbit)	1:500	Cell Signaling Technology	2138
FAK (Rabbit)	1:1000	Cell Signaling Technology	3285
pFAK (Rabbit)	1:1000	Cell Signaling Technology	3281S
Secondary antibody	**Dilution**	**Company**	
Polyclonal-goat-anti-guinea pig IgG-HRP	1:10000	Dianova	106-035-003

Polyclonal Goat-anti-Rabbit IgG-HRP	1:2000	Thermo	NE171565
Polyclonal rabbit-anti-mouse IgG-HRP	1:1000	Dako chemicals	2018-06

3.18. Plasma lipoprotein profiling

Plasma from overnight fasted mice were pooled and lipoproteins were separated by fast protein liquid chromatography (FPLC), Pharmacia FPLC system (Karlsruhe, Germany) using Superose 6 column (Amersham Biosciences, Piscataway, NJ). Two hundred µl of pooled plasma were subjected to FPLC separation and lipoproteins were eluted. Sixty fractions were collected and used for the enzymatic estimation of TG, TC and FC using above mentioned kits. The sensitivity of the reactions was increased by the addition of 3.5-dichloro-2-hydroxy-benzenesulfonate to the reagents.

3.19. Estimation of tissue and fecal cholesterol

Tissues were collected from fed mice. Feces were collected from each mouse for three consecutive days (n=5), dried overnight and weighed. Fecal and tissue lipid extraction was done by Folch's method (Folch et al., 1957). In brief, tissues were weighed and lipids were extracted in chloroform:methanol (2:1) in a volume 20 times the weight of sample. Lipid extracts were then solubilized in freshly prepared 0.2 % Triton X-100 in chloroform, dried under stream of liquid nitrogen and resuspended in ddH_2O. TC and FC concentrations were determined by using commercial kits.

3.20. Estimation of XN in vivo concentration

XN was extracted from pooled liver samples (200 µg protein) and 100 mg dry feces with 300 µl methanol. From plasma (60 µl), XN was extracted with 100 µl methanol. After vortexing for 60s samples were centrifuged at 14,000 rpm for 10 min. Supernatants of liver and feces samples were dried under a stream of nitrogen and re-dissolved in 100 µl methanol. Supernatants of plasma samples were used directly after plasma proteins precipitation. Ten µl of extracts or standards were separated by reverse phase-high

pressure liquid chromatography (Waters HPLC 2690 Seperations Module) at a flow rate of 0.7 ml using a Chromasil C_{18} RP column (150 x 4.6 mm, 5 µm particle size; Altmann Analytik, Munich, Germany). The mobile phase consisted of solvent A (acetonitrile, 0.1% formic acid) and solvent B (20% acetonitrile in water, 0.1% formic acid). Analytes were eluted using a gradient ranging from 40:60 A: B (0-4 min), 50:50 A: B (linear, 4-10 min), 0:100 A: B (linear 10-15 min; hold 15-20 min), and 40:60 A: B (20-23 min, linear; 23-28 min hold). A Waters 2487 absorbance detector set to 370 nm was used for detection. XN (eluting at 15.3 min) concentrations were calculated by peak area comparison with external standards.

3.21. Immunofluorescence

Macrophages were plated on UV sterile glass coverslips. Cells were washed twice with PBS and fixed using 4% paraformaldehyde for 20 min at room temperature. Cells were thoroughly washed, at least 3-4 times till the paraformaldehyde odor is disappeared. Cells were blocked with 3 % skim milk with 0.5 % triton X-100 in water for an hour and primary antibody incubation was carried out for 1 h at RT. Cells were washed gently 2 times and Alexa fluor conjugated secondary antibodies were added and incubated for 1 h at RT. After thorough washing with PBS for 3 times 10 min each, cells were mounted on a glass slide by vectashield containing DAPI (Vector, Burlingame, USA). Images (X63) were taken by confocal laser scanning microscopy using an LSM 510 META microscope system (Carl Zeiss GmbH, Vienna, Austria).

3.22. Aortic root sectioning

To examine plaque formation in the aortic root, mice were fed WTD for 8 weeks. Mice were anesthetized by intra-peritoneal injection of 50 mg/kg Nembutal. Hearts were perfused with PBS for 10 min by inserting the cannula into the left ventricle and the blood vessel of the left kidney was cut. Organs were collected for further experiments. Hearts were incubated in 4 % formalin in PBS for at least a week. Twenty four hour before sectioning, hearts were transferred into tissue tek (Sakura Finetek, Torrance, USA). Seven µm serial sections of aortic root were cut on a cryostat at -20° C.

3.23. Oil red O staining

0.5 g of Oil red O was dissolved in 100 ml of isopropanol with constant stirring overnight and filtered and kept away from direct sunlight.

Working solution: Has to be prepared freshly.

Mix 30 ml of filtered stock solution + 20 ml of distilled water for 10 min.

Aortic root sections were immersed in 4 % formalin-PBS for 10 min. Slides were then dipped into 60 % isopropanol for 5 min and then stained with working solution of oil red O for 15 min. Thereafter, sections were just dipped in 60 % isopropanol for 1 sec to get rid of excess stain and counterstained with hematoxylin for 5 min. Sections were washed in tap water and air dried. Sections were mounted with glycerine jelly. Mean lesion area (μm^2) was calculated from at least 10 consecutive sections per mouse. Quantification of sections was performed by Leica image analysis system.

3.24. Trichrome staining

All sections were incubated in a mordant, Bouin's solution, at room temperature overnight. The next day, sections were washed under running tap water to thoroughly remove yellow color from all sections and once in ddH_2O. Slides were stained in working Weigert's Iron Hematoxylin (equal volume of solution A and B) for 5 minutes at RT. Sections were washed under running tap water and once with ddH_2O for 1 min. Slides were stained in Biebrich Scarlet-Acid Fucshin (150 µl per section) for 5 minutes and washed in ddH_2O for 3X 1 min. Slides were placed in Working phosphotungstic/phosphomolybdic acid solution (1:1:2 ddH_2O) for 5 minutes. Sections were incubated with aniline blue solution (150 µl per section) for 5 minutes. Slides were placed in 1 % acetic acid for 2 minutes. Slides were rinsed just once for a second in ddH_2O and dehydrated for 3s 2X in 95 % ethanol, 3s 2X in 95 % ethanol, 3s 2X in 100 % ethanol, 3 sec 2X in xylene. Section were mounted with Cytoseal 60 and left to dry overnight.

3.25. Separation of fat cake by ultracentrifugation

To separate lipids from water soluble components, 100 µl liver lysates were centrifuged at 100,000 g for 60 min at 4°C. Thereafter images of the ultracentrifuge tubes showing fat cakes on top of liquid fractions were captured.

3.26. ELISA

Serum was collected from overnight fasted WTD and WTD + XN fed *ApoE-/-* mice. Serum MCP-1 and IL-6 levels were measured by ELISA (R&D Systems Inc., Minneapolis, MN) according to the manufacturer's protocol.

3.27. Transmission electron microscopy

(Performed by Dagmar Kolb)

Liver tissue was dissected using a Zeiss OPI1 surgical microscope (Carl Zeiss, Oberkochen, Germany). Small tissue fragments were fixed in 2,5 % (wt/v) glutaraldehyde and 2 % (wt/v) paraformaldehyde in 0.1 M phosphate buffer (pH 7.4) for 2 h, post fixed in 2 % (wt/v) osmium tetroxide for 2 h at room temperature, dehydrated in graded series of ethanol (50 %, 70 %, 80 %, 90 % and two times in 100 %) embedded in a TAAB epoxy resin. Sections (70 nm thick) were contrasted with uranyl acetate and lead citrate. Images were taken using a FEI Tecnai G^2 20 transmission electron microscope (FEI Eindhoven, Eindhoven, Netherlands) with a Gatan ultrascan 1000 CCD camera. Acceleration voltage used was 120 kV.

3.28. Fractional cholesterol absorption

Fractional cholesterol absorption was measured by using the fecal dual-isotope ratio method. *ApoE-/-* mice fed 4 weeks WTD diet with or without XN were fasted for 4 h before they were given a single intragastric dose of 100 µl corn oil containing 0.2 µCi ^{3}H-sitostanol (ARC Inc., St. Louis, MO) and 0.1 µCi ^{14}C-cholesterol (ARC Inc., St. Louis, MO). Feces were collected for 48 h. Fecal lipids were isolated by Folch extraction, and radioactivity was determined by liquid scintillation counting. Fractional cholesterol absorption was calculated by as:

% absorption = ((dose [^{14}C]:[^{3}H]-fecal [^{14}C]:[^{3}H])/dose [^{14}C]:[^{3}H])*100

3.29. Histochemistry

For conventional light microscopy, livers of mice fed WTD or WTD + XN were fixed in 4 % neutral-buffered formalin solution for 24 h and embedded in paraffin. Five µm sections were deparaffinized and subjected to hematoxylin/eosin staining. Sections were rinsed with distilled water and nuclei were stained with hematoxylin (0.7%) for 4 min.

After rinsing with water sections were differentiated with 0.3 % acid alcohol, rinsed with water and stained for 2 min with 1 % eosin. Slides were dried and mounted for microscopy. For histochemical staining with oil red O, 7 µm cryosections were fixed with 10 % formaldehyde. Five min after the fixation, sections were stained with fresh oil red O working solution (see above) for 10 min to detect lipid accumulation. After rinsing with distilled water, the slides were stained with hematoxylin for 5 min, washed with distilled water for 15 min, and mounted. Images of oil red O-stained liver sections were taken with a Nikon Eclipse 80i microscope (Nikon, Vienna, Austria).

3.30. Real time PCR analyses

Total RNA from aorta, liver and small intestine was isolated using TriFast (Peqlab, Erlangen, Germany) according to the manufacturer's protocol. Two µg RNA were reverse transcribed using the High Capacity cDNA Reverse Transcription Kit (Applied Biosystems, Foster City, CA). Real-time PCR was performed on a LightCycler 480 system (Roche, Basel, Switzerland) using the Quantifast SYBR Green PCR kit (Qiagen, Hilden, Germany). Relative expression of genes was normalized to the expression of cyclophilin A as internal reference. Calculations of data were performed using the dd^{-2Ct} method. Following primer sequences were used:

Abcb4_f: AGGCAGCGAGGAAACGGAA
Abcb4_r: TGCTGATGCTGCCTAGTTCAA
Abcg1_f: GGAGTTGCTAAGGACCTTCTTG
Abcg1_r: GACGCTGACTATAAGAGAGACC
Abcg5_f: AGAGGGCCTCACATCAACAGA
Abcg5_r: CTGACGCTGTAGGACACATGC
Abcg8_f: AGTGGTCAGTCCAACACTCTG
Abcg8_r: GAGACCTCCAGGGTATCTTGAA
Cpt-1a_f: CTCCGCCTGAGCCATGAAG
Cpt-1a_r: CACCAGTGATGATGCCATTCT
Scd1_f: CCGGAGACCCCTTAGATCGA
Scd1_r: TAGCCTGTAAAAGATTTCTGCAAACC
Srebp-1c_f: ATCGGCGCGGAAGCTGTCGGGGTAGCGTC
Srebp-1c_r: ACTGTCTTGGTTGTTGATGAGCTGGAGCAT
Srb1_f: GAGCACGTTCTACACGCAG
Srb1_r: GGTCTGACCAAGCTATCAGGTT

3.31. Statistical analyses

Statistical analyses were performed using GraphPad Prism 5.0. Two-tailed, unpaired Student's *t*-test was used to calculate statistical significance. * $P < 0.05$; ** P 0.01; *** P 0.001.

4. RESULTS

4.1. Reduced plasma cholesterol concentrations in XN-fed ApoE-/- mice

Increased plasma lipid levels substantially induce initiation and progression of atherosclerosis (Brown and Goldstein, 1984). To elucidate the effect of XN treatment on atherosclerotic plaque formation, *ApoE-/-* mice were fed WTD ± XN for 8 weeks. Plasma lipid parameters of overnight fasted mice were measured after 4 and 8 weeks of feeding WTD ± XN, respectively. Markedly decreased TC (32 %), FC (27 %) and CE (33 %) concentrations after 4 weeks of feeding WTD + XN (Table 1) were observed. After 8 weeks, plasma TC, FC and CE concentrations were significantly reduced in XN-fed *ApoE-/-* mice by 24 %, 22 % and 24 %, respectively. Plasma TG levels were comparable between both groups. This feeding regimen resulted in 61 nmol/l circulating XN in the plasma of fed animals. In overnight fasted mice XN was not detectable (Table 2).

CE concentrations were calculated as CE=TC-FC (Table 1). Data are expressed as mean values ± SD. **p ≤ 0.01, ***p ≤ 0.001.

Table 1. Reduced plasma cholesterol concentrations in XN-fed *ApoE-/-* mice

	Time (weeks)	N (number)	TC (mmol/l)	FC (mmol/l)	CE (mmol/l)	TG (mmol/l)
WTD	4	10	23.8 ± 1	7.4 ± 0.4	16.2 ± 0.8	0.8 ± 0.1
WTD+XN	4	13	16.3 ± 1***	5.4 ± 0.4**	10.9 ± 0.6 ***	0.8 ± 0.1
WTD	8	8	26.5 ± 0.8	8.3 ± 0.3	18.2 ± 0.6	1.2 ± 0.1
WTD+XN	8	9	0.3 ± 1.1 ***	6.5 ± 0.4 **	13.8 ± 0.7 ***	1.5 ± 0.2

XN plasma concentrations were measured in pooled samples from WTD + XN-fed *ApoE-/-* mice (n=4) after 4 weeks of feeding. n.d., not detected.
(Estimation of XN concentration in the plasma was performed by Branislav Radovic).

Table 2. XN concentration in plasma

	XN plasma concentrations	
	Fasted plasma	Fed plasma
XN (nmol/l)	n.d.	61

Lipoprotein profiling revealed that TC and FC concentrations were markedly decreased in the VLDL fraction with no changes in LDL and HDL fractions (Fig 9A). In addition, I studied effects of XN on food intake and body weight. As shown in Fig 10, food intake (Fig 9B) and body weight (Fig 9C) were comparable between the groups.

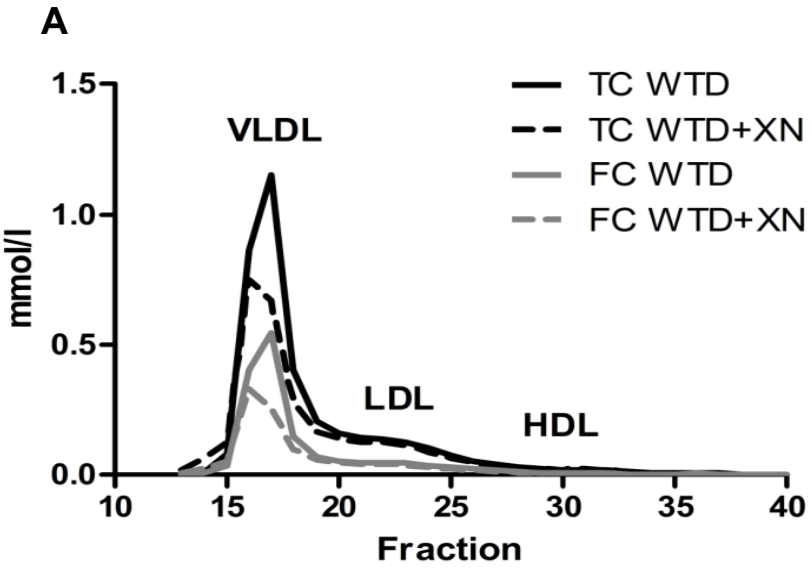

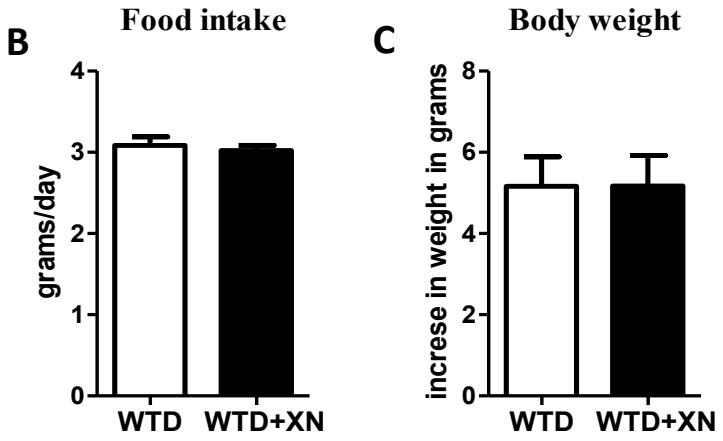

Figure 9. **Decreased cholesterol concentrations in VLDL fraction of XN-fed *ApoE-/-* mice.** Lipoprotein profile of plasma samples from overnight fasted *ApoE-/-* mice (n=5) fed WTD ± XN. TC and FC concentrations in each fraction after FPLC separation were measured enzymatically. Food intake was monitored for three consecutive days during feeding period and body weight is the total increase in weight during feeding. Amount of food intake (B) and gain of body weight (C) remained same in *ApoE-/-* mice fed WTD with or without XN.

4.2. Reduced MCP-1 concentrations in XN-fed *ApoE-/-* mice

To clarify potential anti-inflammatory effects of XN feeding, we determined serum IL-6 and MCP-1 levels in *ApoE-/-* mice fed WTD ± XN. These analyses revealed that MCP-1 concentrations were reduced by 43 %, whereas dietary XN supplementation was without effects on IL-6 levels (Fig 10).

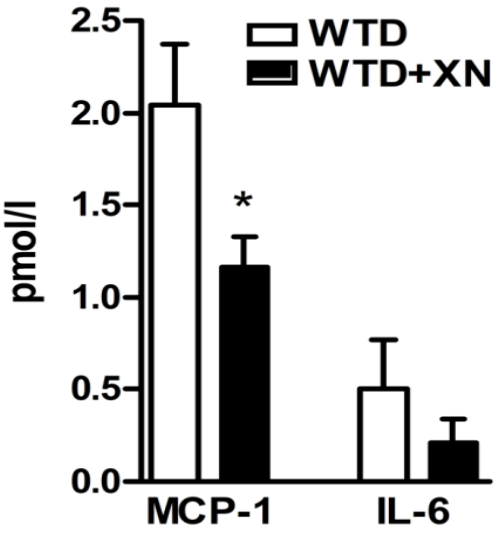

Figure 10. Reduced MCP-1 concentrations in XN-fed *ApoE-/-* mice. Female *ApoE-/-* mice were fed WTD ± XN for 8 weeks. MCP-1 and IL-6 serum concentrations were determined by ELISA. Data represent mean values (n=5) ± SD. *p < 0.05.

4.3. Reduced plaque formation in XN-fed *ApoE-/-* mice

I examined oil red O-stained lesions in aortic valve sections and en face aortas. Mice administered XN exhibited decreased plaque formation (Fig 9) as shown by 43 % reduction in total lesion area of thoracic aorta (Fig 11A) and 33 % reduction in mean lesion area of transverse heart sections in the vicinity of the aortic root (Fig 11B).

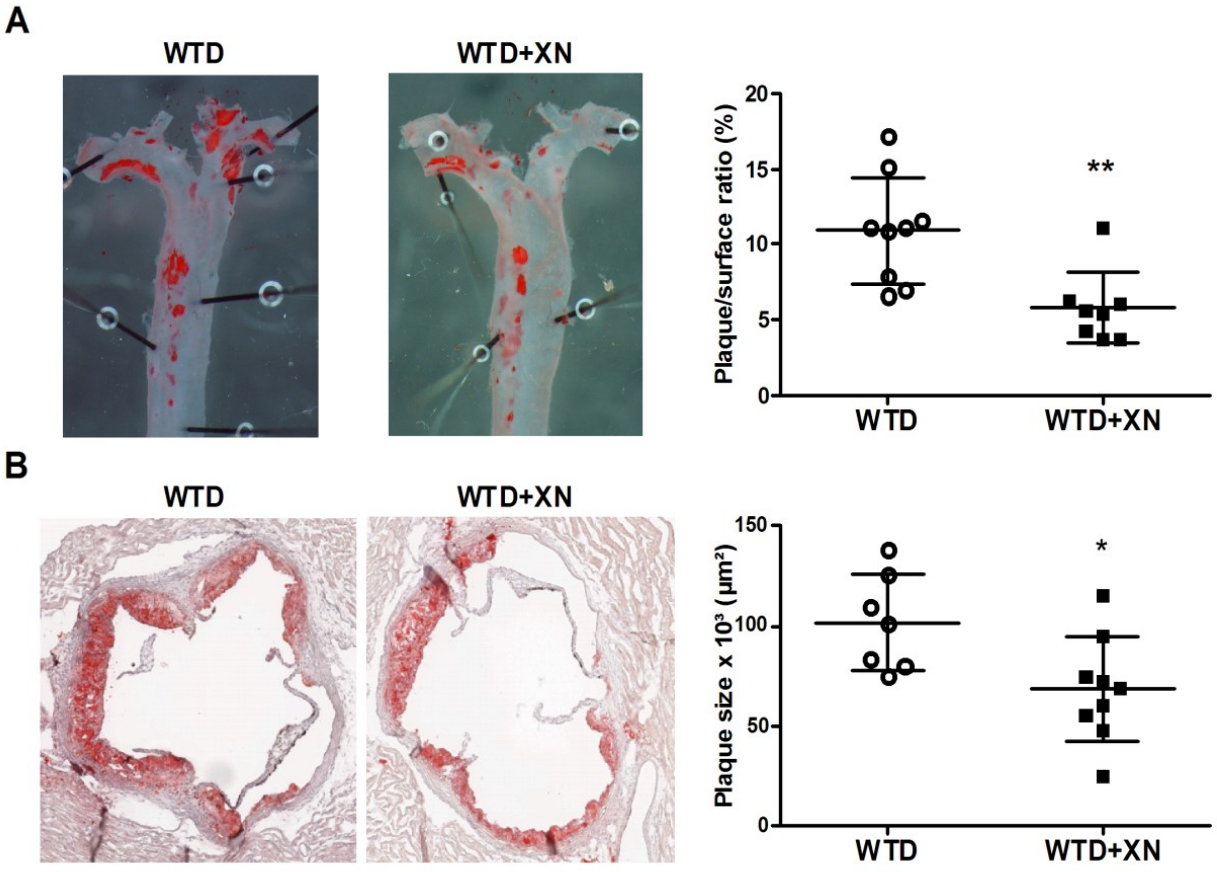

Figure 11. Reduced plaque formation in XN-fed *ApoE-/-* mice. Female *ApoE-/-* mice were fed WTD ± XN for 8 weeks. (A) Representative images of the descending thoracic aorta. The graph represents mean lesion area relative to the total surface area. **p ≤ 0.01. (B) Representative images of aortic valve sections. The graph represents mean plaque area calculated from 5 consecutive sections per mouse. Bars represent the mean values of 7-9 animals ± SD. *p < 0.05.

4.4. Reduced plasma cholesterol concentrations in XN-fed *Ldlr-/-* mice

Next we wanted to elucidate whether XN positively affects plasma cholesterol levels in another mouse model of atherosclerosis. We therefore fed *Ldlr-/-* mice WTD ± XN for 4 weeks. Reduced plasma cholesterol concentrations in XN-treated *Ldlr-/-* mice (Table 3 and Fig 12) indicate that XN regulates plasma cholesterol concentrations during WTD feeding independent on *ApoE* deficiency. Plasma was isolated from overnight fasted mice and TG, TC and FC concentrations were measured enzymatically. CE levels were calculated as CE = TC - FC. Data are expressed as mean values (n=4) ± SD. *p < 0.05.

Table 3. Reduced plasma cholesterol concentrations in XN-fed *Ldlr-/-* mice

	Time (weeks)	N (number)	TC (mmol/l)	FC (mmol/l)	CE (mmol/l)	TG (mmol/l)
WTD	4	4	13.2 ± 1.1	4.3 ± 0.3	8.9 ± 0.8	2.6 ± 0.1
WTD+XN	4	4	9.8 ± 0.6 *	3.3 ± 0.2 *	6.5 ± 0.5 *	2.3 ± 0.1

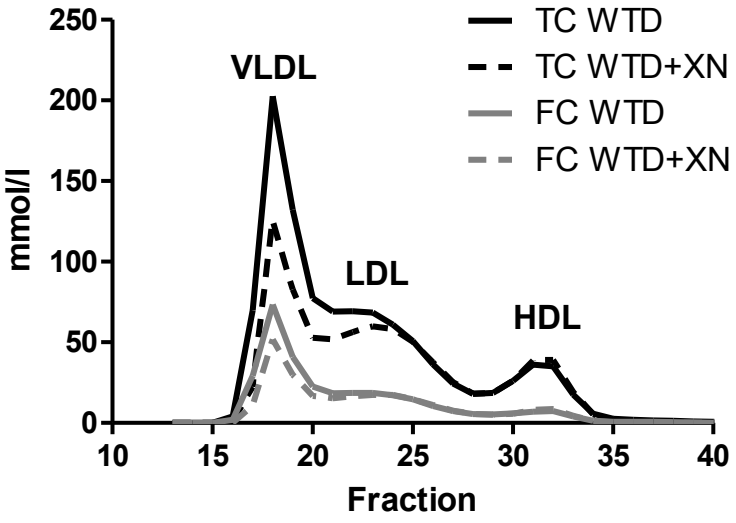

Figure 12. Reduced plasma cholesterol concentrations in XN-fed *Ldlr-/-* mice. Decreased cholesterol concentrations in VLDL fraction. Lipoprotein profile of pooled plasma samples from overnight fasted *Ldlr-/-* mice (n=4) fed WTD or WTD ± XN for 4 weeks.

4.5. Reduced lipid content in livers of XN-fed *ApoE-/-* mice

Liver lipids (especially cholesterol) were markedly reduced in mice administered XN. We found decreased hepatic TC (39%), FC (36%), CE (56%), and TG (27%) concentrations (Table 4). Oil red O staining confirmed reduced neutral lipid content in *ApoE-/-* mice fed XN (Fig 13A). After centrifugation of liver lysates from WTD-fed *ApoE-/-* mice we observed thick fat cakes, which were absent in XN-fed mice (Fig 13B). Additionally, electron microscopy revealed smaller lipid droplets in hepatocytes from XN-fed *ApoE-/-* mice (Fig 13C). No pathological changes were observed in livers of *ApoE-/-* mice fed WTD ± XN according to hematoxylin/eosin staining (Fig 13D). Liver lipids (fed state) from ApoE-/- mice fed 8 weeks WTD or WTD+XN were extracted by Folch extraction and TG, TC and FC concentrations were measured enzymatically. CE levels were calculated as CE = TC - FC. Data represent mean values (n=9) ± SD normalized to wet tissue weight. *$p < 0.05$, **$p \leq 0.01$, ***$p \leq 0.001$.

Table 4. Reduced liver lipid concentrations in XN-fed *ApoE-/-* mice
(Liver lipids were estimated by Katharina Jandl)

	Time (weeks)	N (number)	TC (mg/g)	FC (mg/g)	CE (mg/g)	TG (mg/g)
WTD	8	9	7.1 ± 0.5	4.2 ± 0.4	3.6 ± 0.5	12 ± 1.1
WTD+XN	8	9	4.3 ± 0.1***	2.7 ± 0.2**	1.6 ± 0.2***	8.8 ± 0.7*

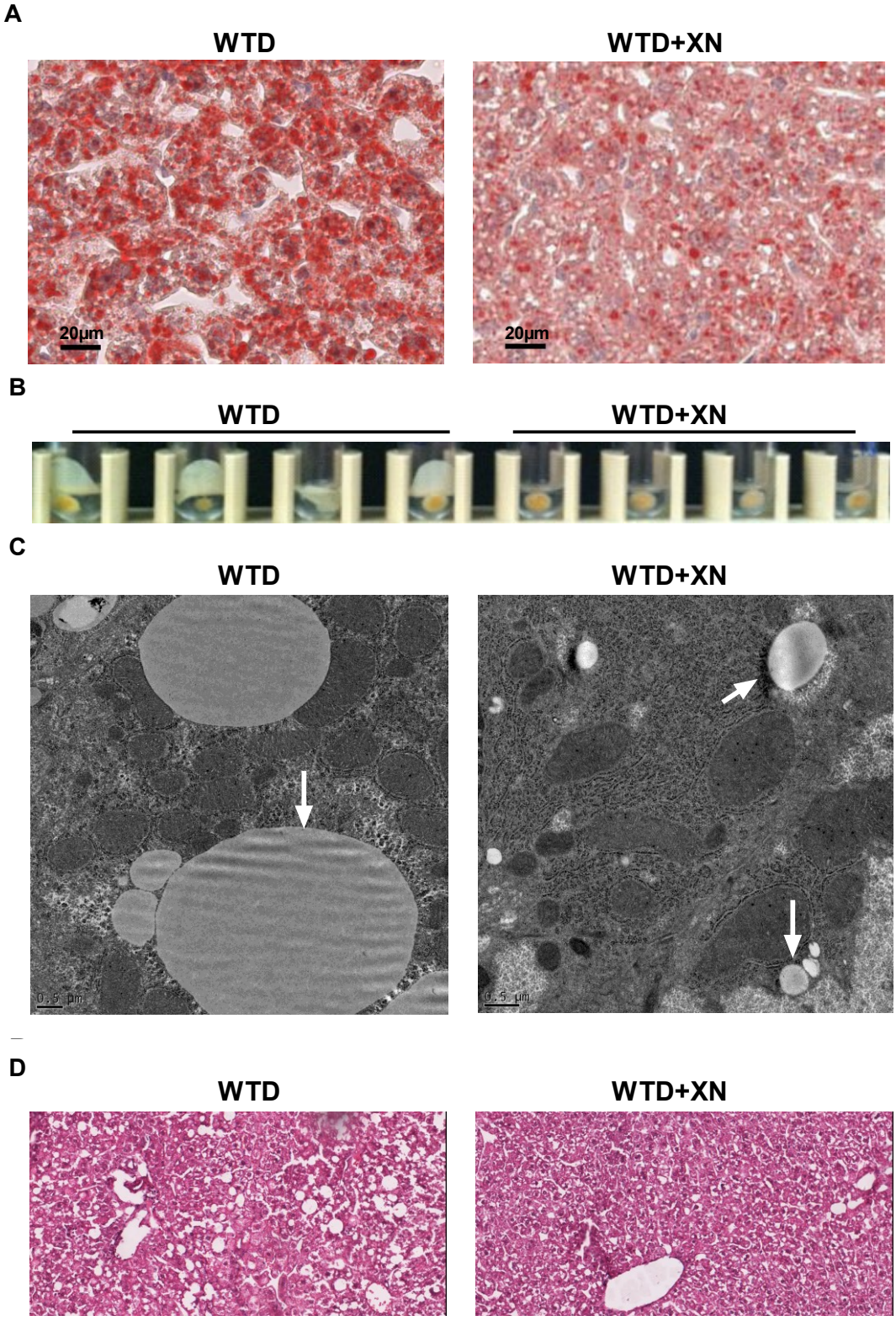

Figure 13. Reduced lipid content in livers of XN-fed *ApoE-/-* mice. Female *ApoE-/-* mice were fed WTD ± XN for 8 weeks. (A) Representative images of oil red O-stained liver sections. (B) Fat layers after separation of lipids from water soluble components by ultracentrifugation at 100,000 g for 60 min at 4°C. (C) Representative electron microscopy images (by Dagmar Kolb)

showing lipid droplets in hepatocytes indicated by white arrows. (D) Representative images of hematoxylin/eosin staining.

4.6. XN reduces hepatic de novo lipogenesis by AMPK activation

To address the question whether the lipid lowering effect of XN is due to increased excretion into the bile or reduced hepatic biosynthesis, proteins involved in fatty acid and cholesterol homeostasis were investigated. Hepatic mRNA expression levels of SREBP-1c and stearoyl CoA desaturase 1 were reduced in XN-treated *ApoE-/-* mice (Fig 14A). Phosphorylation of acetyl-CoA carboxylase (ACC), the key enzyme in de novo fatty acid biosynthesis was significantly induced upon XN treatment (Fig 14B). To investigate the underlying mechanism, I next determined AMPK phosphorylation, which was substantially induced in XN-treated *ApoE-/-* livers but almost absent in control *ApoE-/-* mice. Phosphorylated (p)AMPK is known to phosphorylate and inactivate ACC, thereby inhibiting fatty acid, cholesterol and TG biosynthesis. We therefore hypothesized that lower plasma cholesterol concentrations reflect its decreased supply from the liver as a central organ in de novo cholesterol biosynthesis. We then measured the phosphorylated and inactive form of 3-hydroxy-3-methylglutaryl CoA reductase (HMGCR) and SREBP-2, key proteins in cholesterol biosynthesis. There were comparable changes in protein expression of pHMGCR, whereas mature SREBP-2 was slightly but significantly downregulated (Fig 14B). To investigate transcriptional regulation of carnitine palmitoyltransferase (Cpt)-1a, the protein responsible for fatty acid import into the mitochondria, I performed real time PCR analysis. As shown in Fig 14C, mRNA expression of Cpt-1a was significantly higher in XN-fed animals indicating the possibility of enhanced fatty acid beta-oxidation.

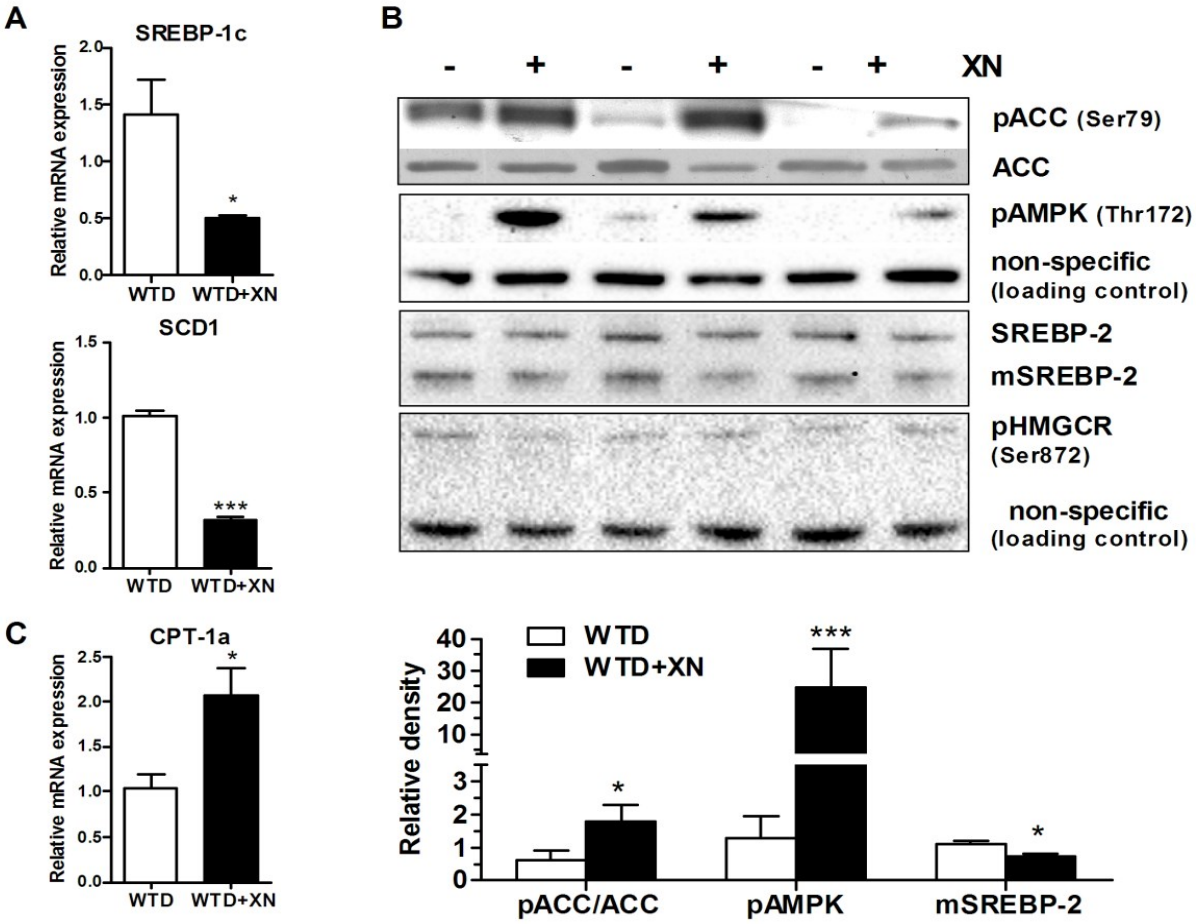

Figure 14. XN treatment inhibits hepatic lipogenesis and induces fatty acid oxidation in *ApoE-/-* mice. Female *ApoE-/-* mice were fed WTD ± XN for 8 weeks. Livers were excised and protein as well as total RNA were isolated. (A) Quantitative real-time PCR analyses of SREBP-1c, SCD1, and (C) CPT-1a normalized to cyclophilin A. Data are expressed as mean values (n=4) ± SD. *$p < 0.05$, ***$p \leq 0.001$. (B) Western blotting analyses of proteins involved in fatty acid and cholesterol biosynthesis. Band intensities were quantitated using Image J software. Data represent the ratios of pACC/ACC, pAMPK/loading control, and mSREBP2/SREBP2 from 3 samples per group ± SD. *$p < 0.05$, ***$p \leq 0.001$.

4.7. Unchanged fractional cholesterol absorption

Fluctuations in circulating lipids mainly reflect activities of liver and intestine during lipid absorption, de novo biosynthesis and/or recycling. We observed no difference in fractional cholesterol absorption in response to XN feeding as determined by the fecal dual-isotope ratio method (Fig 15A). In addition, intestinal cholesterol and TG concentrations were comparable between XN-treated and control *ApoE-/-* mice (Fig 15B). These data suggest that the effect of

XN on plasma lipid levels is not mediated by the small intestine.

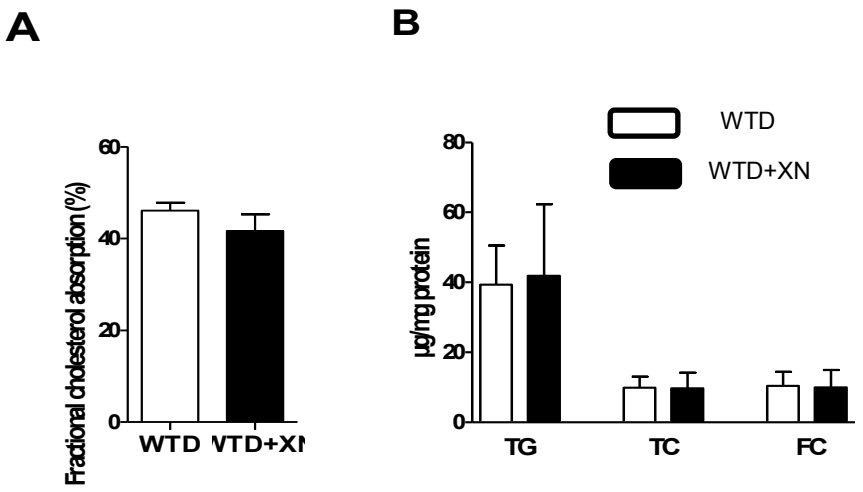

Figure 15. Unchanged fractional cholesterol absorption. (A) Fractional cholesterol absorption in *ApoE-/-* mice (n=5) fed WTD ± XN for 4 weeks. (B) Lipid levels in jejunum of *ApoE-/-* mice (n=9) fed WTD ± XN for 8 weeks

4.8. XN treatment enhances fecal cholesterol excretion in *ApoE-/-* mice fed WTD

Finally, we analyzed expression levels of cholesterol transporters and found a moderate but significant increase in the protein abundance of hepatic ABCG1 in XN-treated *ApoE-/-* mice (Fig 16A). In agreement with our assumption that XN induces cholesterol excretion from the liver, I found elevated concentrations of TC (40%) in feces of XN-fed *ApoE-/-* mice compared with control mice fed WTD for 8 weeks (Fig 16B). The liver tissue was used for the analysis of mRNA expression of genes involved in the cholesterol transport (Fid 16C). However, mRNA levels of ABCG1, ABCG5/G8, ABCB4 and SRB1 were comparable between both groups.

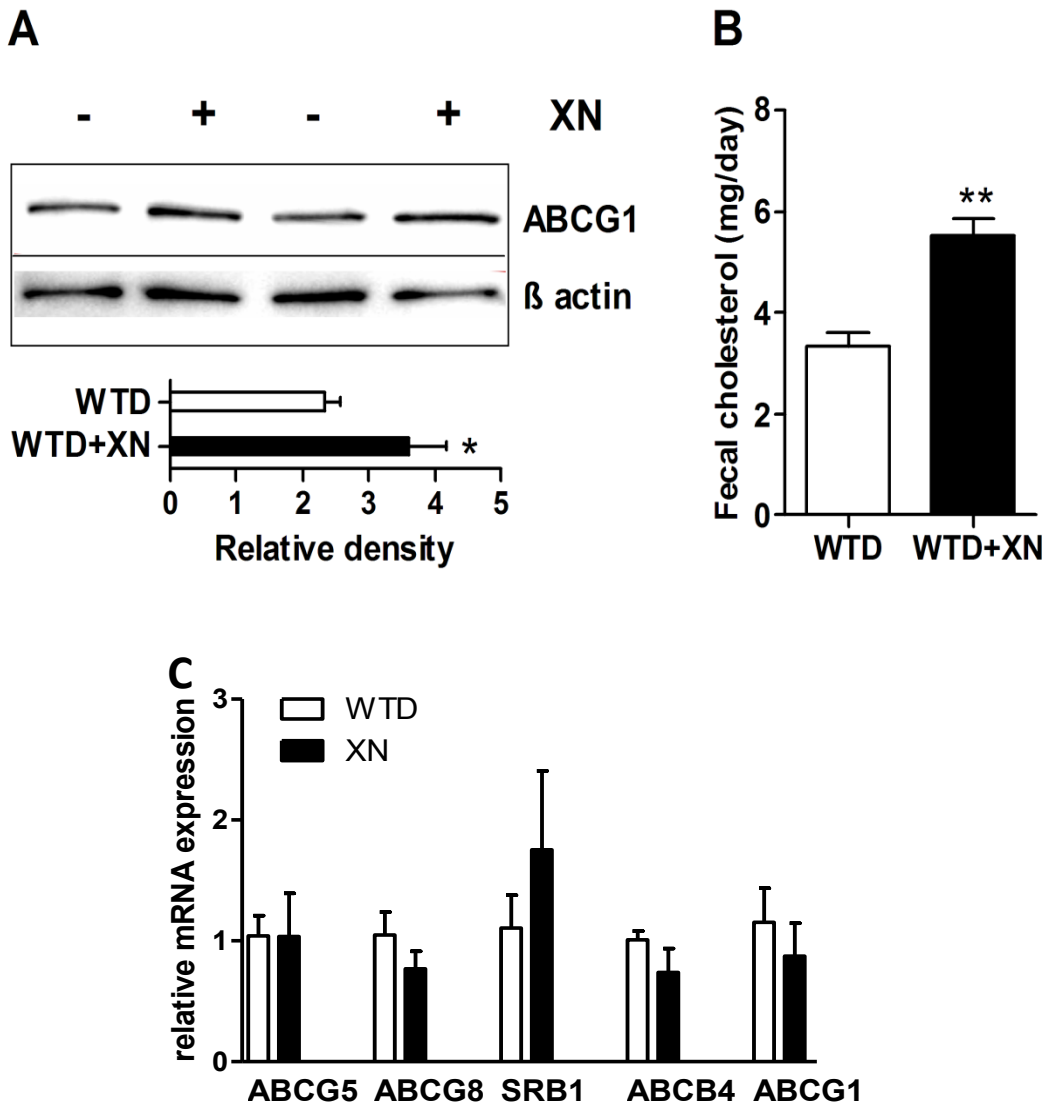

Figure 16. XN treatment enhances fecal cholesterol excretion in *ApoE-/-* mice fed WTD. Female *ApoE-/-* mice were fed WTD ± XN for 8 weeks. (A) Representative Western blot analysis of ABCG1 from liver lysates of 2 untreated (-) and 2 XN-treated (+) mice. The bar graph represents quantifications from samples of n=4 ± SD. *$p < 0.05$. (B) Fecal cholesterol levels calculated as mean concentrations (n=5) ± SD of feces collected for 3 consecutive days. **$p \leq 0.01$. C) Livers were excised and total RNA was isolated. Data are expressed as mean values (n=4) ± SD normalized to cyclophilin A.

5. Discussion

This study demonstrates beneficial effects of the prenylflavonoid, XN, on atherosclerotic plaque formation and hypercholesterolemia in WTD-fed *ApoE-/-* mice. The present data provide evidence that decreased atherosclerosis is a result of combined positive effects on circulating cholesterol and MCP-1 concentrations. Our results also suggest that XN is a potent natural hepatic AMPK activator.

Inflammation and circulating levels of cholesterol are the major cause of atherosclerotic plaque formation. XN is shown to be a potent anti-inflammatory compound. Recently, Ye-Ming Lee showed inhibitory effect of XN on human platelet activation (Lee et al., 2012). Gao et al proved immune suppressive roles on T cell proliferation, IL-2 activated killer cells including cytotoxic T lymphocytes and on the production of Th1 cytokines (Gao et al., 2009). The observed effects are attributed to XN because of its high concentration (80 %) in the probe. There is, however, still the possibility that other prenylflavonoids contribute as well. The strongest candidates are isoxanthohumol (IXN) and 8-prenylnaringenin (8-PN). Nevertheless, taking a compound of a higher purity would still not eliminate the possibility that these XN metabolites are involved. XN, converted to IXN spontaneously or by gut bacteria, can be further metabolized either by gut bacteria or by cytochrome enzymes in the liver into 8-PN (Legette et al., 2012a) (Hanske et al., 2010). Twenty four hours after oral administration of pure XN to rats, concentrations of IXN and 8-PN in the blood reached approximately 50 % and 25 % of XN concentration, respectively (Legette et al., 2012a). According to another similar study IXN concentration was even higher in the blood after 1 h compared with XN, whereas 8-PN was not detected (Hanske et al., 2010). Additional in vivo feeding experiments using IXN are therefore needed to shed more light on this controversial issue.

After feeding *ApoE-/-* mice with XN-supplemented WTD we observed markedly reduced circulating cholesterol and MCP-1 concentrations, which are important determinants of atherosclerotic lesion formation (Hansson and Hermansson, 2011, Boring et al., 1998, Gosling et al., 1999). Recent data showing decreased cholesterol concentrations in atherosclerotic plaques of XN-treated mice expressing human

cholesteryl ester transfer protein (Hirata et al., 2012a) support our findings. XN has been considered an anti-inflammatory substance according to findings in various in vitro and in vivo studies (Dorn et al., 2012, Monteiro et al., 2008, Cho et al., 2008, Cho et al., 2010, Lupinacci et al., 2009, Gao et al., 2009). In order to show the effect of XN on plasma cholesterol levels is independent of *ApoE* deficiency, we fed *Ldlr-/-* mice for 4 weeks. Results obtained from XN feeding were similar irrespective of genetic background. We observed decreased MCP-1 but not significantly reduced IL-6 serum concentrations. In accordance with our results, MCP-1 was the key inflammatory marker found to be increased at the early stage of high fat diet-induced kidney disease, which is characterized by inhibition of AMPK activity (Decleves et al., 2011). In addition, it was reported that AMPK activation in vitro and in vivo reduces MCP-1 in urine and kidney (Decleves et al., 2011), adipocytes (Miyokawa-Gorin et al., 2012), macrophages (Jeong et al., 2009), and endothelial cells (Ewart et al., 2008). Additional studies are needed to understand the possible link between AMPK activation by XN and the reduction of MCP-1 in serum of *ApoE*-/- mice.

The synthetic polyphenol S17834, which was shown to activate AMPK, inhibits SREBP-1 activity, thereby positively affecting dyslipidemia, liver steatosis and atherosclerosis in diet-induced insulin-resistant mice (Li et al., 2011). AMPK plays a major role in the control of hepatic metabolism. AMPK phosphorylates multiple targets in the liver in order to acutely switch on alternative catabolic pathways and switch off anabolic pathways. ACC is an important rate-controlling enzyme for the synthesis of malonyl-CoA, which is a critical precursor of fatty acid and TG biosynthesis (Wakil et al., 1983, Mao et al., 2006) and an inhibitor of fatty acid beta-oxidation (Browning and Horton, 2004). Thus, phosphorylation and inhibition of ACC by AMPK results in reduced malonyl-CoA concentrations followed by decreased fatty acid biosynthesis and increased mitochondrial fatty acid beta-oxidation via regulation of CPT-1 activity (Browning and Horton, 2004). XN treatment induced the protein expression of the inactive, phosphorylated form of ACC in *ApoE*-/- mice. Consequently, TG concentrations were decreased in XN-treated *ApoE*-/- livers.

Despite its ineffective intestinal uptake, XN bioavailability studies (Avula et al., 2004, Hanske et al., 2010, Legette et al., 2012a) report micro molar concentrations of XN in livers and plasma after oral application. The dose of XN used in this study was not

expected to have any adverse effects since it was only one third of the published safety margin in mice (Vanhoecke et al., 2005, Hussong et al., 2005, Dorn et al., 2010). In accordance, no signs of liver toxicity were observed as shown by haematoxylin/eosin staining. XN absorption in the intestine was very low according to the content in feces and compared with plasma and liver concentrations. For potential applications in clinical studies we are currently improving the feeding method as suggested by Legette et al. (Legette et al., 2012a) to reduce XN doses. Here we show that XN exerts its activities in the liver by significantly decreasing hepatic lipid levels at concentrations of only 24 µg/g protein. In agreement with reduced de novo lipogenesis, increased Cpt-1a mRNA expression in livers of *ApoE-/-* mice administered XN imply a higher rate of mitochondrial fatty acid beta-oxidation. Although hepatic cholesterol concentrations were reduced (in agreement with reduced protein expression of mature SREBP-2) pHMGCR was unaffected by XN treatment. This phenomenon is difficult to explain since AMPK was also shown to phosphorylate HMGCR thereby resulting in decreased cholesterol biosynthesis (Sato et al., 1993, Clarke and Hardie, 1990, Winder and Hardie, 1999, Li et al., 2011). AMPK is important but not the solely metabolic regulator of HMGCR. A natural negative regulator of HMGCR activity is cholesterol itself (Sato et al., 1993). Decreased hepatic cholesterol concentration as observed in this study might mask the inhibitory effect of XN on HMGCR via AMPK. Future studies focused on early effects of XN in the liver are needed to proof this assumption.

Activated AMPK also inhibits glycogen synthesis, consecutively increasing glycolysis and glucose transport. AMPK regulates insulin synthesis and secretion as well as modulation of hypothalamic functions involved in the regulation of satiety (Namkoong et al., 2005). This might explain findings by others (Nozawa, 2005, Legette et al., 2012b) showing beneficial effects of XN on obesity, probably by inducing catabolic AMPK-regulated pathways. The mechanism might be the activation of AMPK by inhibition of the Akt pathway. In fact, several publications have so far reported that XN inhibits the Akt pathway (Albini et al., 2006, Dell'Eva et al., 2007, Yang et al., 2008, Deeb et al., 2010, Dorn et al., 2010). Blocking of Akt increases the AMP/ATP ratio and subsequently activates AMPK (Hahn-Windgassen et al., 2005) since the main cause of AMPK phosphorylation is due to a rise in AMP levels when the energy status of the cell is low.

Plasma cholesterol levels reflect the degree of systemic absorption, usage, de novo production, and recycling. Liver and intestine play crucial roles in the regulation of cholesterol homeostasis. Our data indicate that the small intestine is not involved in cholesterol-lowering effects of XN, since we did not find differences in fractional cholesterol absorption. These data suggest that increased cholesterol concentrations in feces of *ApoE-/-* mice fed XN result from increased secretion from the liver into the bile. Nosawa et al. (Nozawa, 2005) reported a 7-fold increased mRNA expression of Cyp7a1, the key enzyme in neutral bile acid biosynthesis, in the liver of KK-A^y mice administered XN. Cyp7a1 mRNA expression, however, was unaffected by XN treatment. Nevertheless, we observed increased cholesterol concentrations in the feces, which might be the result of elevated ABCG1 protein expression. However, there were comparable changes in mRNA expression levels of ABCG5, ABCG8, ABCB4, ABCB1 and SRB1. ABCG1 was identified as an important regulator of liver lipid homeostasis. Although the expression levels of ABCG1 in hepatocytes are much lower compared to Kupffer cells, high cholesterol diet feeding might lead to specific stimulation of ABCG1 in parenchymal cells (Hoekstra et al., 2003). Disruption of ABCG1 in mice induced massive accumulation of both neutral lipids and phospholipids in hepatocytes, whereas overexpression of human ABCG1 protected liver from dietary fat-induced lipid accumulation (Kennedy et al., 2005). Though it might be expected that liver ABCG1 plays a role in efflux of cellular cholesterol to HDL rather than sterol excretion into bile, it was reported by Li et al. (Ji et al., 2012) that ABCG1-deficient primary hepatocytes have a similar capacity to efflux cholesterol to ApoA-I and to form nascent HDL particles compared with control cells. This question is, however, less relevant for our study because we used *ApoE-/-* mice, which are depleted of HDL. Further investigations are needed to clarify whether hepatocytes or Kupffer cells are responsible for increased cholesterol excretion observed in XN-treated *ApoE-/-* mice and to look more closely at the role of ABCG1. Moreover, recent study of XN on human anti-platelet activity (Lee et al., 2012) supported our observation of anti-atherogenic property of the compound. Finally, XN feeding did not affect food intake and body weight both in *ApoE-/-* as well as *Ldlr-/-* mice.

We conclude that XN ameliorates atherosclerotic plaque formation by improving liver and circulating cholesterol and MCP-1 concentrations. Importantly, we discovered a potent natural agent able to activate AMPK (Fig 17) which is, although unspecifically

regulated, an emerging target for the treatment of type 2 diabetes, obesity, dyslipidemia, and atherosclerosis.

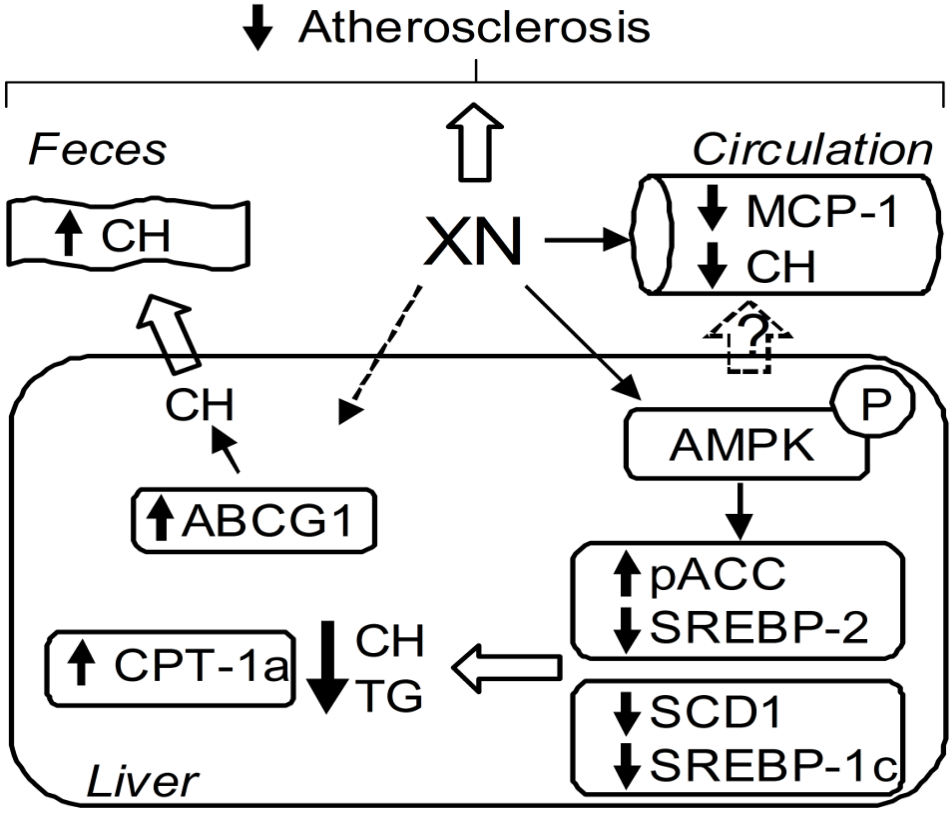

Figure 17. Schematic summary of the effects of XN feeding to *ApoE-/-* mice. XN phosphorylates hepatic AMPK, thereby leading to phosphorylation and inactivation of ACC, reduction of mature SREBP-2 protein and decreased mRNA expression of SREBP-1c and SCD1. In addition, increased expression of CPT-1a suggests increased fatty acid beta-oxidation. As a consequence, de novo lipogenesis in the liver is reduced and fecal cholesterol content is increased. In combination with reduced cholesterol and MCP-1 concentrations in the circulation XN attenuates atherosclerotic plaque formation in WTD-fed *ApoE-/-* mice.
ABC, ATP-binding cassette transporter; ACC, acetyl-CoA carboxylase; AMPK, AMP-activated protein kinase; CH, cholesterol; CPT, carnitine palmitoyltransferase; MCP-1, monocyte chemoattractant protein 1; SREBP, sterol regulatory element-binding protein; TG, triglycerides; XN, xanthohumol.

6. Reduced atherosclerotic plaque formation in ApoE-/- mice lacking perilipin

Abstract

Perilipin1 (PLIN1) is the most abundant protein associated with lipid droplet (LD)s of many cell types. LD-rich macrophage-derived foam cells are a defining feature of atherosclerotic plaque development. Many LD-associated proteins present surrounding intracellular LDs regulate the lipid homeostasis. Increased expression of PLIN1 during differentiation of human monocytes to macrophages prompted us to study the role of PLIN1 in foam cell formation and atherosclerosis. We show that *Plin1* inactivation in apolipoprotein E-deficient (*ApoE-/-*) reduced accumulation of LDs in macrophage-derived foam cells and protected mice against atherosclerosis. Mechanistically, decreased atherosclerosis in *ApoE-/-Plin1-/-* might be the result of increased cholesterol efflux and low levels of circulating triglyceride concentrations in the plasma and the ability of macrophages to maintain reduced foam cell formation. We further show that whole body deletion of *Plin1* results in the increased cell spreading. In conclusion, *Plin1* deletion in *ApoE-/-* mice protects against atherosclerosis and therefore inhibition of PLIN1 might be a good target to treat atherosclerosis.

6.1. Introduction

Lipid droplets (LDs) being recognized as intracellular organelles, store excess free fatty acids (FFA) and sterols in the form of triacylglycerol (TG) and sterol esters to protect cells from lipotoxicity. Lipids are hydrophobic in nature and in order to maintain them in aqueous environment of cytoplasm, cells have evolved a mechanism whereby lipids are maintained in a specialized compartment called LDs, lipid bodies, fat droplets, oil bodies (Martin and Parton, 2006), and adiposomes based on the origin and tissue distribution. LDs consist of TG and cholesterol ester (CE) core surrounded by a monolayer of amphipathic lipids such as phospholipids (PL), cholesterol and LD-associated proteins. Intracellular lipid accumulation in LDs is a balanced process whereby lipid uptake, metabolism and release are tightly regulated. Cells take up CE and hydrolyze it to FC in lysosomes, which can then be used for membrane synthesis. Excess FC can be toxic to cells (Tabas, 2002) and therefore it is effluxed to extracellular acceptors or esterified and stored in LDs. Hydrolysis of neutral lipids in TG-rich LDs (adipocytes, hepatocytes) or CE-rich LDs (steroidogenic cells) also depends upon other specific proteins surrounding LDs, called PERILIPIN family members (Kimmel et al., 2010). LDs are present very close to organelles that are involved in membrane and energy biochemistry such as endoplasmic reticulum, mitochondria and peroxisomes (Fig1).

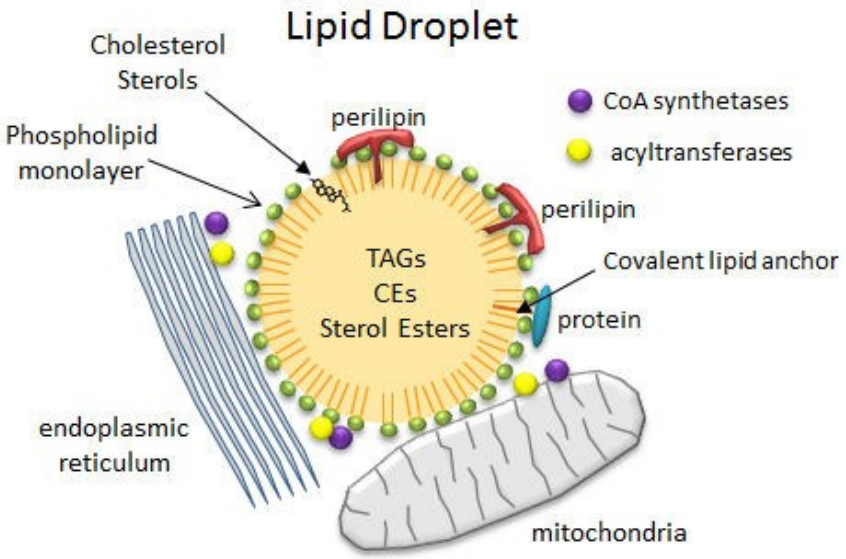

Figure 1. Structure of a lipid droplet and it its association with other cellular organelles. (Fig:http://employees.csbsju.edu/hjakubowski/classes/ch331/lipidstruct/ollipidwater.html)

Formation of cholesterol-rich foam cells from macrophages in the arteries is the hallmark of atherosclerosis. Excessive circulating lipids are stored in intracellular LDs. LD synthesis is a critical step in foam cells formation with regard to atherosclerosis, obesity, diabetes, and hepatic steatosis. Energy imbalance deregulates normal physiology and results in obesity (Rosenbaum et al., 1997). In 2008, around 1.46 billion people worldwide were overweight, of which 502 million were obese and 347 million were affected by diabetes (Finucane et al., 2011, Danaei et al., 2011). High hereditary impact (up to 77%) reflects the influence of genetics on obesity though a small percentage of individuals appear strongly resistant despite the presence of an obesogenic environment (Wardle et al., 2008). It is essential to investigate genes and their regulation involved in lipid metabolism and body fat deposition in order to understand cardiovascular diseases, obesity and associated disorders.

The primary isoform of LD-associated PLIN1 in adipose cell is PLIN1 A, which is the longest isoform exhibiting a unique carboxyl terminus of more than 100 amino acids that are not present in PLIN1 B and C (Greenberg et al., 1993). Excessive TG storage in organs like liver and skeletal muscle is associated with metabolic diseases such as type 2 diabetes and insulin resistance with higher risk of cardiovascular diseases (Bostrom et al., 1988, Andersson et al., 2006). PLIN1 regulates lipolysis under both basal and hormone-stimulated states. PLIN1 promotes TG storage by protecting LDs from the action of lipases. PLIN1 gets phosphorylated when catecholamines bind to the cell surface and activate PKA resulting in enhanced lipolysis.

A decade of studies involving genetic variations in *Plin1* has been related to body weight and obesity-related disorders. Catecholamines increase lipolysis by enhancing adenylate cyclase activity once they bind to cell surface receptors, thereupon activating cAMP-dependent protein kinase A (PKA), which phosphorylates PLIN1 and hormone-sensitive lipase (HSL) (Greenberg et al., 1991, Egan et al., 1992). Extensive studies further led to the discovery of additional functionalities of PLIN1. PLIN1 is a highly abundant protein and its role in lipolysis regulation has been extensively studied. Phosphorylation of PLIN1 is also important for adipose triglyceride lipase (ATGL)-mediated TG hydrolysis. Under basal conditions, comparative gene identification-58 (CGI-58), the co-activator of ATGL, is associated with PLIN1 A. Upon adrenergic

activation, CGI-58 loses contact with Plin1 and binds ATGL to enhance lipolysis (Granneman et al., 2007, Lass et al., 2006, Miyoshi et al., 2007).

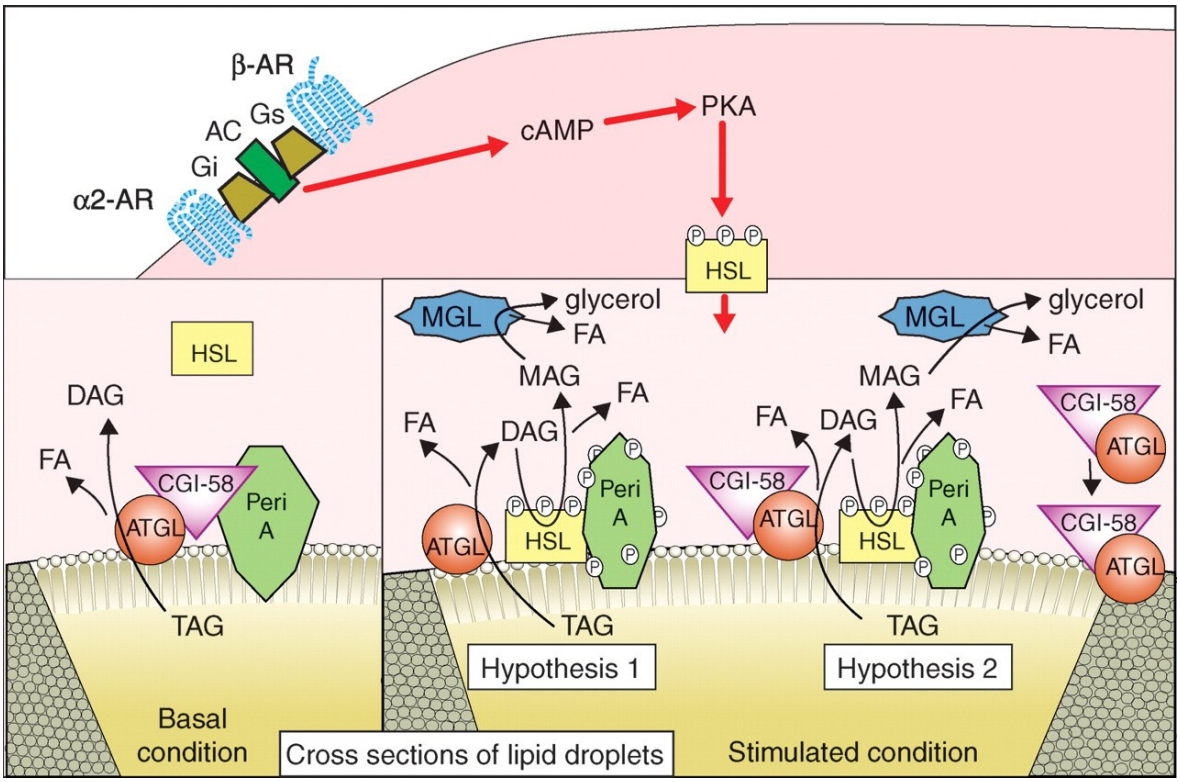

Figure 3. Hypothetical model of basal and stimulated lipolysis in adipocytes. Under basal conditions (lower left panel), ATGL associates with LDs in a PLIN1-independent manner. CGI-58 binds to PLIN1 and facilitates basal lipolysis of triacylglycerol (TG) by ATGL to produce diacylglycerol (DAG) and fatty acids (FA). Hormone-sensitive lipase (HSL) is cytosolic and has limited access to TG stored within LDs or DAG produced during basal lipolysis. When catecholamines bind to β-adrenergic receptors (β-AR), G protein (Gs)-mediated signaling activates adenylyl cyclase (AC) (upper panel). Increased cAMP levels activate cAMP-dependent protein kinase (PKA), which then phosphorylates HSL and PLIN1. Phosphorylated PLIN1 changes its conformation to facilitate increased lipolysis (lower right panel). Phosphorylated HSL docks on phosphorylated PLIN1 and gains access to TG and DAG in lipid droplets. CGI-58 disperses from LDs into the cytoplasm. Two hypotheses are depicted for the roles of CGI-58 and ATGL in stimulated lipolysis. Hypothesis 1: CGI-58 disperses into the cytoplasm, where it has no further role in stimulated lipolysis. ATGL hydrolyzes TG to DAG and FA. Further hydrolysis of DAG to monoacylglycerol (MAG) is catalyzed by HSL bound to PLIN1. Hypothesis 2: CGI-58 enters the cytoplasm, where it forms a complex with ATGL that binds to LDs in a Plin1-independent manner. The ATGL/CGI-58 complex hydrolyzes TG to DAG and FA. HSL hydrolyzes DAG to MAG and FA. For both hypotheses, MAG is hydrolyzed to glycerol and FA by monoglyceride lipase (MGL). FAs and glycerol exit the adipocyte and enter the circulation. Adapted from (Brasaemle, 2007).

6.2. PERILIPIN family members in macrophage lipid metabolism

Though a lot of studies focused on adipocyte biology, the role of Plin1 in TG storage of macrophages has gained a little attention in recent years. Lipid-filled macrophages in the arteries are the result of abnormal lipid deposition and lead to the formation of fatty lesions. Macrophage-derived foam cells also contain a large number of LD-associated proteins including PLIN1, PLIN 2, and PLIN 3 (Persson et al., 2007). Larigauderie et al showed Plin1 expression in human macrophages and that its expression was increased during differentiation from monocytes to macrophages (Larigauderie et al., 2006). Overexpression of *Plin*2 in THP-1 macrophages increased lipid accumulation (Larigauderie et al., 2004). Gu et al showed that increased foam cell formation was associated with Plin3 expression via Toll-like receptor 9-mediated pathway (Gu et al., 2010).

6.3. Mouse models lacking PERILIPIN proteins and atherosclerosis

In vitro and in vivo studies using *Plin1-/-* mice uncovered the dual role of PLIN1 in the regulation of lipid breakdown in adipocytes. PLIN1 forms a barrier around LDs in adipocytes to restrict the action of lipases under fed conditions, when circulating insulin helps in lipid storage (Brasaemle et al., 2000, Martinez-Botas et al., 2000, Tansey et al., 2001). During fasting and exercise, phosphorylated PLIN1 promotes hormonal lipolysis via multiple mechanisms (Brasaemle et al., 2009). *Plin1-/-* mice exhibit resistance to diet-induced obesity, increased basal lipolysis and reduced isoproterenol-stimulated lipolysis despite similar food intake as control mice (Tansey et al., 2001). *Plin2-/-* mice are protected against diet-induced obesity, adipose inflammation and fatty liver disease (McManaman et al., 2013). Miyoshi *et al,* published an interesting observation that overexpression of *Plin1* in mice was protective against diet-induced obesity, glucose tolerance and adipocyte hypertrophy after challenging with high fat diet (Miyoshi et al., 2010). Persson *et al.* identified PLIN 1 and PLIN 2 expression in LDs from human macrophage-derived foam cells using mass spectrometry (Persson et al., 2007). PLIN1 and 2 constitute important PERILIPIN family members. During intra-cellular LD formation PLIN2 expression is increased in macrophages after oxidized LDL treatment (Buechler et al., 2001, Wang et al., 1999). Son et al showed macrophage *Plin2* ablation

protected macrophages against cholesterol-induced toxicity (Son et al., 2012). The role of PLIN2 in macrophage foam cell formation and atherosclerosis was studied using *Plin2* deficiency in *ApoE-/-* background mice (Paul et al., 2008b). Langlois et al showed increased atherosclerosis in *Ldlr-/-Plin1-/-* mice (Langlois et al., 2011) though they found comparable lipid plasma parameters.

6.4. Macrophage spreading and atherosclerosis

Circulating monocytes are attracted and trapped into a damaged arterial intima. Differentiation of circulating monocytes to macrophages leads to changes in shape and affects motility. Cells migrate toward sites of inflammation, infection and injury in a regulated manner that involves gradients of chemokines or bacterial products. Cell migration *in vivo* is a highly integrated multistep process and generally directional (Ridley et al., 2003). During migration, cells form new adhesions at their moving front by breaking old adhesions at the rear side (Fig 4) (Moissoglu and Schwartz, 2006). Focal adhesion kinase (FAK) is one of such non-receptor protein kinases which participates in a number of essential events related to cell motility and directionality (Mitra et al., 2005). It is very well known that macrophage spreading requires actin polymerization to form lamellipodia (Small et al., 2002). Actin polymerization and cell spreading involve sustained phosphorylation of Tyr576/577 in the active site of FAK (Park et al., 2009). Inhibition of tyrosine phosphorylation of FAK is temporally associated with essential modifications in its activities such as disruption of focal adhesions and hence acquisition of a motile phenotype (Matsumoto et al., 1994). This indicates agonists that result in rapid and short-lived induction of FAK will promote migration (Orr et al., 2004), while sustained activation may inhibit migration.

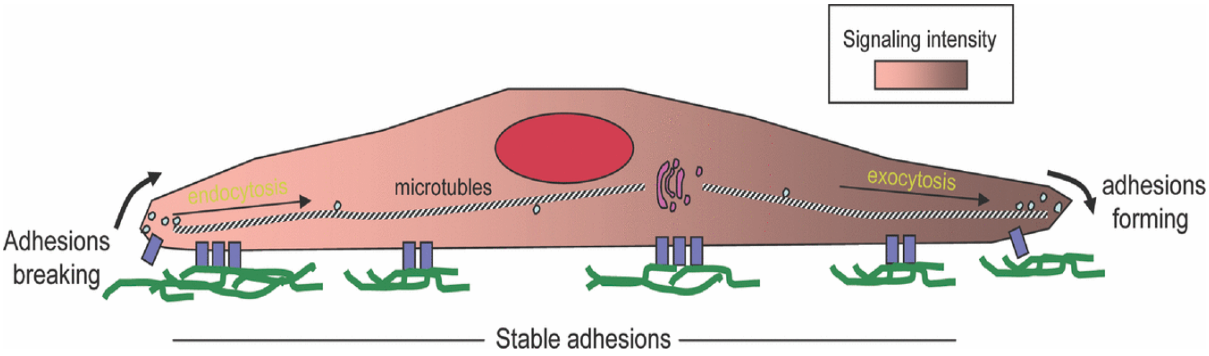

Figure 4. Persistent cell migration. Migrating cells make new stable adhesions at the leading edge while breaking old ones at the trailing edge (Moissoglu and Schwartz, 2006).

7. Aim and objective:

I wanted to investigate whether lack of PLIN1 on an ApoE-/- background has pro- or anti-atherosclerotic consequences.

8. Methods

8.1. Animals

All experimental procedures were performed with the approved standards by the Austrian Federal Ministry of Science and Research, Division of Genetic Engineering and Animal Experiments (Vienna, Austria). *Plin1-/-*, wild type (Himberg, Austria) and *ApoE-/-* mice were on a C57Bl/6 background (Charles River WIGA GesmBH, Sulzfeld, Germany). *ApoE-/-Plin1-/-* mice were obtained by crossbreeding *ApoE-/-* with *Plin1-/-* mice. All mice were maintained on a regular 12 h light and dark cycle and received normal chow diet containing 4.3% fat and 21% protein (Ssniff, Soest, Germany) ad libitum. For studying atherosclerotic plaque formation, female *ApoE-/-* and *ApoE-/-Plin1-/-* mice were challenged with western type diet (WTD; 21% fat, 0.2% cholesterol; Ssniff) for 9 weeks.

8.2. Phalloidin Staining

Macrophages were plated on sterile cover slips and loaded with 100 µg/ml acLDL for 72 h and changing fresh medium and acLDL for every 24 h. Cells were then fixed with 4% paraformaldehyde and permeabilized with 0.5% Triton X-100 for 5 min followed by blocking with 3 % BSA for 30 min. Cells were then incubated with Phalloidin Alexa Fluor® 568 (Molecular Probes, Invitrogen, Vienna, Austria) for 30 min. Cells were washed with PBS and mounted on a glass slide by vectashield containing DAPI (Vector, Burlingame, USA).

8.3. Preparation of LDL, VLDL, HDL and aggregated LDL

Using gradient centrifugation, human plasma HDL, LDL and VLDL were isolated. 1g/l anti-bacterial agent (sodium azide) was added to plasma. Plasma density was corrected to 1.06 g/l with 10g NaCl per 200 ml plasma and 1g/l sodium azide and 1g/l EDTA were added. 40ml of this mixture was centrifuged at 48K rpm for 24 h at 4° C. Two phases formed after centrifugation were separated, upper phase consisted of LDL/VLDL and lower phase had Lp(a) and HDL. Separated phases were dialyzed in distilled water for 30 min. Density of upper phase was adjusted to 1.027 g/l using NaCl and centrifuged at 48K rpm at 15° C for 24 h. After centrifugation, VLDL and LDL were settled in upper

and lower phase respectively. Up to 18 ml of lower phase (LDL) was collected and density was adjusted to 1.063 g/l with NaCl and centrifuged at 48K rpm using 3ml tubes. After centrifugation, approximately 5mm of yellow colored LDL band formed in the middle of each tube. Yellow colored LDL rich band was collected into sterile tubes. HDL rich fraction from lower phase of the first centrifugation step was separated by adjusting the density to 1.063 g/l and centrifuged at 48K rpm. Density was then adjusted set to 1.21 g/l with sodium bromide. After centrifugation, upper phase of HDL_3 layer was collected and dialysed for 48hr in PBS. TG and protein concentrations were measured enzymatically for VLDL fraction. Sterilization of VLDL and LDL was carried out by filtering through 0.8 µm and 0.2 µm filters respectively.

For preparing aggregated LDL, native LDL was vortexed for 2 min.

8.4. Preparation of acetylated LDL

3.2 ml of native LDL fraction was mixed with same volume of saturated NaCl. Throughout the preparation, this mixture was continuously stirred on ice. For every 3 min, 5.4 µl of diethyl ether was added very slowly until the total volume of 57.76 µl was added. To avoid precipitation, 100 µl of 10X PBS was added at the third step of 5.4 µl of diethyl ether addition. After adding total volume of 57.76 µl, stirring was continued for 45 min on ice to get acetylated LDL (acLDL). Using sterile PBS, acLDL was dialyzed for 3hr in at 4° C. TC concentrations were measured by above mentioned enzymatic kit.

8.5. Labeling of acLDL with [3H] cholesterol

Mixture of 100 µg freshly prepared acLDL and 1 µCi [1, 2-^{3}H] cholesterol overlaid with argon and incubated for 16hr at 37° C on a continuous shaking water bath. After incubation time, mixture was passed through PD-10 column for separation of [^{3}H]-acLDL from unincorporated [^{3}H] cholesterol.

8.6. Cholesterol efflux

Peritoneal macrophages were plated in 12-well plates for 24 h. To each well, 100 µg [^{3}H]-acLDL and 1 ml of DMEM medium (0.2% FA-free BSA and 1% P/S) was mixed and added for 36hr. Using warm PBS, cells were washed gently and equilibrated with

medium (DMEM, 0.2% FA-free BSA, 1% P/S and 0.3mM 8-bromo-cAMP) for 16hr. Cells were washed again with warm PBS. Three wells were kept for zero time and other wells for different cholesterol acceptors and time points. Different cholesterol acceptors used in this study were, blank containing only DMEM medium (0.2% FA-free BSA and 1% P/S) as control, 100 µg/ml HDL_3 and 15 µg/ml ApoA1. To each well, 1 ml of acceptor medium was added. 100 µl of medium per well was collected directly in 2 ml scintillation cocktail at each time point 0, 1, 3, 6, 9hr by replacing with the addition of fresh 100 µl acceptor medium to respective well. Scintillation cocktail mixture was vortexed thoroughly and incubated overnight at 4° C. At the end of last time point, remaining medium was discarded and 1 ml of 0.3M NaOH was added to each well to isolated protein. Total efflux from cells to medium was measured by scintillation counting and values were normalized with protein concentrations. Data were presented after subtracting mean % acceptor values with mean % control values.

9. Results

9.1.1. Decreased plasma TG levels in *ApoE-/-Plin1-/-* mice

Lipids parameters were measured in female *ApoE-/-* and *ApoE-/-Plin1-/-* mice after 9 weeks of WTD feeding. There was a slight but statistically significant decline in plasma TG levels (Fig 1A) of *ApoE-/-Plin1-/-* compared to *ApoE-/-* mice. TC and FC concentrations were comparable between the group (Fig 5B and 5C).

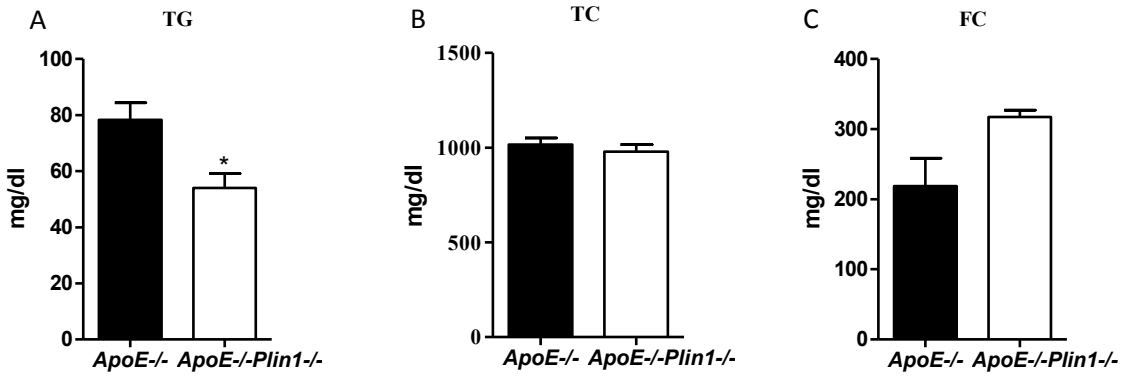

Figure 5. Decreased plasma TG levels in *ApoE-/-Plin1-/-* mice. After 8 weeks of WTD feeding, plasma from overnight fasted female *ApoE-/-* and *ApoE-/-Plin1-/-* mice was collected and estimated enzymatically. Data are presented as a mean values (n=6-8) ± S.E.M. *, $p \leq 0.05$

9.2.2. Reduced plaque formation in *ApoE-/-Plin1-/-* mice

To investigate the effect of PLIN1 deficiency on atherosclerosis development, 8 to 9 week old *ApoE-/-* and *ApoE-/-Plin1-/-* mice were switched to WTD for 9 weeks. Oil red O staining revealed 58 % reduction of lesion formation in *ApoE-/-Plin1-/-* mice compared to *ApoE-/-* mice (Fig 6).

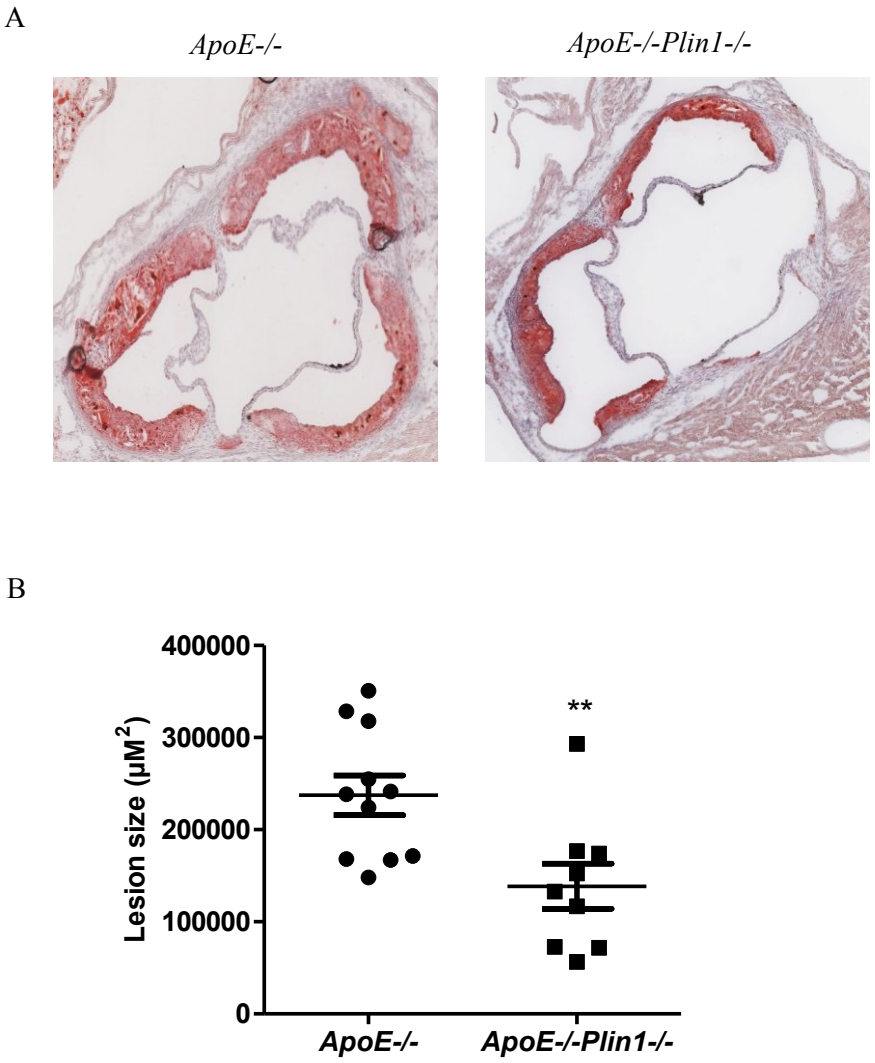

Figure 6. Reduced plaque formation in *ApoE-/-Plin1-/-* mice. Female *ApoE-/- and ApoE-/-Plin1-/-* mice were fed WTD for 9 weeks. Heart was perfused with 4% formalin and neutral lipids were stained with oil red O. (A) Representative images of aortic root sections (oil red O-stained) from female *ApoE-/- and ApoE-/-Plin1-/-* mice. (B) Quantitative analysis of atherosclerotic lesion sizes. Data are represented as mean values of 5 aortic root sections per mouse. Bars represent the mean values of n=9-11 mice per group. **p<0.05.

9.2.3. Increased collagen content in *ApoE-/-Plin1-/-* mice

Collagens provide tensile strength to the fibrous cap in atherosclerotic lesions. The blue color developed by Trichrome staining is the best method to quantify collagen. Masson's trichrome staining showed increased collagen content in the aortic roots of *ApoE-/-Plin1-/-* mice compared to *ApoE-/-* mice (Fig 7A). Collagen content was calculated by percentage per total plaque area (Fig 7B).

A

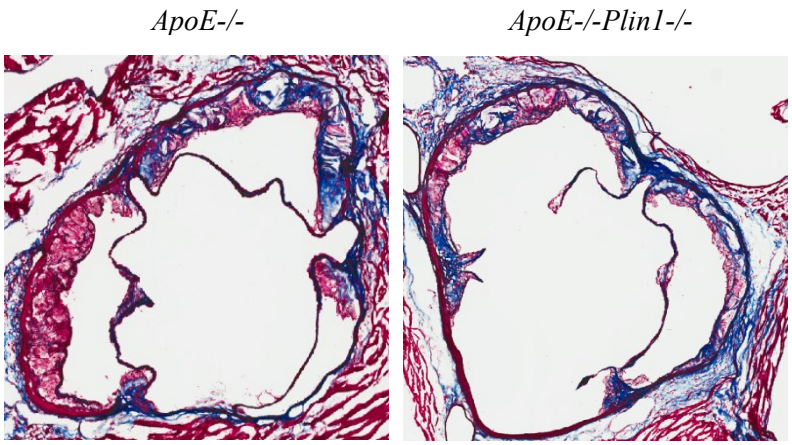

B

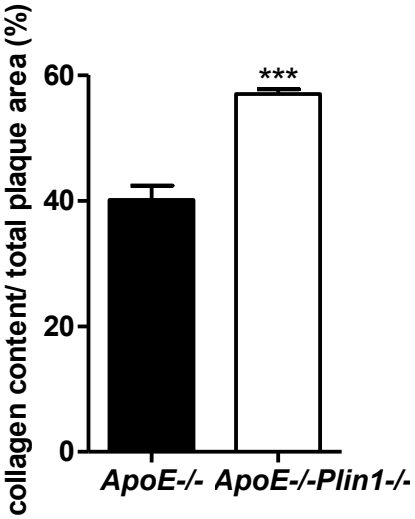

Figure 7. Increased collagen content in *ApoE-/-Plin1-/-* mice. (A) Representative image of Masson's trichrome staining of aortic root sections from female *ApoE-/-* and *ApoE-/-Plin1-/-* mice. (B) Quantitative analysis of collagen content in total plaque area. Data are represented as mean values of 5 aortic root sections per mouse. Bars are the mean values ± S.E.M., (n = 9-11). ***p<0.001.

9.2.4. Reduced foam cell formation in *ApoE-/-Plin1-/-* macrophages

To examine the role of macrophages in reduced atherosclerotic plaque formation, peritoneal macrophages were isolated from chow diet-fed *ApoE-/-* and *ApoE-/-Plin1-/-* mice and treated with 100 µg/ml acLDL and 100 µg/ml VLDL for 24 h. Bodipy green staining of foam cells revealed markedly decreased accumulation of LDs in *ApoE-/-Plin1-/-* compared to ApoE-/- foam cells (Fig 8A). Analysis of foam cell formation indicates that PLIN1 is required for foam cell formation in *ApoE-/-* mice.

In addition, I measured TG, TC and FC concentrations in macrophages and foam cells. TG, TC and FC concentrations were lower in *ApoE-/-Plin1-/-* macrophages. After acLDL loading for 24 h, TC and FC levels were significantly reduced *ApoE-/-Plin1-/-* foam cells, whereas TG levels were decreased but the difference was not statistically significant (Fig 8B). No significant changes were observed in TG, TC, and FC after VLDL loading.

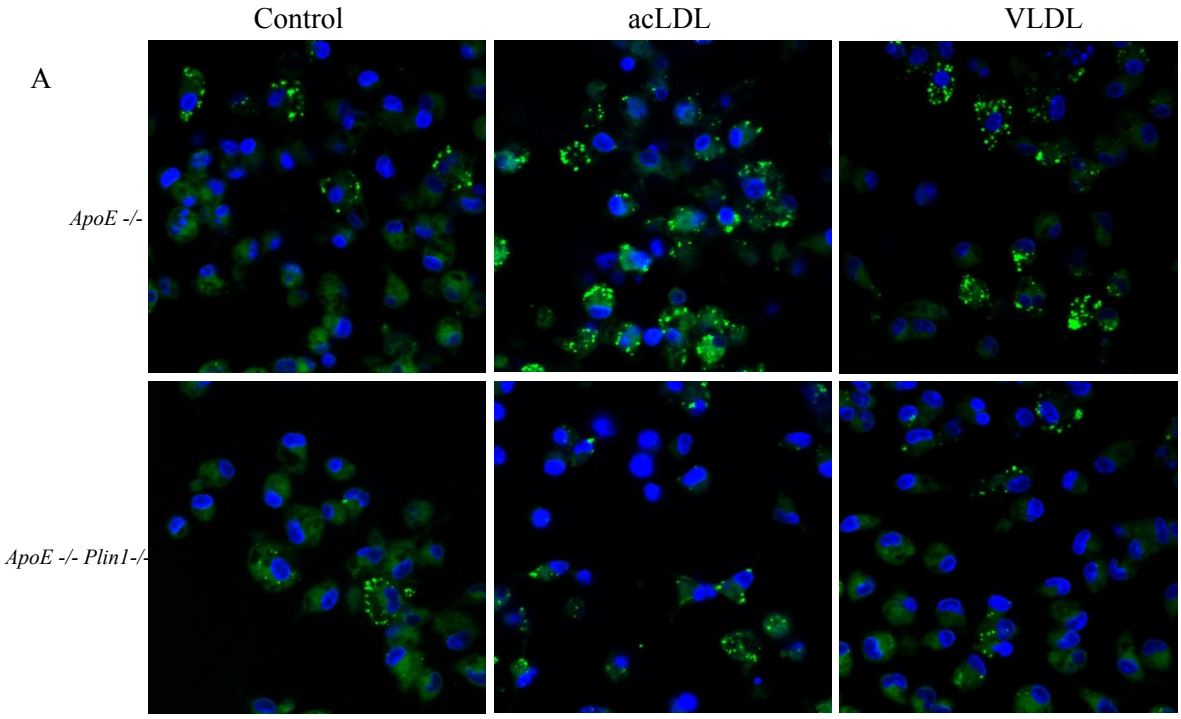

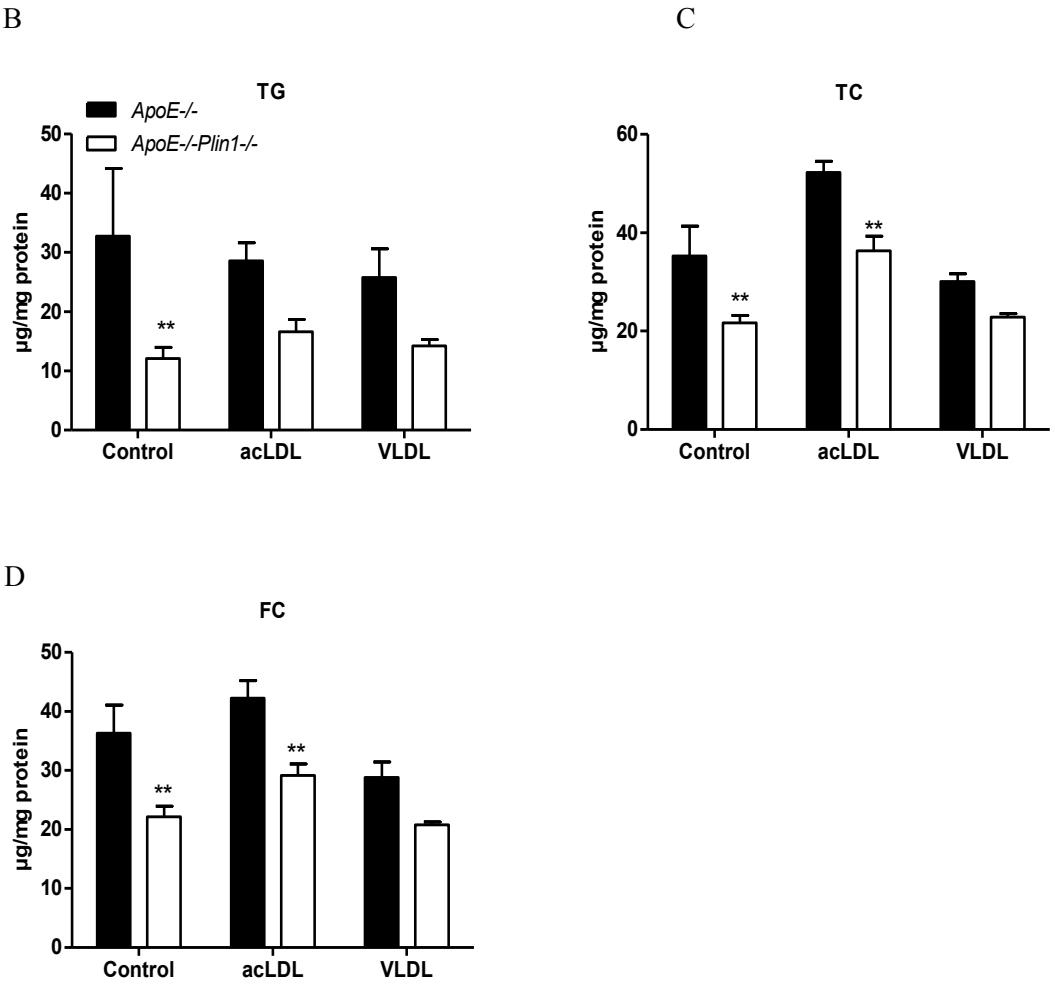

Figure 8. **Reduced foam cell formation in *ApoE-/-Plin1-/-* macrophages**. Peritoneal macrophages from chow diet-fed *ApoE-/-* and *ApoE-/-Plin1-/-* mice were cultured for 24 h in DMEM containing 10% LPDS and acLDL (100 µg/ml) or VLDL (100 µg/ml). A) Representative Bodipy green-stained images of control, acLDL and VLDL-loaded macrophages. Lipids were extracted from peritoneal macrophages. B) TG, C) TC and D) FC concentrations were estimated using commercially available kits. Data presented as a mean values (n=3-5). ± S.E.M. ** $p<0.01$.

9.2.5. Increased cholesterol efflux to ApoA1 in *ApoE-/-Plin1-/-* macrophages

To address whether *ApoE-/-Plin1-/-* macrophages influence reverse cholesterol transport *in vitro*, I treated peritoneal macrophages with ^{3}H-cholesterol-labeled acLDL and analyzed percentage of cholesterol efflux to ApoA1 and HDL_3 as extracellular acceptors. Efflux was increased to ApoA1 (Fig 9A) but no differences were observed to HDL_3 (Fig 9C) in *ApoE-/-Plin1-/-* macrophages compared to *ApoE-/-* macrophages. There was no difference in cholesterol efflux to both acceptors after cAMP stimulation (Fig 9B and 9D). Furthermore, ABCA1 and ABCG1 protein levels were increased in peritoneal macrophages from *ApoE-/-Plin1-/-* compared to *ApoE-/-* mice (Fig 9E). Interestingly, only ABCA1 expression was induced in *ApoE-/-Plin1-/-* compared to *ApoE-/-* macrophage after treating with acLDL for 24 h and protein lysate was used for western blot analysis of cholesterol efflux transporter proteins (Fig 9F).

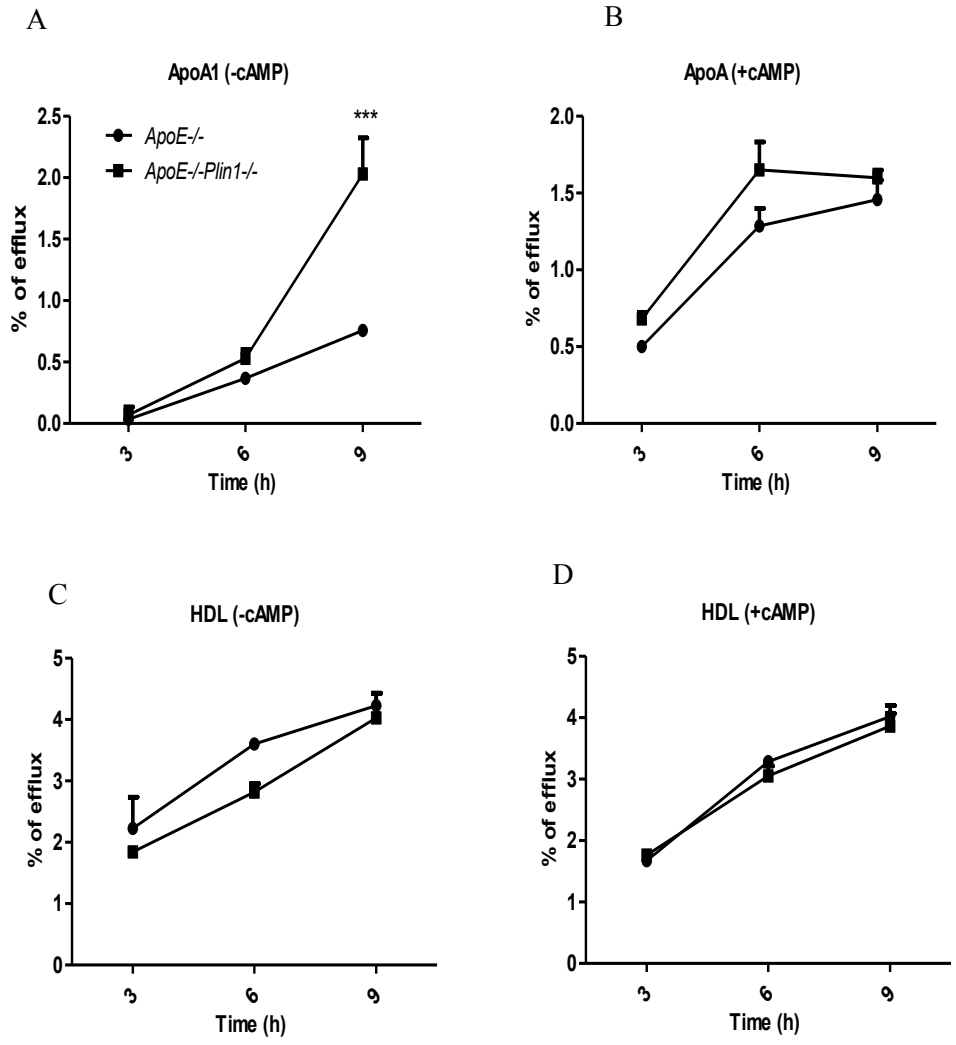

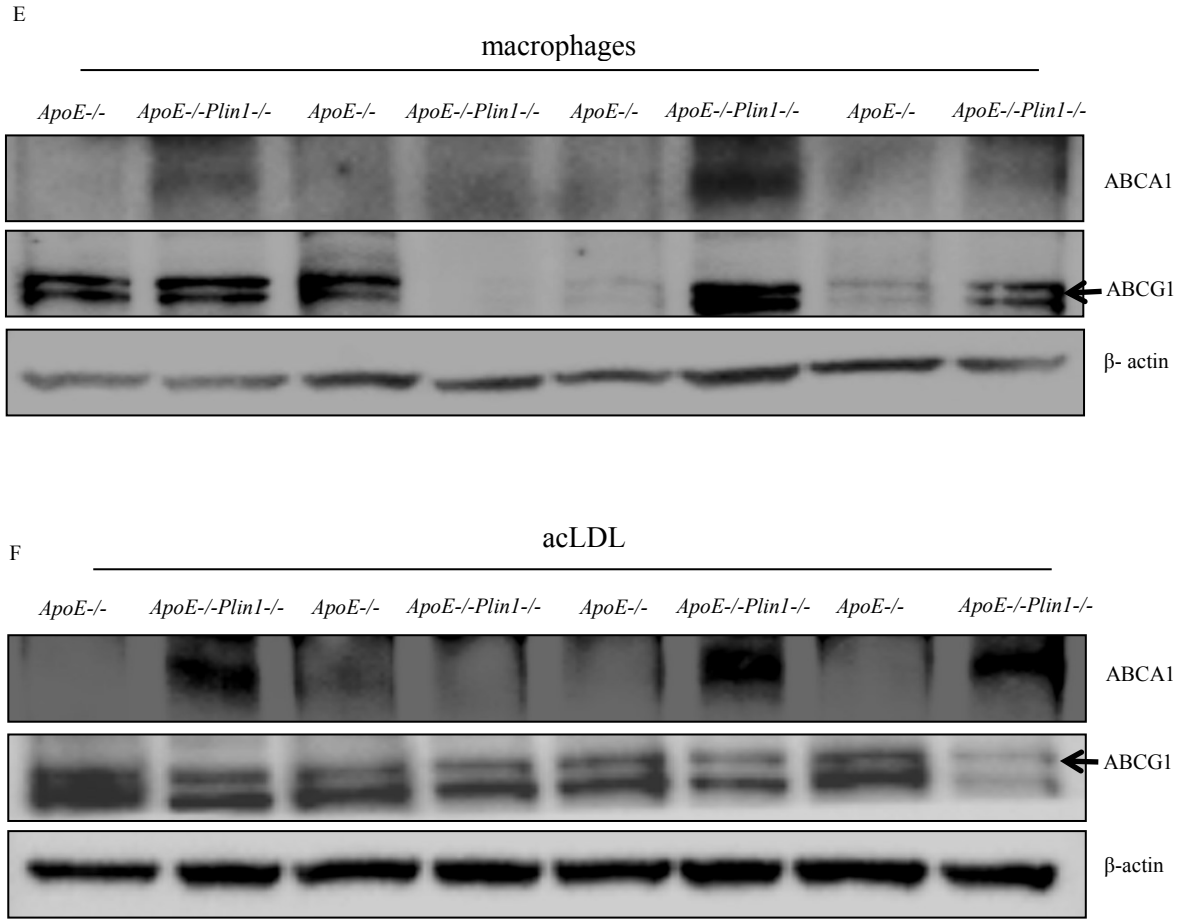

Figure 9. **Increased cholesterol efflux to ApoA1 in *ApoE-/-Plin1-/-* macrophages**. Peritoneal macrophages from chow diet fed *ApoE-/-* and *ApoE-/-Plin1-/-* mice were labeled with ^{3}H-cholesterol and cholesterol efflux to different extracellular acceptors was assessed in the absence (A, C) and presence (B, D) of cAMP. Data show the mean values (n=5) ± S.E.M of triplicate. *** p <0.001.

Cell lysates of (E) macrophages and (F) acLDL (100μg/ml)-treated foam cells (40 μg per lane) were separated by SDS-PAGE. Protein expression of ABCA1 and ABCG1 were analyzed by western blotting relative to the expression of β-actin. Representative western blot images (n=3).

9.3.1. *Plin1* deficiency does not influence foam cell formation in the presence of ApoE

Since *ApoE-/-Plin1-/-* macrophages showed reduced foam cell formation as compared to *ApoE-/-* macrophages, I wanted to check the impact of *Plin1* deficiency on foam cell formation with acLDL and VLDL loading by comparing with Wt macrophages. Both Bodipy

green staining (Fig10 A) and lipid content analysis (Fig10 B) using enzymatic assay revealed comparable foam cell formation in *Plin1-/-* and Wt macrophages.

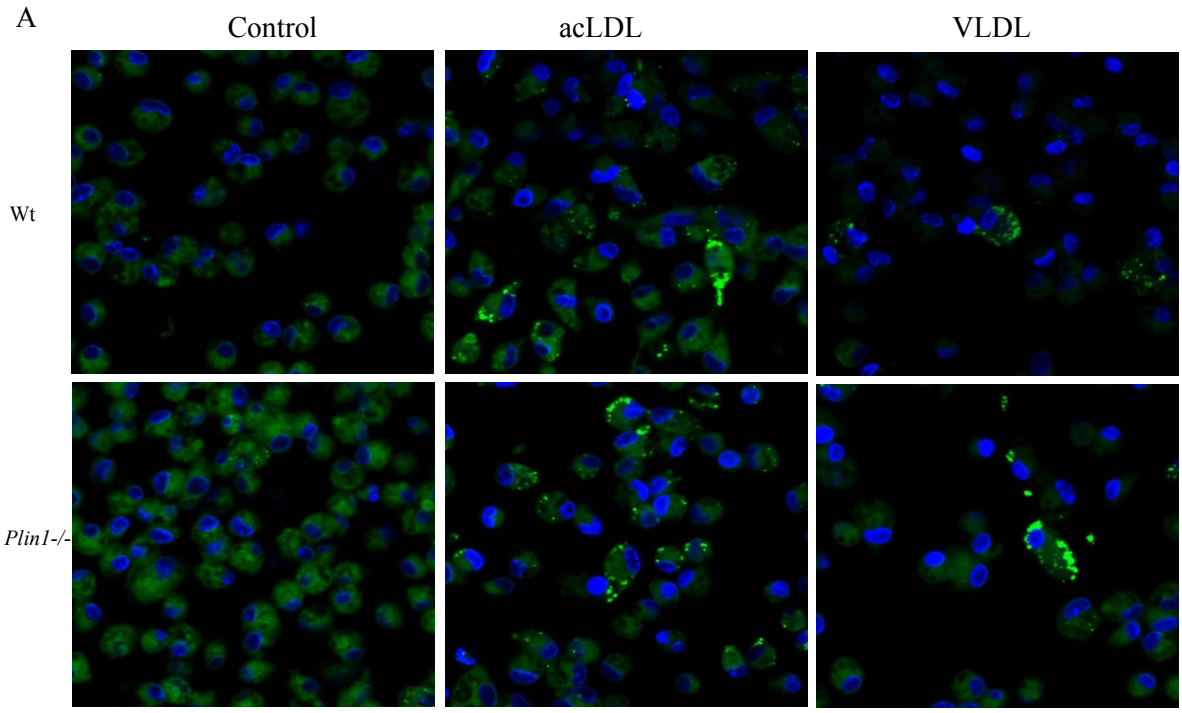

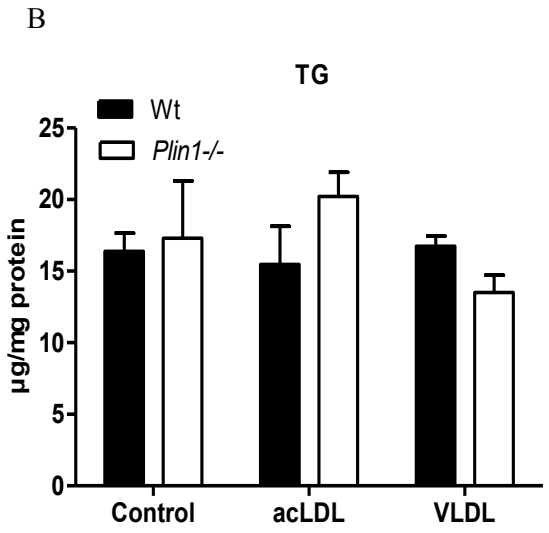

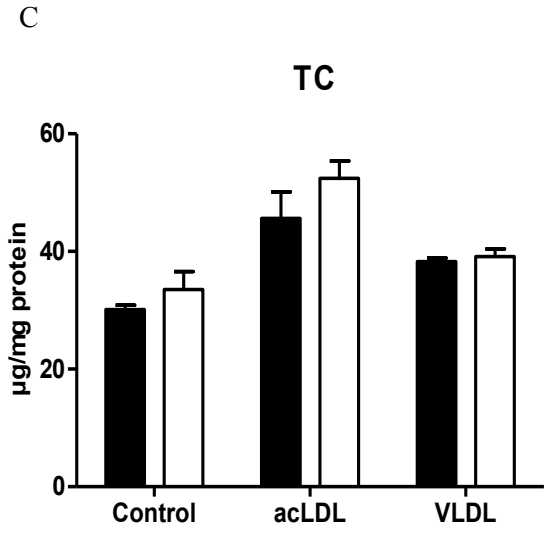

D

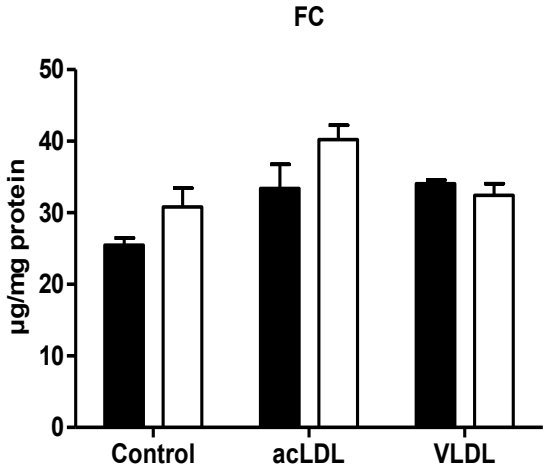

Figure 10. ***Plin1*** **deficiency does not influence foam cell formation in the presence of ApoE**. Peritoneal macrophages from Wt and *Plin1-/-* macrophages were cultured in DMEM medium containing 10% LPDS with or without 100µg/ml acLDL and 100µg/ml VLDL for 24 h. A) Representative images of pooled cells from 4-5 mice per group. Bodipy green staining was performed to visualize LDs of macrophages. Lipids were extracted from peritoneal macrophages of Wt and *Plin1-/-* mice. B) TG, C) TC and D) FC concentrations were estimated using commercially available kits. Data are presented as mean values (n=5) ± S.E.M.

9.3.2. Increased spreading of *Plin1-/-* macrophage foam cells

Monocyte recruitment to the arterial wall and their transformation into macrophages are important early events in the initiation of atherosclerosis. Complex cellular networks such as spreading, disruption of existing focal contacts and formation of newly modified focal contacts are involved in cell migration and trapping into the arterial intima (Stossel, 1994). I therefore examined the effect of acLDL loading on macrophage spreading as the initial step of migration by incubating cells for 3 days and then stained with fluorescein-conjugated phalloidin to detect actin filaments. Interestingly, microscopic analysis showed that increased cell spreading in *Plin1-/-* macrophage-derived foam cells, whereas Wt foam cells showed blunted response (Fig 11A). Furthermore, the increase in FAK phosphorylation (Fig 11B) supports our hypothesis that reduced plaque build-up in *ApoE-/-Plin1-/-* mice might be due to increased cell spreading which hinders trapping of macrophage foam cells into arterial intima.

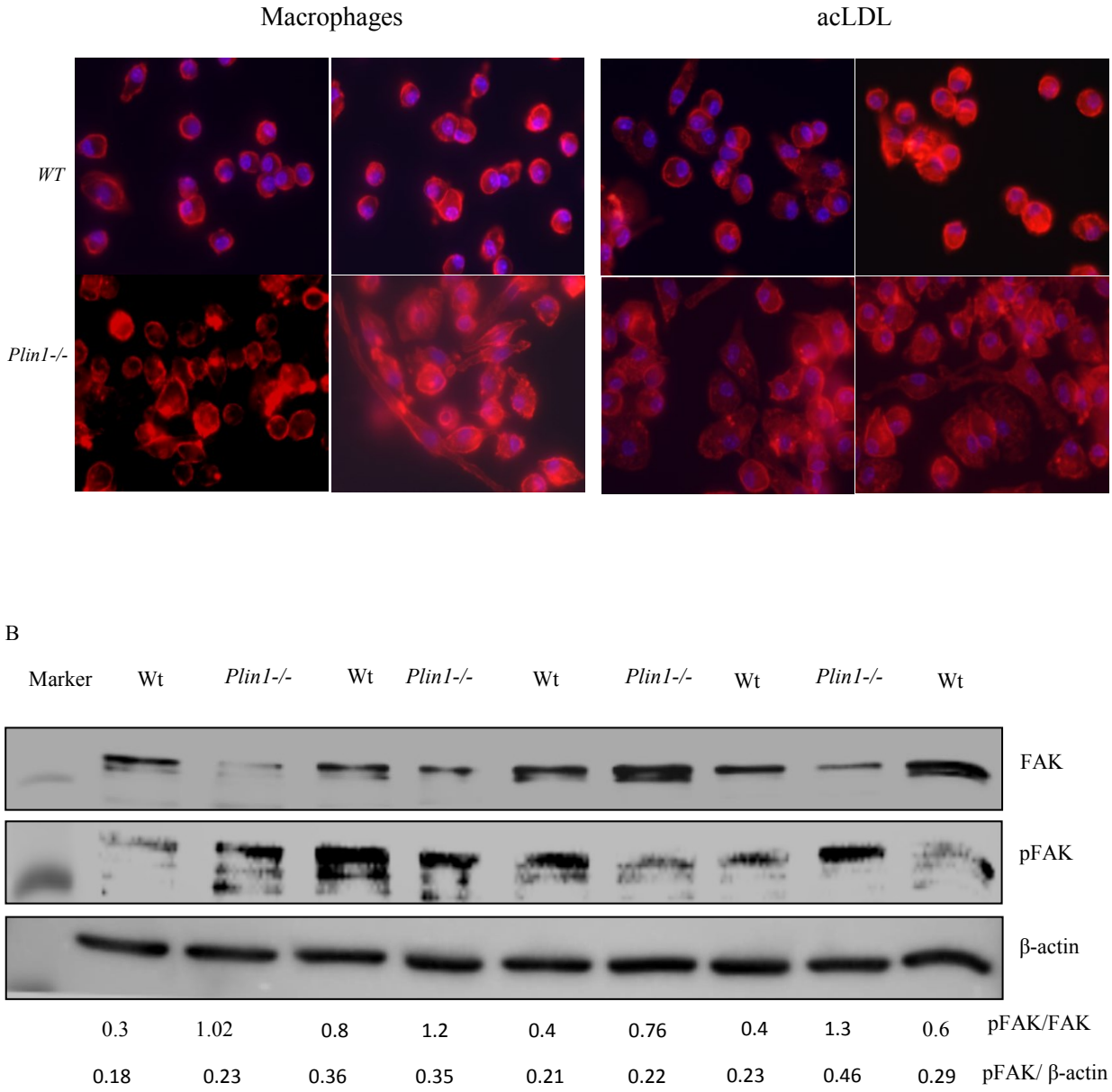

Figure 11. **Increased spreading of *Plin1-/-* macrophage foam cells**. Peritoneal macrophages were exposed to 100 µg/ml acLDL for 3 days. A) Phalloidin staining for f-actin B) Cell lysates were subjected to western blot analysis to detect total and phosphorylated (Tyr576/577) FAK expression using specific antibodies. Immunoblotting with β-actin was used as loading control.

9.3.3. Absence of *Plin1* does not affect expression of other LD-associated proteins

To assess whether *Plin*1 deficiency affects expression of other LD-associated proteins, I determined protein levels of Rab18, Cathepsin B and Plin2. Difference in the expression

pattern of Rab 18 and Cathepsin B were comparable between the groups (Fig 12A). However, PLIN2 protein expression was slightly reduced in *Plin1-/-* macrophages compared to Wt despite no changes in the LD accumulation. Protein expression was normalized to GAPDH (Fig 12B).

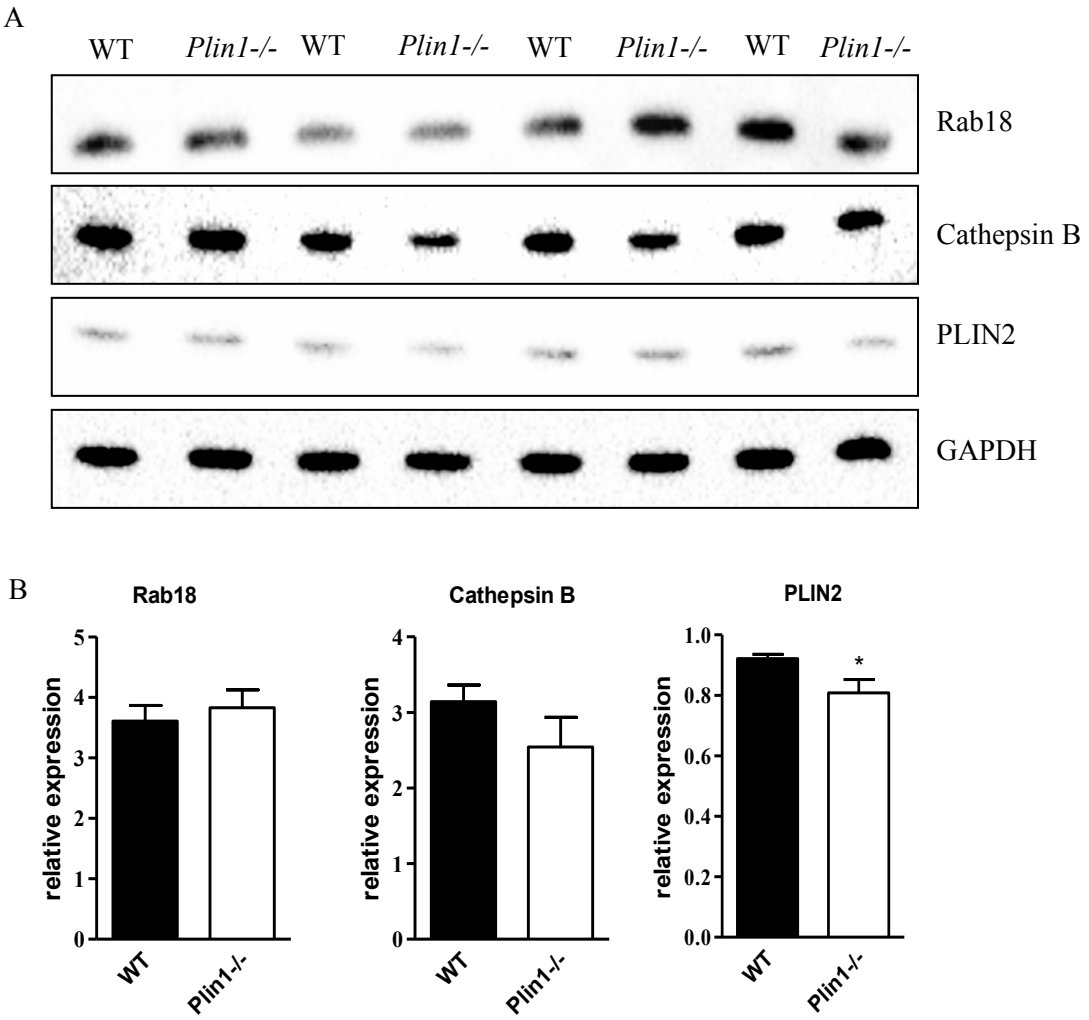

Figure 12. *Plin1* deficiency does not affect expression of other LD-associated proteins. Peritoneal macrophages from Wt and *Plin1-/-* mice were isolated and treated with 100µg/ml acLDL. Cell lysates were used to detect protein expression levels. A). Western blot analysis of Rab18, Cathepsin B and PLIN2. B) Bands were quantified using Image J software and normalized to GAPDH (n=4). *p<0.05

10. Discussion

Macrophages in the arteries take up circulating lipids and store them in intracellular LDs. Intracellular LDs accumulation in macrophage-derived foam cells is closely associated with atherosclerotic lesion development. Studies on the involvement of PERILIPIN family members, which surround LDs on plaque formation, are still limited. PERILIPINs regulate lipid metabolism of LDs in coordination with other cytosolic and LD-bound proteins such as lipases. From our group, it was previously demonstrated the role of ATGL-mediated macrophage function, foam cell formation and its role in atherosclerosis regression (Chandak et al., 2010, Lammers et al., 2011). Lanlois et al showed increased atherosclerosis in *Ldlr-/-Plin1-/-* mice after 20 weeks of atherogenic diet and the effect was independent of plasma lipid levels and inflammation (Langlois et al., 2011). In this thesis and in contrast to Langlois, I demonstrated that whole body ablation of *Plin1* in *ApoE-/-* mice results in reduced plasma TG levels and significantly reduced atherosclerotic plaque formation and increased plaque stability after 9 weeks of WTD feeding. This controversy might be due to the fact that lesion pathology differs between *Ldlr-/-* and *ApoE-/-* mouse models and depends on the type of diet, age of mice (Whitman, 2004). Moreover, lesions have been most thoroughly characterized in *ApoE-/-* mice (Jawien et al., 2004). I found decreased number of LDs in *ApoE-/-Plin1-/-* foam cells and increased cholesterol efflux to ApoAI cholesterol acceptor. In addition, I observed increased cell spreading with concomitant enhanced FAK phosphorylation in *Plin1-/-* macrophages.

After 9 weeks of WTD feeding, *ApoE-/-Plin1-/-* mice had reduced TG concentrations, whereas TC and FC concentrations were comparable between the groups. Plaque development was significantly affected in *ApoE-/-Plin1-/-* mice with 58 % reduction in the lesion size compared to *ApoE-/-* mice. Collagen content, produced mostly by smooth muscle cells and stimulated by factors like platelet-derived growth factor and transforming growth factor-β, strengthens the fibrous cap of lesions by protecting against rupture (Libby, 2006). *ApoE-/-Plin1-/-* mice showed increased collagen accumulation within fatty streaks, suggesting increased plaque stability after WTD feeding.

Macrophage foam cell accumulation is one of the characteristic features of lesion growth and size. It has been reported that whole body *Plin1* ablation results in leanness and reverses obesity by regulating lipolysis and energy balance (Martinez-Botas et al., 2000). Increased circulating FFAs in *Plin1*-/- mice, as a result of enhanced lipolysis, are used by liver, skeletal muscle and adipose tissue with increased beta oxidation and by reducing hepatic glucose production (Saha et al., 2004). Lariguaderie *et al.* showed that increased Plin1 expression was associated with differentiation from human monocytes to macrophages (Larigauderie et al., 2006). It has been reported that PLIN2, the major LD-associated protein in foam cells, is known to regulate foam cell formation and atherosclerosis. *Plin2* ablation in *ApoE-/-* mice reduced foam cell formation and improved atherosclerosis without compensatory increase in mRNA expression of other PERILIPIN family members including *Plin1*. *Plin1* mRNA expression was barely detectable and substantially lower than the expression of *Plin3* and *Plin4* (Paul et al., 2008b). We found slightly reduced expression of Plin2 in *Plin1-/-* foam cells despite comparable cholesterol and TG levels.

It was shown that *Plin1* overexpression in THP-1 macrophages resulted in significant LD formation and TG accumulation and this phenotype was unaffected after silencing *Plin*2 using siRNA approach (Larigauderie et al., 2006). In this study, deficiency of *Plin1* in *ApoE-/-* macrophages reduced the number of LDs and lipid accumulation after acLDL treatment. In contrast, there were no changes in foam cell formation as well as lipid accumulation when macrophages from Wt and *Plin1-/-* mice were incubated in the presence of acLDL or VLDL.

Cellular cholesterol levels are tightly regulated to maintain cell viability as high FC results in disruption of cellular membranes and cell death. Only hepatocytes and adrenocortical cells can degrade excess cholesterol. In many cells and tissues there are two ways to maintain cholesterol levels: primarily, by converting FC to CE, with limited loading capacity, and secondarily, by efflux to extra-cellular acceptors, with unlimited capacity (Low et al., 2012). A large number of studies showed the importance of increased cholesterol efflux with respect to atherosclerosis (Khera et al., 2011, Yancey et al., 2003) as cholesterol efflux is the initial step in reverse cholesterol transport. I found increased cholesterol efflux from *ApoE-/-Plin1-/-* macrophages to ApoA1 cholesterol acceptors and this associated with concomitant increase in ABCA1 protein expression in

acLDL treated cells. ABCA1 and ABCG1 expression was also increased in *ApoE-/-Plin1-/-* macrophages but there was no difference in ABCG1 expression after treating acLDL. This might explain one of the pathways for reduced atherosclerotic lesion formation in *ApoE-/-Plin1-/-* mice compared to *ApoE-/-* mice.

Monocyte recruitment to the arterial wall and their transformation into macrophages is one of the essential early events in the pathogenesis of atherosclerosis. Monocytes migrate toward the site of inflammation in a regulated way involving many changes in the surface adhesion proteins and rearrangement of actin filaments. Actin polymerization coupled with cell spreading involves sustained phosphorylation of Tyr576/577 in the active site of FAK (Park et al., 2009). Inhibition of FAK phosphorylation is temporally associated with acquisition of a motile phenotype (Matsumoto et al., 1994). Agonists that result in rapid and short-lived induction of FAK will promote migration while sustained activation may inhibit migration (Orr et al., 2004). Accordingly, present data show sustained activation of FAK after 3 days of acLDL treatment in *Plin1-/-* macrophages, indicating increased cell spreading which may inhibit their migration and reduced plaque formation.

Adipocyte differention is associated with changes in PERILIPIN protein expression pattern with PLIN2 expression in pre-adipocytes will be replaced by PLIN1 after differentiation into adipocytes (Brasaemle et al., 1997). When we examined the expression of LD-associated proteins including small GTPase like Rab18 that is involved in vesicle transportation and Cathepsin B in *Plin1-/-* macrophages, we could not find any difference except PLIN2 expression which was slightly decreased despite no changes in foam cell formation between the groups.

From my present study, I conclude that whole body ablation of *Plin1* in *ApoE-/-* background plays a very important role in improvement of atherosclerosis. *ApoE-/-Plin1-/-* macrophages showed increased cholesterol efflux to ApoA1 as cholesterol acceptor. Macrophages isolated from *ApoE-/-Plin1-/-* peritoneal macrophages exhibited decreased LD accumulation, which was further confirmed by enzymatic estimation of lipids. Macrophages from *Plin1-/-* mice showed increased spreading with sustained FAK activation. Hence, decreased atherosclerosis in *ApoE-/-Plin1-/-* mice is the combined result of decreased plasma TG concentrations increased cholesterol efflux, impaired

foam cell formation with decreased TG and sterol accumulation. Therefore, inhibition of *Plin1* might be a good target to treat atherosclerosis.

11. Identification and characterization of proteins in foam cell-derived lipid droplets

7.1. Abstract

The structural proteins and hydrolases on lipid droplets (LDs) of macrophage-derived foam cells have a regulatory role in lipid storage and release. PERILIPINs constitute the most abundant structural proteins on LDs. In order to gain insight into the distribution of proteins that govern the flux of lipids into/from LDs, we studied protein composition in macrophage LDs. Since we have found reduced atherosclerosis and decreased number of foam cells in an atherosclerotic mouse model lacking *perilipin1* (*Plin1*), we were interested in differences in LD-associated proteins of wild type (Wt) and *Plin1*-deficient (-/-) foam cells. Foam cell formation was induced by incubating peritoneal macrophages in the presence of acetylated low density lipoprotein (acLDL). LDs were purified by density gradient centrifugation; the LD proteomes were compared by LC-MS/MS after isotopic labelling of peptides. We found a number of LD-associated proteins both that are known to be expressed on LDs and some of unknown functions. Among many differentially expressed proteins, we found reduced expression of ATGL, CGI-58 and Rab18 on the LDs of *Plin1-/-* compared to Wt macrophages.

12. Introduction

One of the key events in the pathogenesis of atherosclerosis is the deposition of macrophage-derived foam cells in the arterial wall. Foam cells store excess cholesterol and fatty acids as cholesterol ester (CE) and triacylglycerol (TG) surrounded by a phospholipid monolayer in lipid droplets (LDs) (Murphy and Vance, 1999, Tauchi-Sato et al., 2002). LD-associated proteins regulate lipolysis, vesicular transport, membrane fusion and cytoskeletal motility. The first observation of LDs dates back to 1674 when van Leeuwenhoek viewed fat globules in milk (Kernohan, 1969, Kernohan and Lepherd, 1969). Once thought an inert organelle, LDs are now proven to be very dynamic and active. PERILIPIN family members are so far known as the major set of LD associated proteins that link regulation of storage and efflux of lipids. PERILIPIN family includes 5 members: PLIN1 (perilipin1), PLIN2 (adipose differentiation-related protein, ADRP, adipophilin, ADFP), PLIN3 (tail interacting protein of 47kDA, TIP47), PLIN4 (S3-12), and PLIN5 (OXPAT, oxidative tissue-enriched PAT protein, lipid storage droplet protein5, LSDP5, myocardial lipid droplet storage droplet protein5, MLDP). PERILIPIN proteins share a common PAT (**P**erilipin, **A**dipophilin, **T**ip47) domain, and are able to bind to a monolayer membrane. PERILIPINs are known to be involved in generation progression, regulation, and stabilization of LDs. LD-associated proteins interact with other regulatory proteins and hydrolases. In addition to PAT proteins, there are a number of LD-associated proteins with known and unknown functions (Bozza et al., 1997, Yu et al., 1998, Fujimoto et al., 2001). Adipocyte biology is best revealed by the recent discoveries of number of LD-associated proteins, specially correlating sequence similarities among PAT proteins (Londos et al., 1999). Recent study by Li et al showed gene expression patterns of proteins during human foam cell formation using microarrays (Li et al., 2010). Hitherto, the macrophage-associated LD proteome has not been studied in detail.

Numerous studies have been reported on the roles of macrophages on atherosclerotic plaque development. However, very little is known about the role of macrophage-derived LDs and LD-associated proteins in the progression or regression of lesion formation. LD-associated proteins have important functions in the maintenance of cellular lipid homeostasis. Identification of these proteins, specially, their dynamic shuttle on and off LDs can give more insight into the biological functions of this

monolayer coated organelle. Through long time LDs have been considered inert storage depots, now they have gained recognition as independent organelles occurring in almost all types of cells playing roles in lipid homeostasis. Imbalance in the lipid homeostasis is known to be one of the key factors during the advancement of lesional area. Therefore it is important to study the macrophage LD proteome. In this study, we have analysed the proteomes of LDs from primary macrophage-derived foam cells isolated from Wt and *Plin1-/-* mice.

12.1. Lipid droplet formation

LDs characteristically increase in numbers in response to elevated fatty acid levels both *in vitro* and *in vivo* (Pol et al., 2004). The most widely accepted model of LD formation deduced from proteomic and microscopic data is that LDs are formed from specific regions on the endoplasmic reticulum (ER) (Serrero et al., 2000, Atshaves et al., 2001). Figure 1 shows three different models of LD formation, firstly, lensing model, where LD are originated from ER monolayer (A), in the second bicelle formation model, LDs are excised from ER membrane (B) and in the third vesicle formation model, rearrangement of the inner leaflet of the bilayer occurs resulting in the neutral lipid-rich LDs.

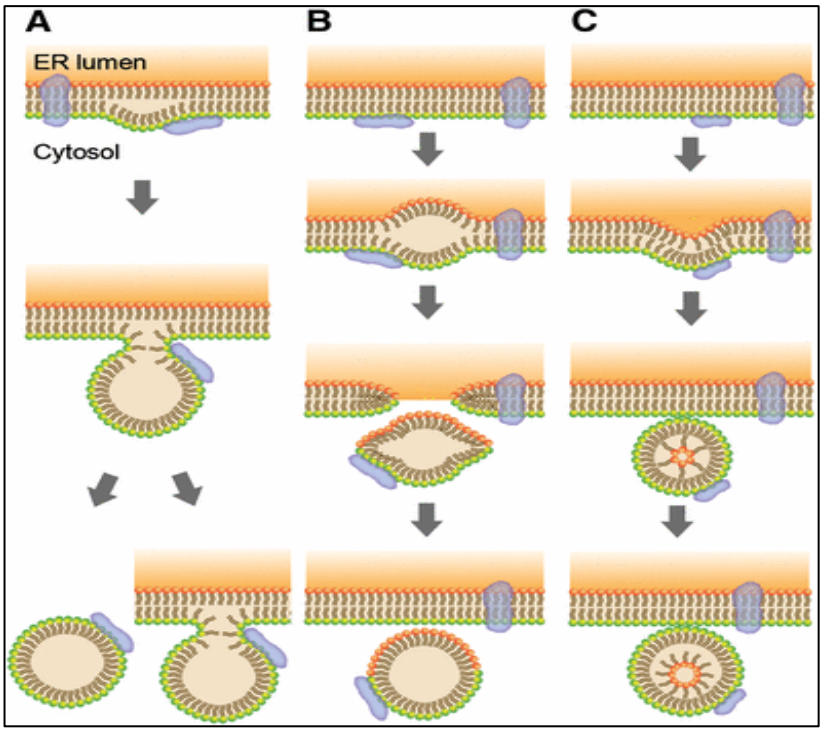

Figure 1. Formation of LDs. (A) According to the "lensing model," neutral lipids are deposited between the leaflets of the ER membrane: after reaching a critical size, the neutral lipid core bulges out and the LD is formed; the LD surface monolayer is derived solely from the cytosolic

leaflet of the ER membrane and contains phospholipids and LD-associated proteins. Subsequently, the LD may completely separate from the ER membrane, or remain attached, with the surface layer forming a continuum with the ER. (B) Bicelle formation: LD formation similar to model in A, but the LD is excised from the ER membrane, and both ER membrane leaflets contribute to the LD surface monolayer. (C) Vesicle formation. Inclusion of the neutral lipid core in the membrane vesicle requires rearrangement of the inner leaflet of the bilayer. These models explain the origin of the phospholipid membrane, which stems either from the cytoplasmic leaflet or from both leaflets of the ER membrane, respectively. Unclear is what limits the expansion of the neutral lipid core between the leaflets, what determines the orientation of LD extrusion toward the cytosol, and how the integrity of the ER membrane is maintained. Notably, none of the intermediate stages representing neutral lipid deposits between the ER membrane leaflets, nascent lipid droplets in the ER, or lipid-filled vesicular structures have been experimentally observed in wild-type cells. Figure adopted from (Kohlwein et al., 2013)

12.2. Intracellular cholesterol regulation

Maintenance of the appropriate cholesterol level in intracellular membranes is crucial for cellular function. Free cholesterol (FC) levels are high in the plasma membrane (60–80% of cellular cholesterol) and low in the ER. Cholesterol is endocytosed as the CE from LDL and moves to endosomes for hydrolysis. FC enters ER where excess cholesterol is converted to CE and stored in LDs or effluxed to cell surface receptors.

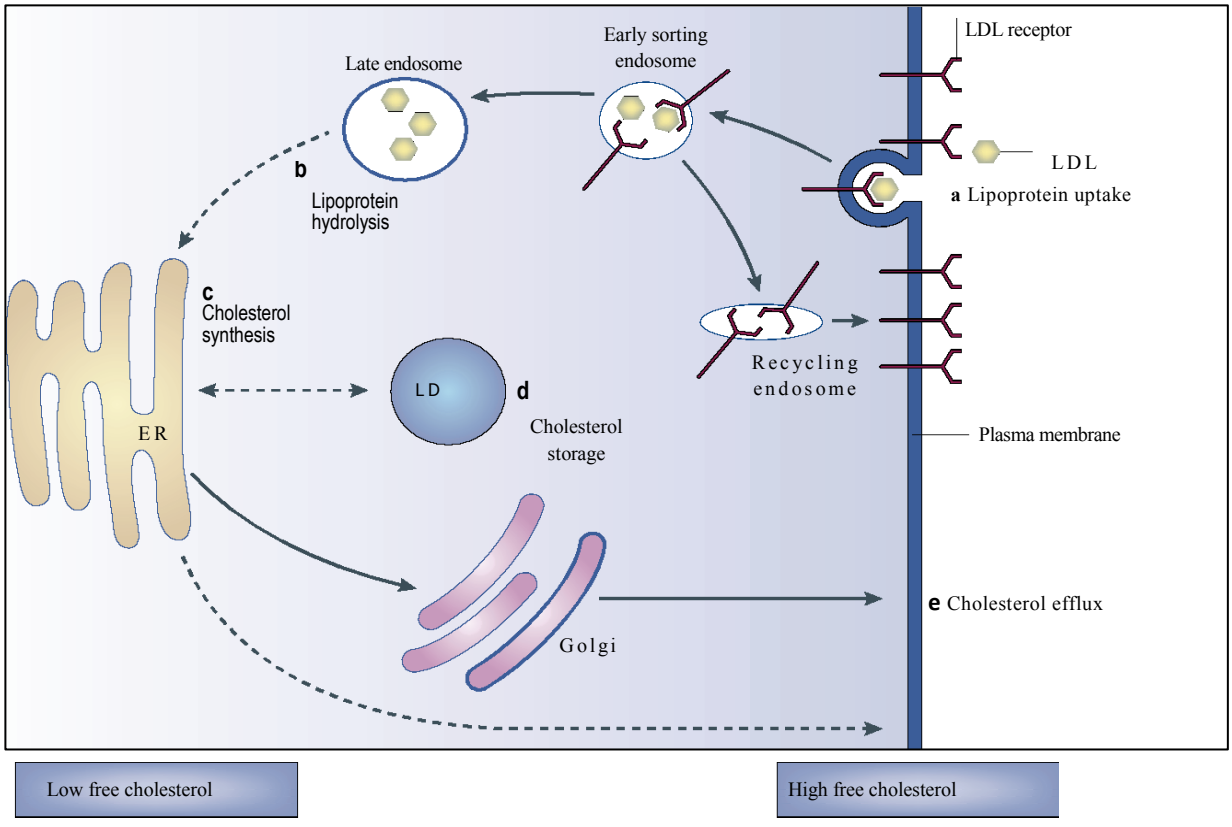

Figure 2. Intracellular cholesterol regulation. Cholesterol is endocytosed as the cholesteryl ester component of LDL (see part a in the figure), and it traffics to the late endosomal system, where it is hydrolyzed to FC and fatty acids (b). FC enters the cellular pool, together with cholesterol synthesized de novo in the ER (c). Excess cholesterol is converted to cholesteryl esters and stored in LDs; d), or effluxed from the cell surface to extracellular acceptors (e). In the figure, solid lines indicate vesicular transport, whereas dashed lines highlight pathways for which there is evidence of both vesicular and non-vesicular trafficking. Figure adopted (Martin and Parton, 2006)

12.3. LD-associated proteins: Role of PERILIPIN family members

Many studies have found that a variety of proteins exist on the surface of intracellular LDs being involved in lipid synthesis, storage, utilization, and degradation (Murphy, 2001). Among these proteins, members of the PERILIPIN are highly abundant. PLIN1 has been found to play a key role in fat metabolism (Saha et al., 2004). Alternative splicing of a *Plin1* common pre mRNA results in three isoforms: Plin1A, Plin1B and Plin1C (Lu et al., 2001). Plin1A and B are expressed in adipocytes with Plin1A form being highly abundant. Plin1C is present in steroidogenic cells (Langlois et al., 2011). PLIN1 promotes lipid storage under basal (= fed) condition by shielding TG-rich LDs from lipases (Brasaemle et al., 2009). PERILIPIN family members share a common PAT domain with the ability to bind intracellular LDs. PLIN1 to PLIN5 differ in their size (Fig 3), tissue expression and affinity for LDs under different metabolic conditions as well as transcriptional regulation (Bickel et al., 2009). Early studies identified PLIN2 on milk droplets secreted from mammary epithelial cells (Heid et al., 1996). PLIN2 is expressed in various cell types that store lipids and in diseases associated with fat accumulation (Heid et al., 1998). PLIN1 and PLIN2 are exclusively present on LDs and undergo proteasomal or lysosomal degradation pathways in unbound form (Paul et al., 2008a). PLIN3 has been found to be associated with TG metabolism in macrophages HOW? (Buers et al., 2009). PLIN4, a peroxisome proliferator–activated receptor-induced PAT domain containing protein, is expressed in highly oxidative tissues such as brown adipose tissue, fasted liver, heart, and slow-twitch muscles and promotes fatty acid (FA)-induced TG accumulation (Wolins et al., 2006b). PLIN5 coats oleate-loaded TG-rich smaller LDs in 3T3-L1 adipocytes *in vitro* and is expressed mostly in white adipose tissue but lower levels are also found in heart and skeletal muscle. Depending on the cell's metabolic state, PLIN3, PLIN4 and PLIN5 exchange on and off LDs and are

stable both when bound to LDs or in cytoplasm, which is in contrast to PLIN1 and PLIN2 (Wolins et al., 2006a, Wolins et al., 2005).

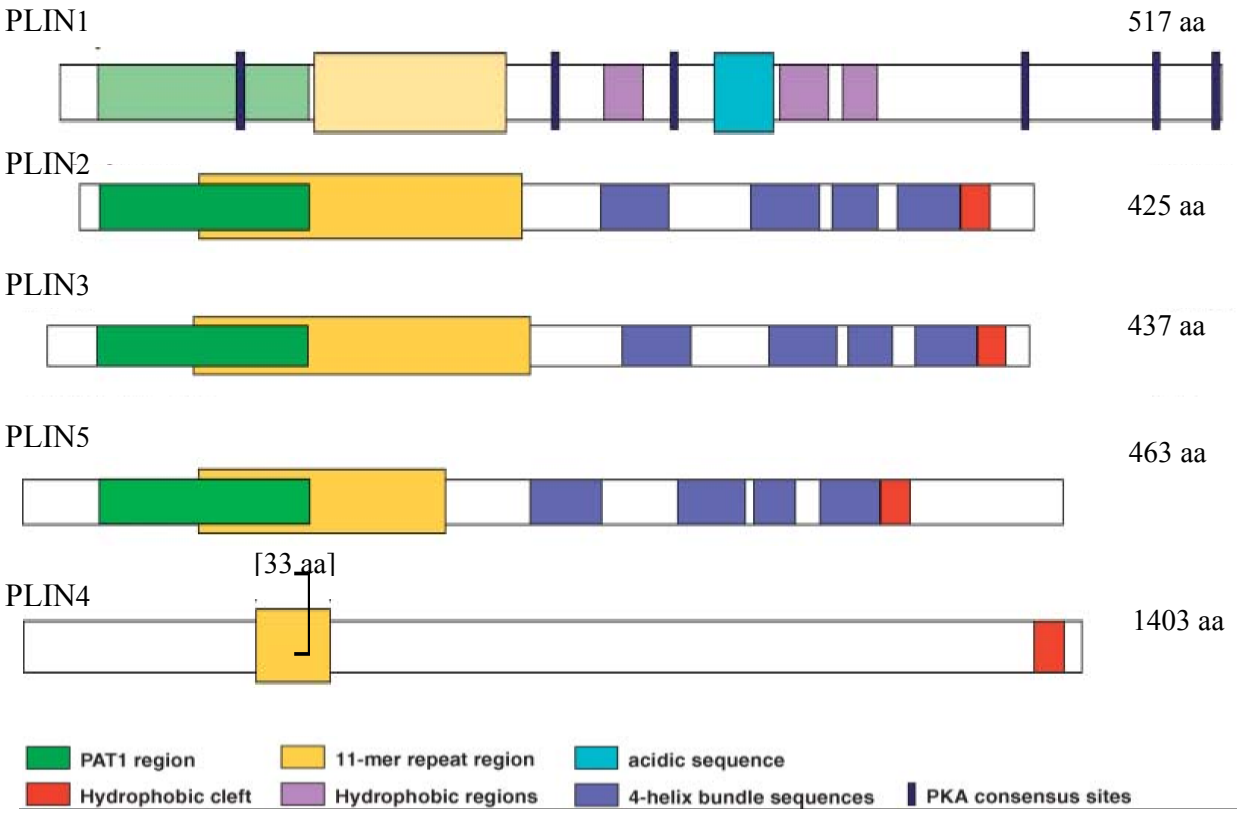

Figure 3. Stuctural features of the PERILIPIN family of proteins. Schematic diagram of the structural features of PLIN1 and related proteins. The positions of structural features that are shared by the PERILIPIN family of proteins are shown; greater intensity of color represents higher similarity of the sequences between family members, whereas lighter color represents reduced sequence similarity. Mouse sequences are depicted. The N termini of PLIN1, PLIN2, PLIN3, and PLIN5, but not PLIN4, contain 100 amino acid (aa) sequences that are highly conserved between members of the family (green). Overlapping with these sequences are stretches of amino acids containing 11-mer repeat sequences that are predicted to fold into amphipathic helices (maize); definition of the exact boundaries of these helical sequences will require elucidation of the structures of the individual proteins. The most extensive section of 11-mer repeat sequences occurs in PLIN4, which has at least 87 tandem 11-mer repeats. Following the putative 11-mer repeats, sequences of PLIN3 fold into a four helix bundle of amphipathic α-helices (blue); both PLIN2 and PLIN5 share sequence similarity in this region. In contrast, within this region, PLIN1 has three sequences of moderate hydrophobicity (lilac) and a highly acidic sequence (cyan). The C termini of PLIN2, PLIN3, PLIN4, and PLIN5, but not PLIN1, contain a highly conserved sequence of 14 amino acids that folds into a hydrophobic cleft in PLIN3 (red). PLIN1 is unique among members of the protein family in having six consensus sequences for the phosphorylation of serine residues by protein kinase A (PKA) (charcoal) dispersed throughout its primary amino acid sequence. Figure modified from (Brasaemle, 2007).

13. Aim and objective

We found reduced foam cell formation and atherosclerosis in an atherosclerotic mouse model lacking whole body PLIN1 gene. Since imbalance in lipid homeostasis is known to be one of the key factors during the advancement of lesional area and LD coat proteins are important regulators of lipid storage and mobilisation we aimed to study the macrophage LD proteome in *Plin1-/-* in comparison to Wt macrophages. Since LC-MS/MS is an effective tool and has become the method of choice for identification and quantification of proteins, we applied this approach to identify LD proteomes from macrophage derived foam cells.

14. Materials and methods

14.1. Animals

C57BL/6 and *Plin1-/-* mice (Londos et al., 1999) on a C57BL/6 background were used. All mice were given unlimited access to food and water. The mice were maintained on regular chow diet, 4.3% (w/w) fat, with no added cholesterol (Ssniff, Soest, Germany) on a regular 12h dark/light cycle. Fourteen to twenty four week old mice were used in the study. All experimental protocols were approved by the Austrian Federal Ministry of Science and Research, Division of Genetic Engineering and Animal Experiments (Vienna, Austria).

14.2. Cell culture

Peritoneal macrophages from Wt and *Plin1-/-* mice were harvested after 3 days of thioglycollate injection (3 ml) intra-peritoneally. Cells were washed with PBS and cultured in Dulbecco's modified Eagle's medium (DMEM) (Gibco, Invitrogen, Vienna, Austria), 10% fetal calf serum (FCS), 100 µg/ml penicillin/streptomycin. After 2 h of plating, cells were washed to remove non-adherent cells and incubated with 100 µg/ml acetylated (ac) LDL for 3 days, constantly changing medium with fresh acLDL for every 24 h.

LDL was isolated from human plasma by density gradient ultracentrifugation. LDL was acetylated as described (Basu et al., 1976).

14.3. Isolation of LDs

Peritoneal macrophages were washed twice with PBS to remove medium. Three ml of ice cold PBS was added to each T-75 cell culture flask for easy detachment and cells were scraped. All the following steps were carried out on ice. The homogenate was centrifuged at 1000 x g, 4^{o} C for 10 min. The supernatant was separated and the pellet was collected into separate tubes. Eight ml of disruption buffer A (100 mM KH_2PO_4, pH 7.4, 250 mM sucrose) containing protease inhibitor complex (PIC) was added and mixed by pipetting up and down and incubated on ice for 15 min. Suspended cell pellet was transferred into a nitrogen bomb for cell disruption at 700 psi for 15 min. Sample was

collected carefully into a separate tubes. All cell content was overlaid with an overlay buffer B (50 mM KH_2PO_4, pH 7.4, 0.1 M KCl, $MgCl_2$) containing PIC. LDs were separated by centrifuging at 40000 rpm for 2 h at 4^o C. Approximately 2 ml of the top layer rich in LDs was taken out into another SW41 centrifuge tube, and 150 mg NaCl was added and overlaid with buffer B+PIC. Tubes were centrifuged for 30 min at 30000 rpm, 4^o C. The enriched LD top layer was removed and transferred into new polypropylene tubes and stored at -80^o C for later usage.

14.4. Mass-spectrum analysis

(Performed by Prof. Ruth Birner-Grünberger)

LD preparations of *Plin1-/-* and Wt macrophages were delipidated by diethylether extraction, reduced and alkylated, digested by sequencing grade trypsin (Promega) over night and acidified to 0.1 % formic acid. Stable isotope dimethyl labeling for semi quantitative analysis was performed according to Boersema et al. (Boersema et al., 2009). This method is based on the reaction of all primary amines with formaldehyde and cyanoborohydride to form dimethylamines, with the exception of N-terminal proline that results in conversion of mono-methylamine (Hsu et al., 2005). By using deuterated or non-deuterated reactants the mass of the dimethyl tag can be changed by 4 or 8 Da. Peptides from Wt LDs were labelled with light (+28 Da) and peptides from the *Plin1-/-* LD with intermediate (+32 Da) dimethyl tags using deuterated or non-deuterated formaldehyde.

The labelled digests of Wt and *Plin1-/-* were pooled in equal amounts according to their spectral counts determined by a LC-MS/MS prerun and prefractionated by strong cation exchange (SCX) into 12 fractions. SCX was performed on an Agilent 1100 HPLC system equipped with a Zorbax BioSCX Series II 0.8 X 50 mm micro-HPLC column (Agilent, Santa Clara, USA) and an automatic fraction collector. The loading buffer consisted of 20 % acetonitrile, 5 mM KH_2PO_4/H_3PO_4, 0.05 % formic acid (pH 2.7). The elution buffer consisted of 350 mM KCl, 20% acetonitrile, 5 mM KH_2PO_4/H_3PO_4, 0.05 % formic acid (pH 2.7). Flow rate during separation was constant at 50 µl/min. For the first 10 min the mobile phase consisted of 100 % loading buffer followed by a gradient to give 35 % elution buffer after 45 min. The gradient was further increased to reach 100 % elution buffer after 51 min and was held constant until the end of measurement after

61 min. Peptide fractions were desalted by solid phase extraction with C18 material in Bond Elut 96 well plates (Agilent). Solid phases were washed and conditioned with 3 x 1 ml 50 % acetonitrile/0.5 % acetic acid and conditioned with 3 x 750 µl triuoroacetic acid (TFA). Fractions were solubilized in 500 µl 0.4 % TFA and applied to the solid phases. Desalting was done with 3 x 1 ml 0.1 % TFA followed by 1 ml 0.5 % acetic acid. Samples were eluted with 250 µl 50 % acetonitrile/0.5 % acetic acid followed by 250 µl 100 % acetonitrile. Samples were collected into Protein LoBind 500 µl DeepWell plates (Eppendorf), dried by centrifugal evaporation, and stored at -20° C for further processing.

The desalted SCX fractions were solubilised in 0.1 % formic acid and separated by nano-HPLC (Agilent 1200 system, Vienna, Austria) equipped with a Zorbax 300SB-C18 enrichment column (5 µm, 5 x 0.3 mm) and a Zorbax 300SB-C18 nanocolumn (3.5 µm, 150 x 0.075 mm). Each fraction was injected and concentrated on the enrichment column for 6 min using 0.1 % formic acid as isocratic solvent at a flow rate of 20 µl/min. The column was then switched in the nanoflow circuit, and the sample was loaded on the nanocolumn at a flow rate of 300 nl/min. Separation was carried out using the following gradient, where solvent A is 0.3 % formic acid in water and solvent B is a mixture of acetonitrile and water (4 : 1, by vol.) containing 0.3 % formic acid: 0-6min: 13 % B; 6-63 min: 13-28 % B; 63-88 min: 28-50 % B, 88-89 min: 50-100 % B; 89-100 min: 100 % B; 100-101 min: 100-13% B; 101-120 min: re-equilibration at 13 % B. The sample was ionized in the nanospray source equipped with nanospray tips (PicoTipTM Stock# FS360-75-15-D-20, Coating: 1P-4P, 15+/- 1µm Emitter, New Objective, Woburn, MA, USA). It was analyzed in a Thermo LTQ-FT mass spectrometer (Thermo Fisher Scientific, Waltham, MA, USA) operated in positive ion mode, applying alternating full scan MS (m/z 400 to 2000) in the ion cyclotron and MS/MS by collision induced dissociation of the 5 most intense peaks in the ion trap with dynamic exclusion enabled. The LC-MS/MS data were analyzed by searching the mouse SwissProt public database with Proteome Discoverer 1.3 (Thermo Fisher Scientific, Waltham, MA, USA) and Mascot 2.3 (MatrixScience, London, UK). Carbamidomethylation on Cys was entered as fixed modification. Intermediate and light dimethylation on lysine and N-terminus were entered as fixed modification in two search nodes, respectively, and oxidation on methionine was entered as variable modification. A maximum false discovery rate of 5 % using decoy database search, an ion score cut off of 20 and a minimum of 2 identified peptides was chosen as identification criteria. For

quantification, ratios of intermediate to light dimethyl labelled peptides and proteins were determined with Proteome Discoverer 1.3.

14.5. Delipidation of LDs, preparation of component proteins, and SDS-PAGE

LD fraction was delipidated with 1 ml of cold acetone overnight at –20 °C followed by centrifugation at 14,000 × *g* for 30 min at 4° C and removal of solvent from the protein pellet. One ml of room temperature acetone was added to further precipitate the pellet and 1:1 acetone:ether (v:v) was added followed by ether. Ether was evaporated under nitrogen and proteins were reduced with 25 mM DTT for 30 min in a water bath sonicator at 37° C with intermittent vortexing. β-mercaptoethanol (4%) was added before loading onto prestained SDS-PAGE gels and proteins were blotted onto a PVDF membrane. The membrane was blocked with 5 % BSA plus 0.1% Tween 20 in TBS for 2 h at room temperature. The blot was incubated with the primary antibody overnight at 4° C and washed three times with TBS for 10 min and then the secondary antibody was added and incubated at RT for 2 h. The blot was washed three times for 10 min and developed using ECL plus plus (Amersham Biosciences, Piscataway, USA) for 5 min. The blot was recorded using ChemiDoc system (BIO-RAD, Vienna, Austria).

15. Results

15.1. Analysis of macrophage foam cell-derived LD-associated proteome by LC-MS/MS

After isolation and precipitation of LD-associated proteins, the samples were subjected to MS analysis. We identified a total of 230 proteins by MS analysis and selected a few known LD-associated proteins for validation by Western blotting (Table 1).

ATGL, CGI-58, Rab18, Rab7, Cathepsin B, PLIN2 and PLIN3 were determined with 14, 3, 9, 15, 8, 13 and 3 unique peptides with sequence coverage of 34 %, 14 %, 46 %, 67 %, 29 %, 42 % and 11 %, respectively. In *Plin1-/-* LDs, only about 1/3rd of the amount of ATGL, 1/6th of CGI-58, half of Rab18 and 2/3rd of Rab7 found on Wt LDs could be detected. Only half of PLIN2 and 1/5th of PLIN3 were detected on *Plin1-/-* compared to Wt LDs. The quantified variability of the ratios of individual peptides was 123 %, 66 %, 102 %, 136 %, 113 % 132 % and 172 %, respectively for ATGL, CGI-58, Rab18, Rab7, PLIN2 and PLIN3. Total fold change in ATGL, CGI-58, Rab18, Rab7, Cathepsin B, PLIN2 and PLIN3 protein amount present on LDs can be represented by the measured ratio of *Plin1-/-*/Wt, respectively, as 0.013, 0.013, 0.032, 0.077, 0.197, 0.198, and 1.558.

Table 1. Selected LD-associated proteins from Wt and *Plin1-/-* macrophage-derived foam cells

Protein	**Σ Coverage**	**Σ# Unique Peptides**	***Ratio Plin1(-/-)/Wt***	***Ratio Plin1(-/-)/Wt* Variability [%]**	**SwissProt Accession number**
ATGL	33.95	14	0.013	122.7	Q8BJ56
CGI-58	14.25	3	0.013	66.2	Q6QA69
Rab18	46.60	9	0.032	102.2	P35293
Rab7	66.67	15	0.077	136.5	P09527
Cathepsin B	29.50	8	0.197	112.9	P10605
PLIN2	42.12	13	0.198	132.2	P43883

PLIN3	11.44	3	1.558	171.9	Q9DBG5

15.2. Protein expression pattern of LD-associated proteins in foam cells

To investigate the changes in LD-associated protein expression pattern, Wt and *Plin1-/-* macrophages were incubated with 100 µg/ml acLDL for 3 days. As shown in Fig 4, there was no difference in the expression patterns of ATGL, CGI-58, Rab18, Rab7 and Cathepsin B in whole cell lysates of Wt versus *Plin1-/-* foam cells.

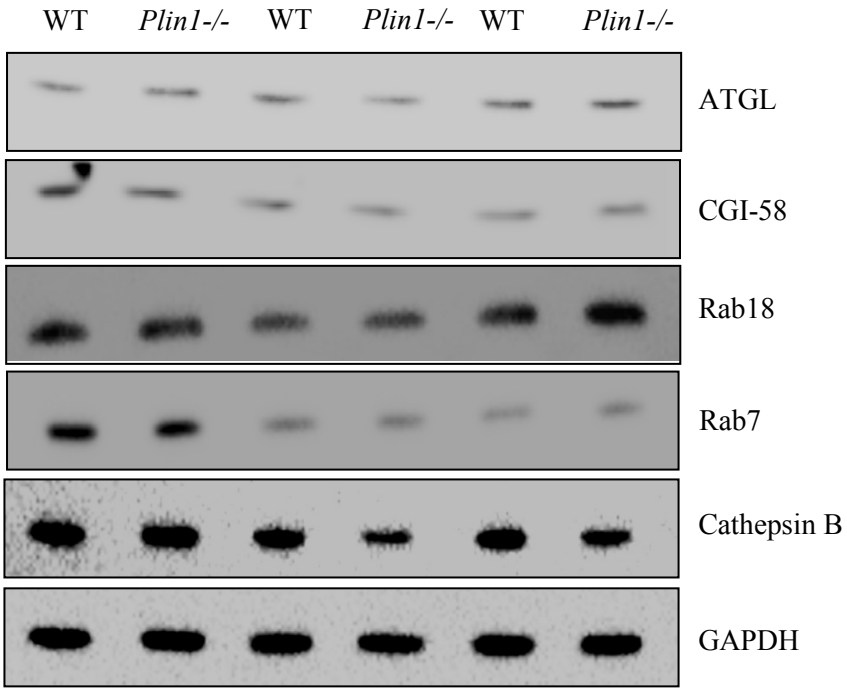

Figure 4. Protein expression pattern of LD-associated proteins in foam cells. Whole cell lysate from Wt and *Plin1-/-* foam cells were separated by SDS PAGE and protein expression of ATGL, CGI-58, Rab18, Rab7 and Cathepsin B was analyzed by western blotting relative to the expression of GAPDH.

15.3. Protein expression pattern found on LDs

After LC-MS/MS analysis of LD-associated proteins from Wt and *Plin1-/-* foam cells, proteins were precipitated and equal volume of proteins were loaded onto a stain-free SDS gel (proteins were available in very small amounts and were hard to precipitate and estimate). From Fig 3A, Wt LD-associated proteins found to be more abundant than proteins from *Plin1-/-* LDs. In line with proteomic data, the expression levels of proteins like ATGL, CGI-58, Rab18 and Cathepsin B were checked as shown in Fig 4B, 4C, 4D, and 4E respectively. It was observed that all these proteins were downregulated but at different levels as also shown by MS data analysis. However, observed differences in western blotting experiments are not completely convincing and reliable because of very low amounts of precipitated proteins. This suggests that the absence of PLIN1 might downregulate these proteins which in turn might play a vital role in foam cell formation.

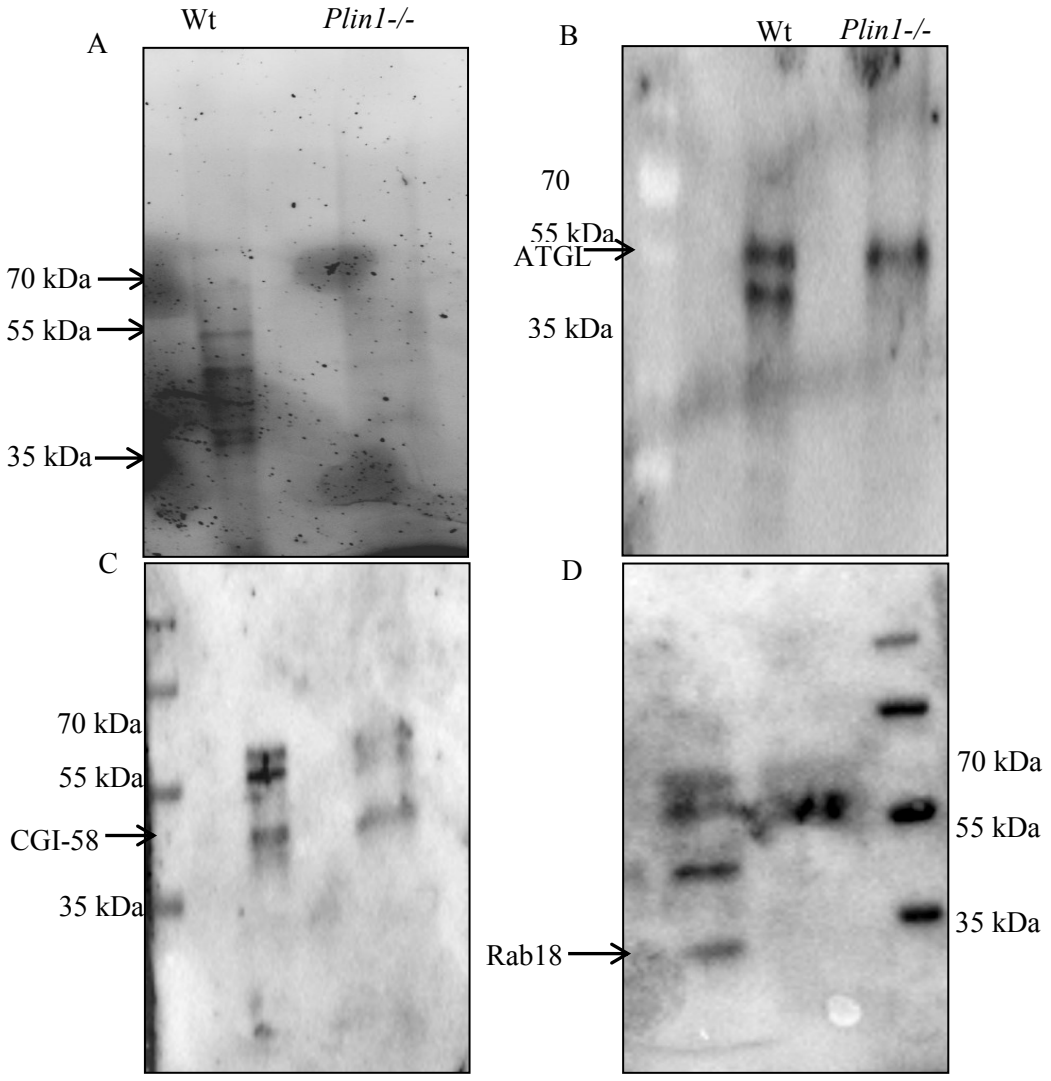

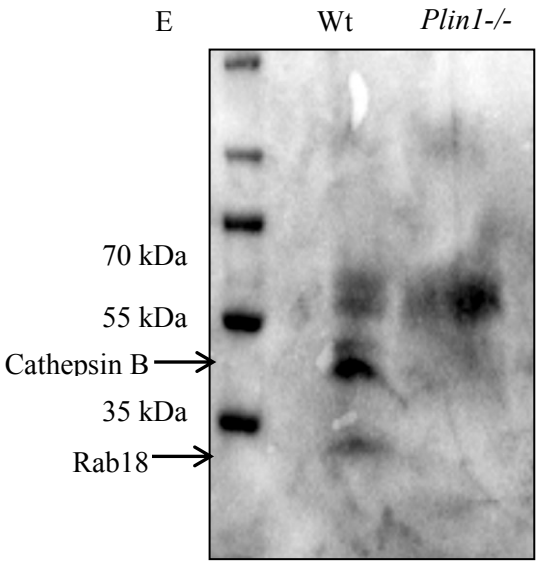

Figure 5. Protein expression pattern found on LDs. A) SDS-PAGE of total proteins precipitated from LDs of Wt and *Plin1-/-* macrophages-derived foam cells after 3 days of acLDL treatment. Position of molecular mass markers is denoted on the left side of the panels. ATGL, CGI-58 and Rab18 were down regulated *Plin1-/-* foam cell-derived LDs. B) ATGL C) CGI-58 D) Rab18 and E) Cathepsin B were determined using specific antibodies.

16. Discussion

Present work was carried out to establish a method for identifying the LD proteome of primary macrophage-derived foam cells using LC-MS/MS. In this study, we observed unchanged expression pattern of ATGL, CGI-58, Rab18, Rab7, and Cathepsin B, which were already known LD-associated proteins, in whole cell lysate from Wt and *Plin1-/-* foam cells; however, LD-proteome analysis by LC-MS/MS revealed reduced expression of these proteins in *Plin1-/-* foam cells. This might be explained by reduced number of lipid droplets and thus reduced localisation of LD-associated proteins on LDs. We observed less LDs in *ApoE-/-Plin1-/-* macrophage-derived foam cells (in the present study of my thesis).

On the other hand, reduced expression of ATGL and CGI-58 might be due to the less important role/s of these proteins in lipid metabolism on *Plin1-/-* compared to Wt LDs. ATGL and its co-activator CGI-58 are involved in a co-ordinated lipolysis in adipocytes where phosphorylation of PLIN1 is also important for ATGL-mediated TG hydrolysis under lipolysis stimulated conditions (Brasaemle, 2007).

Decreased expression of Rab18 and Rab7 GTPases on LDs from *Plin1-/-* compared to Wt foam cells might be the cause for reduced structural rearrangements and foam cell formation. Rab GTPases such as Rab18 and Rab7, present in the cytoplasm, membrane and nucleus, regulate vesicle formation and transport of many proteins as substrates and products between LDs and other organelles involving cytoskeleton. Almahbobi et al showed the interaction of LDs with intermediate filaments in Leydig cells (Almahbobi et al., 1993). LDs are found to move on microtubules in Drosophila embryos (Welte et al., 1998) and homotypic fusion of LDs was shown to be dependent on microtubules (Bostrom et al., 2005). Therefore, the association of LDs with cytoskeleton suggests that LDs might be moving along the cytoskeleton. Furthermore, increased recruitment of vimentin and filamin on LDs suggests that interaction between LDs and cytoskeleton is regulated by PLIN1 protein(s) (Table 2). In addition, we found increased expression of proteins involved in DNA repair and protein synthesis on *Plin1-/-* compared to Wt LDs (Table 2) indicating possible direct or indirect role(s) of PLIN1 in the regulation of cell death and other biological processes. Though results from western blotting experiments

were in line with LC-MS/MS analysis, it was hard to rely on equal amounts of loaded protein concentrations after precipitation of low amounts of LD-associated proteins.

The role of PAT family proteins with regard to LD modification and foam cell formation has been studied in recent years. PLIN2 is a major LD-associated protein that is expressed in different cell types, including macrophage-derived foam cells (Chang and Chan, 2007). In this study, we found decreased PLIN2 protein levels on *Plin1-/-* LDs which might result in the reduced lipid content during foam cell formation (Paul et al., 2008b). Though increased expression of PLIN3 is associated with foam cells formation (Buers et al., 2009), further studies are required to understand the underlying mechanisms.

Numerous studies showed LD-associated proteins regulate many LD functions. The differential expression and identification of several other proteins in the preparations might explain the close neighborhood of LDs with other subcellular organelles. In addition to lipases, PERILIPINs such as PLIN2 and PLIN3 as well as small GTPases, we found differential expression of heat shock proteins, DNA binding proteins including histones and elongation factors, most of which regulate metabolic processes. However, we cannot rule out the possibility of contamination of proteins from neighboring organelles.

In addition to decreased expression of ATGL, CGI-58, Rab18, Rab7 Cathepsin B and PLIN2, we found a number of proteins with varying degree of expression on LDs of *Plin1-/-* compared to Wt foam cells by LC-MS/MS analysis (Tables 2 and 3). In summary, LC-MS/MS constitutes an effective tool to identify LD-associated proteins from macrophage-derived foam cells. However, further studies are required to understand the functional roles of LD associated proteins during foam cell formation.

Table 2. Identification of upregulated lipid droplet-associated proteins

Accession	Description	ΣCoverage	Σ# Unique Peptides	Ratio Plin1(-/-)/Wt	*Ratio Plin1(-/-)/Wt Variability [%]*
Q64433	10 kDa heat shock protein	52.94	6	24.540	150.4
Q9CQX8	28S ribosomal protein S36	44.12	2	6.534	34.6
P62264	40S ribosomal protein S14	9.27	2	12.653	95.7
P62908	40S ribosomal protein S3	17.28	3	45.396	160.6
P14206	40S ribosomal protein SA	33.22	6	26.342	60.9
P99027	60S acidic ribosomal protein P2	70.43	6	23.027	90.0
P35979	60S ribosomal protein L12	21.21	2	19.034	17.8
Q9DCD0	6-phosphogluconate dehydrogenase	13.87	6	24.024	107.2
P20029	78 kDa glucose-regulated protein	38.02	21	12.101	155.4
Q99KI0	Aconitate hydratase, mitochondrial	4.74	2	4.395	138.1
P60710	Actin, cytoplasmic 1	44.53	14	4.779	107.6
P59999	Actin-related protein	16.07	3	122.237	128.2
Q9CPW4	Actin-related protein	31.13	2	75.642	54.0
Q99JY9	Actin-related protein 3	22.49	6	21.852	72.9
P31786	Acyl-CoA-binding protein	27.59	2	9.920	59.0
P40124	Adenylyl cyclase-associated protein 1	21.10	7	9.628	29.7
Q9JII6	Alcohol dehydrogenase [NADP(+)]	26.46	7	35.370	150.0
P47738	Aldehyde dehydrogenase, mitochondrial	18.69	8	20.576	103.1
P45377	Aldose reductase-related protein 2	10.13	2	5.622	59.5
P55302	Alpha-2-macroglobulin receptor-associated protein	23.33	6	8.715	73.1
P57780	Alpha-actinin-4	5.15	3	42.053	127.7
P17182	Alpha-enolase	40.55	14	19.243	137.3
P70295	Ancient ubiquitous protein 1	15.61	6	13.871	198.0
P10107	Annexin A1	41.04	12	21.561	59.3
P07356	Annexin A2	48.97	18	18.782	68.0
O35639	Annexin A3	36.22	12	55.710	72.5
P97429	Annexin A4	33.23	10	24.896	116.4
P48036	Annexin A5	34.48	12	35.480	114.7
P14824	Annexin A6	15.75	7	41.578	128.0
Q8VBT6	Apolipoprotein B receptor	19.21	14	21.793	125.3
Q61176	Arginase-1	34.37	8	67.434	192.4
P05201	Aspartate aminotransferase, cytoplasmic	11.62	4	25.560	101.8
P12265	Beta-glucuronidase	5.40	2	15.723	6.4
P29416	Beta-hexosaminidase subunit alpha	5.30	2	4.914	141.1
P62204	Calmodulin	45.64	6	19.204	67.7
P14211	Calreticulin	26.68	8	16.812	93.4
O35887	Calumenin	6.98	2	7.703	140.5
O70370	Cathepsin S	34.12	8	13.445	151.5
Q9Z1Q5	Chloride intracellular channel protein 1	14.94	2	34.653	114.2
Q68FD5	Clathrin heavy chain 1	2.33	3	46.574	132.3
Q9CQI6	Coactosin-like protein	40.14	6	8.701	83.7
P18760	Cofilin-1	50.60	10	51.897	172.1
O08997	Copper transport protein ATOX1	58.82	4	45.701	7.0
Q62426	Cystatin-B	51.02	6	11.976	106.6
P62897	Cytochrome c, somatic	32.38	4	12.772	17.2

Q9D1A2	Cytosolic non-specific dipeptidase	23.16	8	37.993	151.5
Q99L04	Dehydrogenase/reductase SDR family member 1	64.22	16	1.343	182.8
Q9WVK4	EH domain-containing protein 1	9.74	3	20.951	58.5
P10126	Elongation factor 1-alpha 1	25.76	8	13.878	149.7
P57776	Elongation factor 1-delta	18.86	3	61.025	63.8
P58252	Elongation factor 2	9.79	7	47.720	152.7
P08113	Endoplasmin	14.59	8	25.225	171.2
P60843	Eukaryotic initiation factor 4A-I	15.76	4	49.510	151.8
P63242	Eukaryotic translation initiation factor 5A-1	32.47	5	31.516	67.3
Q3U7R1	Extended synaptotagmin-1	4.49	4	1.599	171.9
P47753	F-actin-capping protein subunit alpha-1	11.54	2	6.440	57.3
P47757	F-actin-capping protein subunit beta	6.86	2	2.069	74.0
P04117	Fatty acid-binding protein, adipocyte	54.55	7	7.353	122.1
Q05816	Fatty acid-binding protein, epidermal	73.33	9	4.449	129.6
P09528	Ferritin heavy chain	17.58	5	2.400	183.2
P29391	Ferritin light chain 1	38.25	5	4.772	42.3
Q8BTM8	Filamin-A	23.35	42	29.428	93.1
Q923D2	Flavin reductase (NADPH)	36.41	6	6.515	154.1
P05064	Fructose-bisphosphate aldolase A	47.25	10	13.886	50.0
P16045	Galectin-1	31.85	4	24.235	95.1
P16110	Galectin-3	26.89	7	2.581	145.2
P13020	Gelsolin	10.26	6	99.996	158.4
P06745	Glucose-6-phosphate isomerase	15.77	7	29.070	15.1
P11352	Glutathione peroxidase 1	37.31	7	62.840	62.2
P47791	Glutathione reductase, mitochondrial	15.20	4	66.875	123.5
P16858	Glyceraldehyde-3-phosphate dehydrogenase	29.73	8	14.218	122.3
O70310	Glycylpeptide N-tetradecanoyltransferase 1	6.45	2	23.497	84.8
Q60631	Growth factor receptor-bound protein 2	11.06	3	11.023	68.1
P62827	GTP-binding nuclear protein Ran	16.67	3	33.023	86.7
Q9R111	Guanine deaminase	8.59	4	18.297	77.2
P63017	Heat shock cognate 71 kDa protein	40.56	22	32.579	116.2
P07901	Heat shock protein HSP 90-alpha	19.78	6	49.950	127.5
P11499	Heat shock protein HSP 90-beta	19.89	6	10.876	70.7
P49710	Hematopoietic lineage cell-specific protein	17.70	7	5.063	55.3
P51859	Hepatoma-derived growth factor	29.96	3	39.503	108.4
Q9Z2X1	Heterogeneous nuclear ribonucleoprotein F	6.51	2	35.966	0.5
O88569	Heterogeneous nuclear ribonucleoproteins A2/B1	20.68	5	15.135	109.9
P63158	High mobility group protein B1	26.51	3	6.996	128.0
P30681	High mobility group protein B2	30.95	4	18.802	19.9
P62748	Hippocalcin-like protein 1	15.54	3	48.194	93.9
P70349	Histidine triad nucleotide-binding protein 1	50.00	3	13.049	127.7
P10853	Histone H2B type 1-F/J/L	16.67	3	125.621	131.6
P62806	Histone H4	40.78	4	150.682	125.7
P11835	Integrin beta-2	7.65	5	2.275	135.3

O88844	Isocitrate dehydrogenase [NADP] cytoplasmic	5.07	2	5.514	122.8
Q6IFX2	Keratin, type I cytoskeletal 42	12.83	4	8.253	172.7
P14733	Lamin-B1	12.41	6	18.009	143.1
Q9ERE7	LDLR chaperone MESD	10.27	2	4.769	74.9
P06151	L-lactate dehydrogenase A chain	32.53	11	17.657	128.8
P19973	Lymphocyte-specific protein 1	13.33	3	4.873	39.6
Q8BYI6	Lysophosphatidylcholine acyltransferase 2	7.90	5	1.985	142.2
P34884	Macrophage migration inhibitory factor	7.83	1	3.914	114.7
P24452	Macrophage-capping protein	27.27	8	19.803	177.7
Q9CXI5	Mesencephalic astrocyte-derived neurotrophic factor	26.82	3	39.442	90.6
P26041	Moesin	26.17	11	7.379	33.0
Q60605	Myosin light polypeptide 6	47.68	7	29.726	76.5
Q3THE2	Myosin regulatory light chain 12B	18.60	3	14.759	133.0
Q8VDD5	Myosin-9	6.38	9	16.279	100.3
P62774	Myotrophin	38.14	3	6.132	117.9
P70441	Na(+)/H(+) exchange regulatory cofactor NHE-RF1	13.24	4	9.121	90.7
P29595	NEDD8	23.46	2	14.931	43.7
Q8BHN3	Neutral alpha-glucosidase AB	2.97	3	29.319	62.3
Q99KQ4	Nicotinamide phosphoribosyltransferase	9.98	4	49.487	79.4
P62960	Nuclease-sensitive element-binding protein 1	15.22	2	4.140	62.2
Q02819	Nucleobindin-1	9.59	3	3.897	42.0
Q01768	Nucleoside diphosphate kinase B	35.53	4	17.270	69.1
Q62422	Osteoclast-stimulating factor 1	20.93	3	9.493	17.8
P17742	Peptidyl-prolyl cis-trans isomerase A	58.54	8	20.367	97.9
P24369	Peptidyl-prolyl cis-trans isomerase B	38.89	7	26.496	170.7
Q9DBG5	Perilipin-3	11.44	3	1.558	171.9
P35700	Peroxiredoxin-1	75.38	16	8.028	103.2
P99029	Peroxiredoxin-5, mitochondrial	45.24	9	46.459	111.6
O08709	Peroxiredoxin-6	35.27	7	47.895	126.5
P51660	Peroxisomal multifunctional enzyme type 2	5.71	2	2.583	106.4
P70296	Phosphatidylethanolamine-binding protein 1	28.34	3	1.532	44.5
Q8BSF4	Phosphatidylserine decarboxylase proenzyme	7.64	3	1.902	100.7
P09411	Phosphoglycerate kinase 1	24.70	7	11.581	78.5
Q9DBJ1	Phosphoglycerate mutase 1	51.57	11	29.326	135.5
Q61233	Plastin-2	50.72	24	31.615	144.6
Q8K124	Pleckstrin homology domain-containing family O member 2	10.30	2	1.004	129.1
P0CG49	Polyubiquitin-B	64.26	6	15.087	167.3
P48678	Prelamin-A/C	13.53	7	46.054	144.5
P62962	Profilin-1	59.29	7	77.796	138.9
Q9R0Q7	Prostaglandin E synthase 3	15.00	2	20.175	52.9
Q91YR9	Prostaglandin reductase 1	4.56	2	13.900	67.6
Q4VAA2	Protein CDV3	22.42	3	48.986	118.4
P27773	Protein disulfide-isomerase A3	48.32	21	13.118	110.2
P08003	Protein disulfide-isomerase A4	16.77	8	19.745	167.2

P09103	Protein disulfide-isomerase	40.67	17	13.890	134.3
Q9DCL8	Protein phosphatase inhibitor 2	17.48	3	10.485	78.9
P08207	Protein S100-A10	17.53	2	124.922	167.9
P97352	Protein S100-A13	33.67	3	27.396	108.5
P31725	Protein S100-A9	19.47	2	15.177	56.3
Q9EQU5	Protein SET	10.73	3	269.203	120.6
P23492	Purine nucleoside phosphorylase	11.42	2	43.566	113.5
P52480	Pyruvate kinase isozymes M1/M2	38.42	18	35.264	146.6
Q05144	Ras-related C3 botulinum toxin substrate 2	23.96	2	65.776	141.4
Q91V41	Ras-related protein Rab-14	49.30	8	2.782	213.3
Q99PT1	Rho GDP-dissociation inhibitor 1	34.31	6	85.293	140.9
Q61599	Rho GDP-dissociation inhibitor 2	40.00	4	10.735	68.3
Q91VI7	Ribonuclease inhibitor	30.04	10	35.269	77.7
P84104	Serine/arginine-rich splicing factor 3	11.59	2	6.788	118.7
Q8BL97	Serine/arginine-rich splicing factor 7	17.23	4	7.495	75.7
Q76MZ3	Serine/threonine-protein phosphatase 2A 65 kDa regulatory subunit A alpha isoform	6.79	2	26.396	65.5
Q9R0P3	S-formylglutathione hydrolase	14.54	3	30.054	47.9
O70493	Sorting nexin-12	20.00	3	42.599	92.7
O70492	Sorting nexin-3	14.81	2	59.592	138.9
Q9D8U8	Sorting nexin-5	7.43	3	16.593	97.7
Q60864	Stress-induced-phosphoprotein 1	10.31	4	81.020	129.8
Q61207	Sulfated glycoprotein 1	28.37	14	18.598	135.2
P08228	Superoxide dismutase [Cu-Zn]	32.47	4	2.286	92.6
Q9D5V6	Synapse-associated protein 1	19.18	3	23.600	5.1
P26039	Talin-1	6.26	10	30.388	92.5
P42932	T-complex protein 1 subunit theta	6.39	3	38.918	92.8
Q9CQU0	Thioredoxin domain-containing protein 12	8.82	1	5.531	101.0
P10639	Thioredoxin	34.29	3	52.919	133.8
Q9JMH6	Thioredoxin reductase 1, cytoplasmic	5.06	3	37.432	125.7
Q93092	Transaldolase	21.66	8	64.150	84.4
Q6Y685	Transforming acidic coiled-coil-containing protein 1	7.36	3	20.793	141.1
Q9WVA4	Transgelin-2	31.66	6	13.278	121.9
Q01853	Transitional endoplasmic reticulum ATPase	18.11	11	26.567	131.8
P40142	Transketolase	34.35	17	48.027	67.9
P63028	Translationally-controlled tumor protein	23.26	3	103.866	44.6
P17751	Triosephosphate isomerase	30.77	8	24.732	144.3
P21107	Tropomyosin alpha-3 chain	27.11	8	185.727	125.8
Q6IRU2	Tropomyosin alpha-4 chain	26.61	7	19.629	99.2
P68373	Tubulin alpha-1C chain	19.60	6	32.466	130.7
Q62393	Tumor protein D52	31.70	4	10.135	129.9
P29351	Tyrosine-protein phosphatase non-receptor type 6	8.57	4	47.984	105.0
P68037	Ubiquitin-conjugating enzyme E2 L3	15.58	2	12.520	0.5
Q9DBP5	UMP-CMP kinase	16.33	3	93.622	141.4
Q8BVA5	UPF0554 protein C2orf43 homolog	10.43	3	2.660	123.3
P20152	Vimentin	43.78	22	15.357	109.8

P50516	V-type proton ATPase catalytic subunit A	19.29	9	1.023	138.4
P62814	V-type proton ATPase subunit B, brain isoform	24.27	10	12.884	214.2
P50518	V-type proton ATPase subunit E 1	18.14	5	6.449	162.4
Q9D1K2	V-type proton ATPase subunit F	18.49	3	53.086	171.3
O88342	WD repeat-containing protein 1	13.37	8	67.395	131.2

Table 3. Identification of downregulated lipid droplet-associated proteins

Accession	Description	ΣCoverage	Σ# Unique Peptides	*Ratio Plin1(-/-)/Wt*	*Ratio Plin1(-/-)/Wt Variability [%]*
O70404	Vesicle-associated membrane protein 8	23.76	2	0.009	43.3
O88653	Ragulator complex protein LAMTOR3	18.55	2	0.018	0.4
O88876	Short-chain dehydrogenase/reductase 3	37.09	12	0.547	155.8
P02535	Keratin, type I cytoskeletal 10	12.11	5	0.016	124.7
P04104	Keratin, type II cytoskeletal 1	5.18	2	0.441	17.5
P07724	Serum albumin	4.44	2	0.249	69.5
P08905	Lysozyme C-2	39.86	5	0.107	151.5
P10605	Cathepsin B	29.50	8	0.197	112.9
P11438	Lysosome-associated membrane glycoprotein 1	10.34	4	0.016	119.9
P18242	Cathepsin D	34.15	13	0.010	82.2
P24270	Catalase	14.99	6	0.217	123.3
P28798	Granulins	20.71	7	0.227	54.7
P35293	Ras-related protein Rab-18	46.60	9	0.032	102.2
P37040	NADPH--cytochrome P450 reductase	3.24	1	0.537	0.5
P43883	Perilipin-2	42.12	13	0.198	132.2
P46638	Ras-related protein Rab-11B	28.44	5	0.210	139.7
P51150	Ras-related protein Rab-7a	66.67	15	0.077	136.5
P61027	Ras-related protein Rab-10	22.50	2	0.177	121.9
P84096	Rho-related GTP-binding protein RhoG	31.94	4	0.021	99.5
P97449	Aminopeptidase N	3.42	2	0.019	100.2
Q08857	Platelet glycoprotein 4	9.32	3	0.013	109.1
Q3TDN2	FAS-associated factor 2	25.39	8	0.096	149.9
Q3TTY5	Keratin, type II cytoskeletal 2 epidermal	6.22	4	0.162	102.2
Q60766	Immunity-related GTPase family M protein 1	5.13	2	0.013	105.8
Q62159	Rho-related GTP-binding protein RhoC	7.77	2	0.213	132.1
Q62465	Synaptic vesicle membrane protein VAT-1 homolog	44.09	15	0.104	225.1
Q6ZWY3	40S ribosomal protein S27-like	13.10	1	0.577	18.9
Q8BJ56	Patatin-like phospholipase domain-containing protein 2	33.95	14	0.013	122.7
Q8BUE4	Apoptosis-inducing factor 2	15.82	6	0.008	63.0
Q8R127	Saccharopine dehydrogenase-like oxidoreductase	5.36	2	0.206	122.0
Q8VBZ0	Dehydrogenase/reductase SDR family	10.45	3	0.228	105.7

	member on chromosome X homolog				
Q91XV3	Brain acid soluble protein 1	35.84	4	0.255	136.3
Q922U2	Keratin, type II cytoskeletal 5	9.14	3	0.138	111.9
Q99JI6	Ras-related protein Rap-1b	33.15	5	0.014	13.9
Q99P91	Transmembrane glycoprotein NMB	4.70	3	0.016	80.9
Q9CQW2	ADP-ribosylation factor-like protein 8B	22.58	4	0.283	83.5
Q9CR51	V-type proton ATPase subunit G 1	13.56	2	0.260	129.7
Q9DBL9	1-acylglycerol-3-phosphate O-acyltransferase ABHD5	14.25	3	0.013	66.2
Q9DCN2	NADH-cytochrome b5 reductase 3	49.50	12	0.059	187.8
Q9EQ06	Estradiol 17-beta-dehydrogenase 11	52.68	15	0.063	204.5
Q9EQC1	3 beta-hydroxysteroid dehydrogenase type 7	10.84	3	0.009	103.6
Q9EQK5	Major vault protein	4.53	3	0.189	143.7
Q9QUJ7	Long-chain-fatty-acid--CoA ligase 4	14.49	7	0.016	104.4
Q9WUU7	Cathepsin Z	7.52	2	0.434	19.4
Q9Z0J0	Epididymal secretory protein E1	18.79	2	0.669	0.8
Q9Z2K1	Keratin, type I cytoskeletal 16	10.02	2	0.252	88.0

17. Reference

AHMADIAN, M., ABBOTT, M. J., TANG, T., HUDAK, C. S., KIM, Y., BRUSS, M., HELLERSTEIN, M. K., LEE, H. Y., SAMUEL, V. T., SHULMAN, G. I., WANG, Y., DUNCAN, R. E., KANG, C. & SUL, H. S. 2011. Desnutrin/ATGL is regulated by AMPK and is required for a brown adipose phenotype. *Cell Metab,* 13**,** 739-48.

ALBINI, A., DELL'EVA, R., VENE, R., FERRARI, N., BUHLER, D. R., NOONAN, D. M. & FASSINA, G. 2006. Mechanisms of the antiangiogenic activity by the hop flavonoid xanthohumol: NF-kappaB and Akt as targets. *FASEB J,* 20**,** 527-9.

ANDERSSON, L., BOSTROM, P., ERICSON, J., RUTBERG, M., MAGNUSSON, B., MARCHESAN, D., RUIZ, M., ASP, L., HUANG, P., FROHMAN, M. A., BOREN, J. & OLOFSSON, S. O. 2006. PLD1 and ERK2 regulate cytosolic lipid droplet formation. *J Cell Sci,* 119**,** 2246-57.

ATSHAVES, B. P., STOREY, S. M., MCINTOSH, A. L., PETRESCU, A. D., LYUKSYUTOVA, O. I., GREENBERG, A. S. & SCHROEDER, F. 2001. Sterol carrier protein-2 expression modulates protein and lipid composition of lipid droplets. *J Biol Chem,* 276**,** 25324-35.

AUSTIN, M. A. 1994. Small, dense low-density lipoprotein as a risk factor for coronary heart disease. *Int J Clin Lab Res,* 24**,** 187-92.

AVULA, B., GANZERA, M., WARNICK, J. E., FELTENSTEIN, M. W., SUFKA, K. J. & KHAN, I. A. 2004. High-performance liquid chromatographic determination of xanthohumol in rat plasma, urine, and fecal samples. *J Chromatogr Sci,* 42**,** 378-82.

BASU, S. K., GOLDSTEIN, J. L., ANDERSON, G. W. & BROWN, M. S. 1976. Degradation of cationized low density lipoprotein and regulation of cholesterol metabolism in homozygous familial hypercholesterolemia fibroblasts. *Proc Natl Acad Sci U S A,* 73**,** 3178-82.

BENELLI, R., VENE, R., CIARLO, M., CARLONE, S., BARBIERI, O. & FERRARI, N. 2012. The AKT/NF-kappaB inhibitor xanthohumol is a potent anti-lymphocytic leukemia drug overcoming chemoresistance and cell infiltration. *Biochem Pharmacol,* 83**,** 1634-42.

BICKEL, P. E., TANSEY, J. T. & WELTE, M. A. 2009. PAT proteins, an ancient family of lipid droplet proteins that regulate cellular lipid stores. *Biochim Biophys Acta,* 1791**,** 419-40.

BLANCHETTE-MACKIE, E. J., DWYER, N. K., BARBER, T., COXEY, R. A., TAKEDA, T., RONDINONE, C. M., THEODORAKIS, J. L., GREENBERG, A. S. & LONDOS, C. 1995. Perilipin is located on the surface layer of intracellular lipid droplets in adipocytes. *J Lipid Res,* 36**,** 1211-26.

BOERSEMA, P. J., RAIJMAKERS, R., LEMEER, S., MOHAMMED, S. & HECK, A. J. 2009. Multiplex peptide stable isotope dimethyl labeling for quantitative proteomics. *Nat Protoc,* 4**,** 484-94.

BORING, L., GOSLING, J., CLEARY, M. & CHARO, I. F. 1998. Decreased lesion formation in CCR2-/- mice reveals a role for chemokines in the initiation of atherosclerosis. *Nature,* 394**,** 894-7.

BOSTROM, K., BOREN, J., WETTESTEN, M., SJOBERG, A., BONDJERS, G., WIKLUND, O., CARLSSON, P. & OLOFSSON, S. O. 1988. Studies on the assembly of apo B-100-containing lipoproteins in HepG2 cells. *J Biol Chem,* 263**,** 4434-42.

BOZZA, P. T., YU, W., PENROSE, J. F., MORGAN, E. S., DVORAK, A. M. & WELLER, P. F. 1997. Eosinophil lipid bodies: specific, inducible intracellular sites for enhanced eicosanoid formation. *J Exp Med,* 186**,** 909-20.

BRASAEMLE, D. L. 2007. Thematic review series: adipocyte biology. The perilipin family of structural lipid droplet proteins: stabilization of lipid droplets and control of lipolysis. *J Lipid Res,* 48**,** 2547-59.

BRASAEMLE, D. L., BARBER, T., WOLINS, N. E., SERRERO, G., BLANCHETTE-MACKIE, E. J. & LONDOS, C. 1997. Adipose differentiation-related protein is an ubiquitously expressed lipid storage droplet-associated protein. *J Lipid Res,* 38**,** 2249-63.

BRASAEMLE, D. L., RUBIN, B., HARTEN, I. A., GRUIA-GRAY, J., KIMMEL, A. R. & LONDOS, C. 2000. Perilipin A increases triacylglycerol storage by decreasing the rate of triacylglycerol hydrolysis. *J Biol Chem,* 275**,** 38486-93.

BRASAEMLE, D. L., SUBRAMANIAN, V., GARCIA, A., MARCINKIEWICZ, A. & ROTHENBERG, A. 2009. Perilipin A and the control of triacylglycerol metabolism. *Mol Cell Biochem,* 326**,** 15-21.

BRESLOW, J. L. 1996. Mouse models of atherosclerosis. *Science,* 272**,** 685-8.

BROWN, M. S. & GOLDSTEIN, J. L. 1979. Receptor-mediated endocytosis: insights from the lipoprotein receptor system. *Proc Natl Acad Sci U S A,* 76**,** 3330-7.

BROWN, M. S. & GOLDSTEIN, J. L. 1984. How LDL receptors influence cholesterol and atherosclerosis. *Sci Am,* 251**,** 58-66.

BROWN, M. S. & GOLDSTEIN, J. L. 1999. A proteolytic pathway that controls the cholesterol content of membranes, cells, and blood. *Proc Natl Acad Sci U S A,* 96**,** 11041-8.

BROWNING, J. D. & HORTON, J. D. 2004. Molecular mediators of hepatic steatosis and liver injury. *J Clin Invest,* 114**,** 147-52.

BUECHLER, C., RITTER, M., DUONG, C. Q., ORSO, E., KAPINSKY, M. & SCHMITZ, G. 2001. Adipophilin is a sensitive marker for lipid loading in human blood monocytes. *Biochim Biophys Acta,* 1532**,** 97-104.

BUERS, I., ROBENEK, H., LORKOWSKI, S., NITSCHKE, Y., SEVERS, N. J. & HOFNAGEL, O. 2009. TIP47, a lipid cargo protein involved in macrophage triglyceride metabolism. *Arterioscler Thromb Vasc Biol,* 29**,** 767-73.

CASASCHI, A., MAIYOH, G. K., RUBIO, B. K., LI, R. W., ADELI, K. & THERIAULT, A. G. 2004. The chalcone xanthohumol inhibits triglyceride and apolipoprotein B secretion in HepG2 cells. *J Nutr,* 134**,** 1340-6.

CHANDAK, P. G., RADOVIC, B., AFLAKI, E., KOLB, D., BUCHEBNER, M., FROHLICH, E., MAGNES, C., SINNER, F., HAEMMERLE, G., ZECHNER, R., TABAS, I., LEVAK-FRANK, S. & KRATKY, D. 2010. Efficient phagocytosis requires triacylglycerol hydrolysis by adipose triglyceride lipase. *J Biol Chem,* 285**,** 20192-201.

CHO, Y. C., KIM, H. J., KIM, Y. J., LEE, K. Y., CHOI, H. J., LEE, I. S. & KANG, B. Y. 2008. Differential anti-inflammatory pathway by xanthohumol in IFN-gamma and LPS-activated macrophages. *Int Immunopharmacol,* 8**,** 567-73.

CHO, Y. C., YOU, S. K., KIM, H. J., CHO, C. W., LEE, I. S. & KANG, B. Y. 2010. Xanthohumol inhibits IL-12 production and reduces chronic allergic contact dermatitis. *Int Immunopharmacol,* 10**,** 556-61.

CLARKE, P. R. & HARDIE, D. G. 1990. Regulation of HMG-CoA reductase: identification of the site phosphorylated by the AMP-activated protein kinase in vitro and in intact rat liver. *EMBO J,* 9**,** 2439-46.

DANAEI, G., FINUCANE, M. M., LU, Y., SINGH, G. M., COWAN, M. J., PACIOREK, C. J., LIN, J. K., FARZADFAR, F., KHANG, Y. H., STEVENS, G. A., RAO, M., ALI, M. K., RILEY, L. M., ROBINSON, C. A., EZZATI, M. & GLOBAL BURDEN OF METABOLIC RISK FACTORS OF CHRONIC DISEASES COLLABORATING, G. 2011. National, regional, and global trends in fasting plasma glucose and diabetes prevalence since 1980: systematic analysis of health examination surveys and epidemiological studies with 370 country-years and 2.7 million participants. *Lancet,* 378**,** 31-40.

DECLEVES, A. E., MATHEW, A. V., CUNARD, R. & SHARMA, K. 2011. AMPK mediates the initiation of kidney disease induced by a high-fat diet. *J Am Soc Nephrol,* 22**,** 1846-55.

DEEB, D., GAO, X., JIANG, H., ARBAB, A. S., DULCHAVSKY, S. A. & GAUTAM, S. C. 2010. Growth inhibitory and apoptosis-inducing effects of xanthohumol, a prenylated chalone present in hops, in human prostate cancer cells. *Anticancer Res,* 30**,** 3333-9.

DELL'EVA, R., AMBROSINI, C., VANNINI, N., PIAGGIO, G., ALBINI, A. & FERRARI, N. 2007. AKT/NF-kappaB inhibitor xanthohumol targets cell growth and angiogenesis in hematologic malignancies. *Cancer,* 110**,** 2007-11.

DOBRZYN, P., DOBRZYN, A., MIYAZAKI, M., COHEN, P., ASILMAZ, E., HARDIE, D. G., FRIEDMAN, J. M. & NTAMBI, J. M. 2004. Stearoyl-CoA desaturase 1 deficiency increases fatty acid oxidation by activating AMP-activated protein kinase in liver. *Proc Natl Acad Sci U S A,* 101**,** 6409-14.

DORN, C., BATAILLE, F., GAEBELE, E., HEILMANN, J. & HELLERBRAND, C. 2010. Xanthohumol feeding does not impair organ function and homoeostasis in mice. *Food Chem Toxicol,* 48**,** 1890-7.

DORN, C., MASSINGER, S., WUZIK, A., HEILMANN, J. & HELLERBRAND, C. 2012. Xanthohumol suppresses inflammatory response to warm ischemia-reperfusion induced liver injury. *Exp Mol Pathol*.

EGAN, J. J., GREENBERG, A. S., CHANG, M. K., WEK, S. A., MOOS, M. C., JR. & LONDOS, C. 1992. Mechanism of hormone-stimulated lipolysis in adipocytes: translocation of hormone-sensitive lipase to the lipid storage droplet. *Proc Natl Acad Sci U S A,* 89**,** 8537-41.

EWART, M. A., KOHLHAAS, C. F. & SALT, I. P. 2008. Inhibition of tumor necrosis factor alpha-stimulated monocyte adhesion to human aortic endothelial cells by AMP-activated protein kinase. *Arterioscler Thromb Vasc Biol,* 28**,** 2255-7.

FINUCANE, M. M., STEVENS, G. A., COWAN, M. J., DANAEI, G., LIN, J. K., PACIOREK, C. J., SINGH, G. M., GUTIERREZ, H. R., LU, Y., BAHALIM, A. N., FARZADFAR, F., RILEY, L. M., EZZATI, M. & GLOBAL BURDEN OF METABOLIC RISK FACTORS OF CHRONIC DISEASES COLLABORATING, G. 2011. National, regional, and global trends in body-mass index since 1980: systematic analysis of health examination surveys and epidemiological studies with 960 country-years and 9.1 million participants. *Lancet,* 377**,** 557-67.

FOLCH, J., LEES, M. & SLOANE STANLEY, G. H. 1957. A simple method for the isolation and purification of total lipides from animal tissues. *J Biol Chem,* 226**,** 497-509.

FUJIMOTO, T., KOGO, H., ISHIGURO, K., TAUCHI, K. & NOMURA, R. 2001. Caveolin-2 is targeted to lipid droplets, a new "membrane domain" in the cell. *J Cell Biol,* 152**,** 1079-85.

GAO, X., DEEB, D., LIU, Y., GAUTAM, S., DULCHAVSKY, S. A. & GAUTAM, S. C. 2009. Immunomodulatory activity of xanthohumol: inhibition of T cell proliferation, cell-mediated cytotoxicity and Th1 cytokine production through suppression of NF-kappaB. *Immunopharmacol Immunotoxicol,* 31**,** 477-84.

GOSLING, J., SLAYMAKER, S., GU, L., TSENG, S., ZLOT, C. H., YOUNG, S. G., ROLLINS, B. J. & CHARO, I. F. 1999. MCP-1 deficiency reduces susceptibility to atherosclerosis in mice that overexpress human apolipoprotein B. *J Clin Invest,* 103**,** 773-8.

GRANNEMAN, J. G., MOORE, H. P., GRANNEMAN, R. L., GREENBERG, A. S., OBIN, M. S. & ZHU, Z. 2007. Analysis of lipolytic protein trafficking and interactions in adipocytes. *J Biol Chem,* 282**,** 5726-35.

GREENBERG, A. S., EGAN, J. J., WEK, S. A., GARTY, N. B., BLANCHETTE-MACKIE, E. J. & LONDOS, C. 1991. Perilipin, a major hormonally regulated adipocyte-specific

phosphoprotein associated with the periphery of lipid storage droplets. *J Biol Chem,* 266**,** 11341-6.

GREENBERG, A. S., EGAN, J. J., WEK, S. A., MOOS, M. C., JR., LONDOS, C. & KIMMEL, A. R. 1993. Isolation of cDNAs for perilipins A and B: sequence and expression of lipid droplet-associated proteins of adipocytes. *Proc Natl Acad Sci U S A,* 90**,** 12035-9.

GU, J. Q., WANG, D. F., YAN, X. G., ZHONG, W. L., ZHANG, J., FAN, B. & IKUYAMA, S. 2010. A Toll-like receptor 9-mediated pathway stimulates perilipin 3 (TIP47) expression and induces lipid accumulation in macrophages. *Am J Physiol Endocrinol Metab,* 299**,** E593-600.

HAHN-WINDGASSEN, A., NOGUEIRA, V., CHEN, C. C., SKEEN, J. E., SONENBERG, N. & HAY, N. 2005. Akt activates the mammalian target of rapamycin by regulating cellular ATP level and AMPK activity. *J Biol Chem,* 280**,** 32081-9.

HANSKE, L., LOH, G., SCZESNY, S., BLAUT, M. & BRAUNE, A. 2010. Recovery and metabolism of xanthohumol in germ-free and human microbiota-associated rats. *Mol Nutr Food Res,* 54**,** 1405-13.

HANSSON, G. K. & HERMANSSON, A. 2011. The immune system in atherosclerosis. *Nat Immunol,* 12**,** 204-12.

HEID, H. W., MOLL, R., SCHWETLICK, I., RACKWITZ, H. R. & KEENAN, T. W. 1998. Adipophilin is a specific marker of lipid accumulation in diverse cell types and diseases. *Cell Tissue Res,* 294**,** 309-21.

HEID, H. W., SCHNOLZER, M. & KEENAN, T. W. 1996. Adipocyte differentiation-related protein is secreted into milk as a constituent of milk lipid globule membrane. *Biochem J,* 320 (Pt 3)**,** 1025-30.

HIRATA, H., YIMIN, SEGAWA, S., OZAKI, M., KOBAYASHI, N., SHIGYO, T. & CHIBA, H. 2012a. Xanthohumol Prevents Atherosclerosis by Reducing Arterial Cholesterol Content via CETP and Apolipoprotein E in CETP-Transgenic Mice. *PLoS One,* 7**,** 8.

HIRATA, H., YIMIN, SEGAWA, S., OZAKI, M., KOBAYASHI, N., SHIGYO, T. & CHIBA, H. 2012b. Xanthohumol prevents atherosclerosis by reducing arterial cholesterol content via CETP and apolipoprotein E in CETP-transgenic mice. *PLoS One,* 7**,** e49415.

HOEKSTRA, M., KRUIJT, J. K., VAN ECK, M. & VAN BERKEL, T. J. 2003. Specific gene expression of ATP-binding cassette transporters and nuclear hormone receptors in rat liver parenchymal, endothelial, and Kupffer cells. *J Biol Chem,* 278**,** 25448-53.

HORTON, J. D., GOLDSTEIN, J. L. & BROWN, M. S. 2002. SREBPs: activators of the complete program of cholesterol and fatty acid synthesis in the liver. *J Clin Invest,* 109**,** 1125-31.

HSU, J. L., HUANG, S. Y., SHIEA, J. T., HUANG, W. Y. & CHEN, S. H. 2005. Beyond quantitative proteomics: signal enhancement of the a1 ion as a mass tag for peptide sequencing using dimethyl labeling. *J Proteome Res,* 4**,** 101-8.

HUSSONG, R., FRANK, N., KNAUFT, J., ITTRICH, C., OWEN, R., BECKER, H. & GERHAUSER, C. 2005. A safety study of oral xanthohumol administration and its influence on fertility in Sprague Dawley rats. *Mol Nutr Food Res,* 49**,** 861-7.

ISHIBASHI, S., GOLDSTEIN, J. L., BROWN, M. S., HERZ, J. & BURNS, D. K. 1994. Massive xanthomatosis and atherosclerosis in cholesterol-fed low density lipoprotein receptor-negative mice. *J Clin Invest,* 93**,** 1885-93.

JAWIEN, J., NASTALEK, P. & KORBUT, R. 2004. Mouse models of experimental atherosclerosis. *J Physiol Pharmacol,* 55**,** 503-17.

JEONG, H. W., HSU, K. C., LEE, J. W., HAM, M., HUH, J. Y., SHIN, H. J., KIM, W. S. & KIM, J. B. 2009. Berberine suppresses proinflammatory responses through AMPK activation in macrophages. *Am J Physiol Endocrinol Metab,* 296**,** E955-64.

JI, A., WROBLEWSKI, J. M., CAI, L., DE BEER, M. C., WEBB, N. R. & VAN DER WESTHUYZEN, D. R. 2012. Nascent HDL formation in hepatocytes and role of ABCA1, ABCG1, and SR-BI. *J Lipid Res,* 53**,** 446-55.

KENNEDY, M. A., BARRERA, G. C., NAKAMURA, K., BALDAN, A., TARR, P., FISHBEIN, M. C., FRANK, J., FRANCONE, O. L. & EDWARDS, P. A. 2005. ABCG1 has a critical role in mediating cholesterol efflux to HDL and preventing cellular lipid accumulation. *Cell Metab,* 1**,** 121-31.

KERNOHAN, E. A. & LEPHERD, E. E. 1969. Size distribution of fat globules in cow's milk during milking, measured with a Coulter counter. *Journal of Dairy Research,* 36**,** 177-182.

KERNOHAN, E. A. A. L., E. E. 1969. Size distribution of fat globules in cow's milk during milking, measured with a Coulter counter. *Journal of Dairy Research,* 36**,** 177-182.

KHERA, A. V., CUCHEL, M., DE LA LLERA-MOYA, M., RODRIGUES, A., BURKE, M. F., JAFRI, K., FRENCH, B. C., PHILLIPS, J. A., MUCKSAVAGE, M. L., WILENSKY, R. L., MOHLER, E. R., ROTHBLAT, G. H. & RADER, D. J. 2011. Cholesterol efflux capacity, high-density lipoprotein function, and atherosclerosis. *N Engl J Med,* 364**,** 127-35.

KIMMEL, A. R., BRASAEMLE, D. L., MCANDREWS-HILL, M., SZTALRYD, C. & LONDOS, C. 2010. Adoption of PERILIPIN as a unifying nomenclature for the mammalian PAT-family of intracellular lipid storage droplet proteins. *J Lipid Res,* 51**,** 468-71.

KNOWLES, J. W. & MAEDA, N. 2000. Genetic modifiers of atherosclerosis in mice. *Arterioscler Thromb Vasc Biol,* 20**,** 2336-45.

LAGE, R., DIEGUEZ, C., VIDAL-PUIG, A. & LOPEZ, M. 2008. AMPK: a metabolic gauge regulating whole-body energy homeostasis. *Trends Mol Med,* 14**,** 539-49.

LAMMERS, B., CHANDAK, P. G., AFLAKI, E., VAN PUIJVELDE, G. H., RADOVIC, B., HILDEBRAND, R. B., MEURS, I., OUT, R., KUIPER, J., VAN BERKEL, T. J., KOLB, D., HAEMMERLE, G., ZECHNER, R., LEVAK-FRANK, S., VAN ECK, M. & KRATKY, D. 2011. Macrophage adipose triglyceride lipase deficiency attenuates atherosclerotic lesion development in low-density lipoprotein receptor knockout mice. *Arterioscler Thromb Vasc Biol,* 31**,** 67-73.

LANGLOIS, D., FORCHERON, F., LI, J. Y., DEL CARMINE, P., NEGGAZI, S. & BEYLOT, M. 2011. Increased atherosclerosis in mice deficient in perilipin1. *Lipids Health Dis,* 10**,** 169.

LARIGAUDERIE, G., BOUHLEL, M. A., FURMAN, C., JAYE, M., FRUCHART, J. C. & ROUIS, M. 2006. Perilipin, a potential substitute for adipophilin in triglyceride storage in human macrophages. *Atherosclerosis,* 189**,** 142-8.

LARIGAUDERIE, G., FURMAN, C., JAYE, M., LASSELIN, C., COPIN, C., FRUCHART, J. C., CASTRO, G. & ROUIS, M. 2004. Adipophilin enhances lipid accumulation and prevents lipid efflux from THP-1 macrophages: potential role in atherogenesis. *Arterioscler Thromb Vasc Biol,* 24**,** 504-10.

LASS, A., ZIMMERMANN, R., HAEMMERLE, G., RIEDERER, M., SCHOISWOHL, G., SCHWEIGER, M., KIENESBERGER, P., STRAUSS, J. G., GORKIEWICZ, G. & ZECHNER, R. 2006. Adipose triglyceride lipase-mediated lipolysis of cellular fat stores is activated by CGI-58 and defective in Chanarin-Dorfman Syndrome. *Cell Metab,* 3**,** 309-19.

LEE, Y. M., HSIEH, K. H., LU, W. J., CHOU, H. C., CHOU, D. S., LIEN, L. M., SHEU, J. R. & LIN, K. H. 2012. Xanthohumol, a Prenylated Flavonoid from Hops (Humulus lupulus), Prevents Platelet Activation in Human Platelets. *Evid Based Complement Alternat Med,* 2012**,** 852362.

LEGETTE, L., MA, L., REED, R. L., MIRANDA, C. L., CHRISTENSEN, J. M., RODRIGUEZ-PROTEAU, R. & STEVENS, J. F. 2012a. Pharmacokinetics of

xanthohumol and metabolites in rats after oral and intravenous administration. *Mol Nutr Food Res,* 56**,** 466-74.

LEGETTE, L. L., MORENO LUNA, A. Y., REED, R. L., MIRANDA, C. L., BOBE, G., PROTEAU, R. R. & STEVENS, J. F. 2012b. Xanthohumol lowers body weight and fasting plasma glucose in obese male Zucker fa/fa rats. *Phytochemistry*.

LEWIS, G. F. & RADER, D. J. 2005. New insights into the regulation of HDL metabolism and reverse cholesterol transport. *Circ Res,* 96**,** 1221-32.

LI, H., SONG, Y., LI, F., ZHANG, L., GU, Y., ZHANG, L., JIANG, L., DONG, W., YE, J. & LI, Q. 2010. Identification of lipid droplet-associated proteins in the formation of macrophage-derived foam cells using microarrays. *Int J Mol Med,* 26**,** 231-9.

LI, Y., XU, S., MIHAYLOVA, M. M., ZHENG, B., HOU, X., JIANG, B., PARK, O., LUO, Z., LEFAI, E., SHYY, J. Y., GAO, B., WIERZBICKI, M., VERBEUREN, T. J., SHAW, R. J., COHEN, R. A. & ZANG, M. 2011. AMPK phosphorylates and inhibits SREBP activity to attenuate hepatic steatosis and atherosclerosis in diet-induced insulin-resistant mice. *Cell Metab,* 13**,** 376-88.

LIBBY, P. 2002. Inflammation in atherosclerosis. *Nature,* 420**,** 868-74.

LIBBY, P. 2006. Inflammation and cardiovascular disease mechanisms. *Am J Clin Nutr,* 83**,** 456S-460S.

LONDOS, C., BRASAEMLE, D. L., SCHULTZ, C. J., SEGREST, J. P. & KIMMEL, A. R. 1999. Perilipins, ADRP, and other proteins that associate with intracellular neutral lipid droplets in animal cells. *Semin Cell Dev Biol,* 10**,** 51-8.

LONG, Y. C. & ZIERATH, J. R. 2006. AMP-activated protein kinase signaling in metabolic regulation. *J Clin Invest,* 116**,** 1776-83.

LOW, H., HOANG, A. & SVIRIDOV, D. 2012. Cholesterol efflux assay. *J Vis Exp***,** e3810.

LU, X., GRUIA-GRAY, J., COPELAND, N. G., GILBERT, D. J., JENKINS, N. A., LONDOS, C. & KIMMEL, A. R. 2001. The murine perilipin gene: the lipid droplet-associated perilipins derive from tissue-specific, mRNA splice variants and define a gene family of ancient origin. *Mamm Genome,* 12**,** 741-9.

LUPINACCI, E., MEIJERINK, J., VINCKEN, J. P., GABRIELE, B., GRUPPEN, H. & WITKAMP, R. F. 2009. Xanthohumol from hop (Humulus lupulus L.) is an efficient inhibitor of monocyte chemoattractant protein-1 and tumor necrosis factor-alpha release in LPS-stimulated RAW 264.7 mouse macrophages and U937 human monocytes. *J Agric Food Chem,* 57**,** 7274-81.

MAO, J., DEMAYO, F. J., LI, H., ABU-ELHEIGA, L., GU, Z., SHAIKENOV, T. E., KORDARI, P., CHIRALA, S. S., HEIRD, W. C. & WAKIL, S. J. 2006. Liver-specific deletion of acetyl-CoA carboxylase 1 reduces hepatic triglyceride accumulation without affecting glucose homeostasis. *Proc Natl Acad Sci U S A,* 103**,** 8552-7.

MARTIN, S. & PARTON, R. G. 2006. Lipid droplets: a unified view of a dynamic organelle. *Nat Rev Mol Cell Biol,* 7**,** 373-8.

MARTINEZ-BOTAS, J., ANDERSON, J. B., TESSIER, D., LAPILLONNE, A., CHANG, B. H., QUAST, M. J., GORENSTEIN, D., CHEN, K. H. & CHAN, L. 2000. Absence of perilipin results in leanness and reverses obesity in Lepr(db/db) mice. *Nat Genet,* 26**,** 474-9.

MATSUMOTO, K., MATSUMOTO, K., NAKAMURA, T. & KRAMER, R. H. 1994. Hepatocyte growth factor/scatter factor induces tyrosine phosphorylation of focal adhesion kinase (p125FAK) and promotes migration and invasion by oral squamous cell carcinoma cells. *J Biol Chem,* 269**,** 31807-13.

MCMANAMAN, J. L., BALES, E. S., ORLICKY, D. J., JACKMAN, M., MACLEAN, P. S., CAIN, S., CRUNK, A. E., MANSUR, A., GRAHAM, C. E., BOWMAN, T. A. & GREENBERG, A. S. 2013. Perilipin-2-null mice are protected against diet-induced obesity, adipose inflammation, and fatty liver disease. *J Lipid Res,* 54**,** 1346-59.

MERRILL, G. F., KURTH, E. J., HARDIE, D. G. & WINDER, W. W. 1997. AICA riboside increases AMP-activated protein kinase, fatty acid oxidation, and glucose uptake in rat muscle. *Am J Physiol,* 273**,** E1107-12.

MIRANDA, C. L., YANG, Y. H., HENDERSON, M. C., STEVENS, J. F., SANTANA-RIOS, G., DEINZER, M. L. & BUHLER, D. R. 2000. Prenylflavonoids from hops inhibit the metabolic activation of the carcinogenic heterocyclic amine 2-amino-3-methylimidazo[4, 5-f]quinoline, mediated by cDNA-expressed human CYP1A2. *Drug Metab Dispos,* 28**,** 1297-302.

MITRA, S. K., HANSON, D. A. & SCHLAEPFER, D. D. 2005. Focal adhesion kinase: in command and control of cell motility. *Nat Rev Mol Cell Biol,* 6**,** 56-68.

MIYOKAWA-GORIN, K., TAKAHASHI, K., HANDA, K., KITAHARA, A., SUMITANI, Y., KATSUTA, H., TANAKA, T., NISHIDA, S., YOSHIMOTO, K., OHNO, H. & ISHIDA, H. 2012. Induction of mitochondrial uncoupling enhances VEGF(1)(2)(0) but reduces MCP-1 release in mature 3T3-L1 adipocytes: possible regulatory mechanism through endogenous ER stress and AMPK-related pathways. *Biochem Biophys Res Commun,* 419**,** 200-5.

MIYOSHI, H., PERFIELD, J. W., 2ND, SOUZA, S. C., SHEN, W. J., ZHANG, H. H., STANCHEVA, Z. S., KRAEMER, F. B., OBIN, M. S. & GREENBERG, A. S. 2007. Control of adipose triglyceride lipase action by serine 517 of perilipin A globally regulates protein kinase A-stimulated lipolysis in adipocytes. *J Biol Chem,* 282**,** 996-1002.

MIYOSHI, H., SOUZA, S. C., ENDO, M., SAWADA, T., PERFIELD, J. W., 2ND, SHIMIZU, C., STANCHEVA, Z., NAGAI, S., STRISSEL, K. J., YOSHIOKA, N., OBIN, M. S., KOIKE, T. & GREENBERG, A. S. 2010. Perilipin overexpression in mice protects against diet-induced obesity. *J Lipid Res,* 51**,** 975-82.

MOISSOGLU, K. & SCHWARTZ, M. A. 2006. Integrin signalling in directed cell migration. *Biol Cell,* 98**,** 547-55.

MONTEIRO, R., CALHAU, C., SILVA, A. O., PINHEIRO-SILVA, S., GUERREIRO, S., GARTNER, F., AZEVEDO, I. & SOARES, R. 2008. Xanthohumol inhibits inflammatory factor production and angiogenesis in breast cancer xenografts. *J Cell Biochem,* 104**,** 1699-707.

MUNDAY, M. R., CAMPBELL, D. G., CARLING, D. & HARDIE, D. G. 1988. Identification by amino acid sequencing of three major regulatory phosphorylation sites on rat acetyl-CoA carboxylase. *Eur J Biochem,* 175**,** 331-8.

MURPHY, D. J. 2001. The biogenesis and functions of lipid bodies in animals, plants and microorganisms. *Prog Lipid Res,* 40**,** 325-438.

MURPHY, D. J. & VANCE, J. 1999. Mechanisms of lipid-body formation. *Trends Biochem Sci,* 24**,** 109-15.

NAKASHIMA, Y., PLUMP, A. S., RAINES, E. W., BRESLOW, J. L. & ROSS, R. 1994. ApoE-deficient mice develop lesions of all phases of atherosclerosis throughout the arterial tree. *Arterioscler Thromb,* 14**,** 133-40.

NAMKOONG, C., KIM, M. S., JANG, P. G., HAN, S. M., PARK, H. S., KOH, E. H., LEE, W. J., KIM, J. Y., PARK, I. S., PARK, J. Y. & LEE, K. U. 2005. Enhanced hypothalamic AMP-activated protein kinase activity contributes to hyperphagia in diabetic rats. *Diabetes,* 54**,** 63-8.

NOZAWA, H. 2005. Xanthohumol, the chalcone from beer hops (Humulus lupulus L.), is the ligand for farnesoid X receptor and ameliorates lipid and glucose metabolism in KK-A(y) mice. *Biochem Biophys Res Commun,* 336**,** 754-61.

ORR, A. W., PALLERO, M. A., XIONG, W. C. & MURPHY-ULLRICH, J. E. 2004. Thrombospondin induces RhoA inactivation through FAK-dependent signaling to stimulate focal adhesion disassembly. *J Biol Chem,* 279**,** 48983-92.

PARK, Y. M., FEBBRAIO, M. & SILVERSTEIN, R. L. 2009. CD36 modulates migration of mouse and human macrophages in response to oxidized LDL and may contribute to macrophage trapping in the arterial intima. *J Clin Invest,* 119**,** 136-45.

PAUL, A., CHAN, L. & BICKEL, P. E. 2008a. The PAT family of lipid droplet proteins in heart and vascular cells. *Curr Hypertens Rep,* 10**,** 461-6.

PAUL, A., CHANG, B. H., LI, L., YECHOOR, V. K. & CHAN, L. 2008b. Deficiency of adipose differentiation-related protein impairs foam cell formation and protects against atherosclerosis. *Circ Res,* 102**,** 1492-501.

PERSSON, J., DEGERMAN, E., NILSSON, J. & LINDHOLM, M. W. 2007. Perilipin and adipophilin expression in lipid loaded macrophages. *Biochem Biophys Res Commun,* 363**,** 1020-6.

PLUMP, A. S. & BRESLOW, J. L. 1995. Apolipoprotein E and the apolipoprotein E-deficient mouse. *Annu Rev Nutr,* 15**,** 495-518.

POL, A., MARTIN, S., FERNANDEZ, M. A., FERGUSON, C., CAROZZI, A., LUETTERFORST, R., ENRICH, C. & PARTON, R. G. 2004. Dynamic and regulated association of caveolin with lipid bodies: modulation of lipid body motility and function by a dominant negative mutant. *Mol Biol Cell,* 15**,** 99-110.

REN, G., RUDENKO, G., LUDTKE, S. J., DEISENHOFER, J., CHIU, W. & POWNALL, H. J. 2010. Model of human low-density lipoprotein and bound receptor based on cryoEM. *Proc Natl Acad Sci U S A,* 107**,** 1059-64.

RIDLEY, A. J., SCHWARTZ, M. A., BURRIDGE, K., FIRTEL, R. A., GINSBERG, M. H., BORISY, G., PARSONS, J. T. & HORWITZ, A. R. 2003. Cell migration: integrating signals from front to back. *Science,* 302**,** 1704-9.

ROSENBAUM, M., LEIBEL, R. L. & HIRSCH, J. 1997. Obesity. *New England Journal of Medicine,* 337**,** 396-407.

RUDENKO, G., HENRY, L., HENDERSON, K., ICHTCHENKO, K., BROWN, M. S., GOLDSTEIN, J. L. & DEISENHOFER, J. 2002. Structure of the LDL receptor extracellular domain at endosomal pH. *Science,* 298**,** 2353-8.

SAHA, P. K., KOJIMA, H., MARTINEZ-BOTAS, J., SUNEHAG, A. L. & CHAN, L. 2004. Metabolic adaptations in the absence of perilipin: increased beta-oxidation and decreased hepatic glucose production associated with peripheral insulin resistance but normal glucose tolerance in perilipin-null mice. *J Biol Chem,* 279**,** 35150-8.

SATO, R., GOLDSTEIN, J. L. & BROWN, M. S. 1993. Replacement of serine-871 of hamster 3-hydroxy-3-methylglutaryl-CoA reductase prevents phosphorylation by AMP-activated kinase and blocks inhibition of sterol synthesis induced by ATP depletion. *Proc Natl Acad Sci U S A,* 90**,** 9261-5.

SERRERO, G., FROLOV, A., SCHROEDER, F., TANAKA, K. & GELHAAR, L. 2000. Adipose differentiation related protein: expression, purification of recombinant protein in Escherichia coli and characterization of its fatty acid binding properties. *Biochim Biophys Acta,* 1488**,** 245-54.

SMALL, J. V., STRADAL, T., VIGNAL, E. & ROTTNER, K. 2002. The lamellipodium: where motility begins. *Trends Cell Biol,* 12**,** 112-20.

SON, S. H., GOO, Y. H., CHANG, B. H. & PAUL, A. 2012. Perilipin 2 (PLIN2)-deficiency does not increase cholesterol-induced toxicity in macrophages. *PLoS One,* 7**,** e33063.

STOSSEL, T. P. 1994. The machinery of cell crawling. *Sci Am,* 271**,** 54-5, 58-63.

SUBRAMANIAN, V., ROTHENBERG, A., GOMEZ, C., COHEN, A. W., GARCIA, A., BHATTACHARYYA, S., SHAPIRO, L., DOLIOS, G., WANG, R., LISANTI, M. P. & BRASAEMLE, D. L. 2004. Perilipin A mediates the reversible binding of CGI-58 to lipid droplets in 3T3-L1 adipocytes. *J Biol Chem,* 279**,** 42062-71.

TABAS, I. 2002. Consequences of cellular cholesterol accumulation: basic concepts and physiological implications. *J Clin Invest,* 110**,** 905-11.

TABATA, N., ITO, M., TOMODA, H. & OMURA, S. 1997. Xanthohumols, diacylglycerol acyltransferase inhibitors, from Humulus lupulus. *Phytochemistry,* 46**,** 683-7.

TANSEY, J. T., SZTALRYD, C., GRUIA-GRAY, J., ROUSH, D. L., ZEE, J. V., GAVRILOVA, O., REITMAN, M. L., DENG, C. X., LI, C., KIMMEL, A. R. & LONDOS, C. 2001. Perilipin ablation results in a lean mouse with aberrant adipocyte lipolysis, enhanced leptin production, and resistance to diet-induced obesity. *Proc Natl Acad Sci U S A,* 98**,** 6494-9.

TAUCHI-SATO, K., OZEKI, S., HOUJOU, T., TAGUCHI, R. & FUJIMOTO, T. 2002. The surface of lipid droplets is a phospholipid monolayer with a unique Fatty Acid composition. *J Biol Chem,* 277**,** 44507-12.

TENGER, C. & ZHOU, X. 2003. Apolipoprotein E modulates immune activation by acting on the antigen-presenting cell. *Immunology,* 109**,** 392-7.

VAN ANTWERPEN, R., LA BELLE, M., NAVRATILOVA, E. & KRAUSS, R. M. 1999. Structural heterogeneity of apoB-containing serum lipoproteins visualized using cryo-electron microscopy. *J Lipid Res,* 40**,** 1827-36.

VANHOECKE, B. W., DELPORTE, F., VAN BRAECKEL, E., HEYERICK, A., DEPYPERE, H. T., NUYTINCK, M., DE KEUKELEIRE, D. & BRACKE, M. E. 2005. A safety study of oral tangeretin and xanthohumol administration to laboratory mice. *In Vivo,* 19**,** 103-7.

VIOLLET, B., ANDREELLI, F., JORGENSEN, S. B., PERRIN, C., FLAMEZ, D., MU, J., WOJTASZEWSKI, J. F., SCHUIT, F. C., BIRNBAUM, M., RICHTER, E., BURCELIN, R. & VAULONT, S. 2003. Physiological role of AMP-activated protein kinase (AMPK): insights from knockout mouse models. *Biochem Soc Trans,* 31**,** 216-9.

WAKIL, S. J., STOOPS, J. K. & JOSHI, V. C. 1983. Fatty acid synthesis and its regulation. *Annu Rev Biochem,* 52**,** 537-79.

WANG, X., REAPE, T. J., LI, X., RAYNER, K., WEBB, C. L., BURNAND, K. G. & LYSKO, P. G. 1999. Induced expression of adipophilin mRNA in human macrophages stimulated with oxidized low-density lipoprotein and in atherosclerotic lesions. *FEBS Lett,* 462**,** 145-50.

WARDLE, J., CARNELL, S., HAWORTH, C. M. & PLOMIN, R. 2008. Evidence for a strong genetic influence on childhood adiposity despite the force of the obesogenic environment. *Am J Clin Nutr,* 87**,** 398-404.

WHITMAN, S. C. 2004. A practical approach to using mice in atherosclerosis research. *Clin Biochem Rev,* 25**,** 81-93.

WINDER, W. W. & HARDIE, D. G. 1999. AMP-activated protein kinase, a metabolic master switch: possible roles in type 2 diabetes. *Am J Physiol,* 277**,** E1-10.

WOLINS, N. E., BRASAEMLE, D. L. & BICKEL, P. E. 2006a. A proposed model of fat packaging by exchangeable lipid droplet proteins. *FEBS Lett,* 580**,** 5484-91.

WOLINS, N. E., QUAYNOR, B. K., SKINNER, J. R., SCHOENFISH, M. J., TZEKOV, A. & BICKEL, P. E. 2005. S3-12, Adipophilin, and TIP47 package lipid in adipocytes. *J Biol Chem,* 280**,** 19146-55.

WOLINS, N. E., QUAYNOR, B. K., SKINNER, J. R., TZEKOV, A., CROCE, M. A., GROPLER, M. C., VARMA, V., YAO-BORENGASSER, A., RASOULI, N., KERN, P. A., FINCK, B. N. & BICKEL, P. E. 2006b. OXPAT/PAT-1 is a PPAR-induced lipid droplet protein that promotes fatty acid utilization. *Diabetes,* 55**,** 3418-28.

WONG, B. W., MEREDITH, A., LIN, D. & MCMANUS, B. M. 2012. The biological role of inflammation in atherosclerosis. *Can J Cardiol,* 28**,** 631-41.

YANCEY, P. G., BORTNICK, A. E., KELLNER-WEIBEL, G., DE LA LLERA-MOYA, M., PHILLIPS, M. C. & ROTHBLAT, G. H. 2003. Importance of different pathways of cellular cholesterol efflux. *Arterioscler Thromb Vasc Biol,* 23**,** 712-9.

YANG, J. Y., DELLA-FERA, M. A., RAYALAM, S. & BAILE, C. A. 2008. Enhanced effects of xanthohumol plus honokiol on apoptosis in 3T3-L1 adipocytes. *Obesity (Silver Spring),* 16**,** 1232-8.

YU, W., BOZZA, P. T., TZIZIK, D. M., GRAY, J. P., CASSARA, J., DVORAK, A. M. & WELLER, P. F. 1998. Co-compartmentalization of MAP kinases and cytosolic phospholipase A2 at cytoplasmic arachidonate-rich lipid bodies. *Am J Pathol,* 152**,** 759-69.

ZADELAAR, S., KLEEMANN, R., VERSCHUREN, L., DE VRIES-VAN DER WEIJ, J., VAN DER HOORN, J., PRINCEN, H. M. & KOOISTRA, T. 2007. Mouse models for atherosclerosis and pharmaceutical modifiers. *Arterioscler Thromb Vasc Biol,* 27**,** 1706-21.

ZANOLI, P. & ZAVATTI, M. 2008. Pharmacognostic and pharmacological profile of Humulus lupulus L. *J Ethnopharmacol,* 116**,** 383-96.

ZHANG, S. H., REDDICK, R. L., PIEDRAHITA, J. A. & MAEDA, N. 1992. Spontaneous hypercholesterolemia and arterial lesions in mice lacking apolipoprotein E. *Science,* 258**,** 468-71.

ZHAO, F., NOZAWA, H., DAIKONNYA, A., KONDO, K. & KITANAKA, S. 2003. Inhibitors of nitric oxide production from hops (Humulus lupulus L.). *Biol Pharm Bull,* 26**,** 61-5.

ZHOU, G., MYERS, R., LI, Y., CHEN, Y., SHEN, X., FENYK-MELODY, J., WU, M., VENTRE, J., DOEBBER, T., FUJII, N., MUSI, N., HIRSHMAN, M. F., GOODYEAR, L. J. & MOLLER, D. E. 2001. Role of AMP-activated protein kinase in mechanism of metformin action. *J Clin Invest,* 108**,** 1167-74.

18. Abbreviations

Adipose triglyceride lipase	ATGL
Acyl-CoA: cholesterol acyltransferase1	ACAT1
Apolipoprotein E knockout	ApoE-/-
ATP-binding cassette transporter A1	Abca1
ATP-binding cassette transporter G1	Abcg1
Adipocyte differentiation-related protein	ADRP
Apolipoprotein AI	ApoAI
Adenosine monophosphate-activated protein kinase	AMPK
Acetylated LDL	acLDL
Aggregated LDL	aggLDL
Bone marrow-derived macrophages	BMDM
Cholesteryl esters	CE
Cardiovascular diseases	CVDs
Cluster of differentiation 36	Cd36
Comparative gene identification-58	CGI-58
Carnitine palymitoyltransferase 1 alpha	Cpt1α
Diaglycerides	DG
Diacylglycerol acyltransferase	DGAT
Diethyl pyrocarbonate	DEPC
Endoplasmic reticulum	ER
Fatty acids	FAs
Free fatty acid	FFA

Free cholesterol	FC
Intracellular adhesion molecule	ICAM-1
Intermediate-density lipoproteins	IDL
Glyceraldehyde phosphate dehydrogenase	GAPDH
Hypoxanthine phophoribosyl transferase	HPRT
High density lipoprotein	HDL
Hormone sensitive lipase	Hsl
Lipid droplets	LDs
Lipopolysaccharides	LPS
Lipoprotein-deficient serum	LPDS
Low-density lipoprotein	LDL
Lipoprotein lipase	LPL
Liposomal acid lipase	LAL
Low-density lipoprotein receptor knockout	Ldlr-/-
Monoglyceride lipase	MGL
Monoglycerides	MG
Macrophage colony-stimulating factor	M-CSF
Macrophage-chemoattractant protein 1	MCP-1
Monoclonal antibody to macrophages-2	MOMA-2
Mouse peritoneal macrophages	MPM
Oxidized LDL	oxLDL
Protein kinase A	PKA
Phosphatidylcholine	PC
Phosphatidylinositol	PI

Phospholipids	PL
Perilipin	Plin1
Peroxisome proliferator-activated receptors	PPAR
1 % Penicillin/1 % streptomycin 1 %	P/S
SDS-polyacrylamid gel	SDS-PAGE
Tail interacting protein 47	TIP47
Triglycerides	TG
Total cholesterol	TC
Tumor necrosis factor α	TNFα
Thin layer chromatography	TLC
Toll-like receptor	TLR
Vascular cell-adhesion molecule	VCAM-1
Wild-type	Wt
Western-type diet	WTD
White adipose tissue	WAT